COMPRESSION BEHAVIOR OF FIRE-DAMAGED CONCRETE-FILLED STEEL TUBULAR COLUMNS CONFINED WITH FIBER-REINFORCED POLYMER SHEETS

Mr. Dat Thanh Vu

A Thesis Submitted in Partial Fulfillment of the Requirements
for the Degree of Master of Engineering in Civil Engineering
Department of Civil Engineering
Faculty of Engineering
Chulalongkorn University
Academic Year 2018

พฤติกรรมรับแรงอัดของเสาท่อเหล็กเติมด้วยคอนกรีตที่เสียหายจากไฟถูกโอบรัดด้วยแผ่นพอลิเมอร์เสริมเส้นใย

นายแดท ถาน วู

วิทยานิพนธ์นี้เป็นส่วนหนึ่งของการศึกษาตามหลักสูตรปริญญาวิศวกรรมศาสตรมหาบัณฑิต
สาขาวิชาวิศวกรรมโยธา ภาควิชาวิศวกรรมโยธา
คณะวิศวกรรมศาสตร์ จุฬาลงกรณ์มหาวิทยาลัย
ปีการศึกษา 2561

Thesis Title	COMPRESSION BEHAVIOR OF FIRE-DAMAGED CONCRETE-FILLED STEEL TUBULAR COLUMNS CONFINED WITH FIBER-REINFORCED POLYMER SHEETS
By	Mr. Dat Thanh Vu
Field of Study	Civil Engineering
Thesis Advisor	Associate Professor AKHRAWAT LENWARI, Ph.D.

Accepted by the Faculty of Engineering, Chulalongkorn University in Partial Fulfillment of the Requirement for the Master of Engineering

..... Dean of the Faculty of Engineering
(Professor SUPOT TEACHAVORASINSKUN, D.Eng.)

THESIS COMMITTEE

..... Chairman
(Professor THANYAWAT POTHISIRI, Ph.D.)

..... Thesis Advisor
(Associate Professor AKHRAWAT LENWARI, Ph.D.)

..... Examiner
(Assistant Professor PITCHA JONGVIVATSAKUL, Ph.D.)

..... External Examiner
(Professor Thaksin Thepchatri, Ph.D.)

แดท ถาน วู : พฤติกรรมรับแรงอัดของเสาท่อเหล็กเติมด้วยคอนกรีตที่เสียหายจากไฟถูกโอบรัดด้วยแผ่นพอลิเมอร์เสริมเส้นใย. (COMPRESSION BEHAVIOR OF FIRE-DAMAGED CONCRETE-FILLED STEEL TUBULAR COLUMNS CONFINED WITH FIBER-REINFORCED POLYMER SHEETS) อ.ที่ปรึกษาหลัก : รศ. ดร.อัครวัชร เล่นวารี

งานวิจัยนี้ศึกษาพฤติกรรมรับแรงอัดของเสาสั้นท่อเหล็กกลมเติมด้วยคอนกรีตที่เสียหายจากไฟและถูกโอบรัดภายนอกด้วยแผ่นพอลิเมอร์เสริมเส้นใย ในการศึกษานี้ได้ทำการทดสอบเสาตัวอย่างภายใต้แรงอัดจำนวน 38 ชิ้นงานเพื่อศึกษากำลังรับแรงอัด ความเหนียว และสติฟเนสของเสา ทั้งก่อนและภายหลังการเสริมกำลังด้วยแผ่นพอลิเมอร์เสริมเส้นใย โดยมีตัวแปรในการทดสอบประกอบ คือ ระดับความเสียหายจากไฟ (ไม่มีความเสียหาย และได้รับความเสียหายจากการเผาไฟภายใต้เพลิงไหม้มาตรฐานไอเอสโอเป็นระยะเวลา 2 ชั่วโมง) กำลังรับแรงอัดของคอนกรีต (24 และ 55 เมกะปาสคาล) ประเภทของเส้นใย (คาร์บอน และแก้ว) และ จำนวนชั้นที่พันรอบด้วยแผ่นพอลิเมอร์เสริมเส้นใย (0 1 และ 2 ชั้น) จากผลการทดสอบพบว่า เสาวัสดุผสมที่เติมด้วยคอนกรีต 55 เมกะปาสคาล ได้รับผลกระทบจากการเผาไฟมากกว่าเสาวัสดุผสมที่เติมด้วยคอนกรีต 24 เมกะปาสคาล แต่แสดงประสิทธิภาพของการเสริมกำลังที่ไม่แตกต่างกัน ทั้งนี้ ระดับการเพิ่มขึ้นของกำลังรับแรงอัดเนื่องจากการเสริมกำลังในกรณีเสาวัสดุผสมที่เสียหายจากไฟมีค่าต่ำกว่ากรณีเสาที่ไม่เสียหาย และแผ่นพอลิเมอร์เสริมเส้นใยไม่สามารถเพิ่มสติฟเนสของเสาวัสดุผสมที่เสียหายจากไฟได้เหมือนในกรณีเสาที่ไม่เสียหาย นอกจากนั้น การเพิ่มจำนวนชั้นที่พันรอบด้วยแผ่นพอลิเมอร์เสริมเส้นใยสามารถเพิ่มกำลังรับแรงอัดแต่ความเหนียวของเสาลดลง เส้นใยแก้วให้ระดับการเพิ่มขึ้นของกำลังรับแรงอัดที่ใกล้เคียงและให้ระดับการเพิ่มขึ้นของความเหนียวที่สูงกว่าเส้นใยคาร์บอน งานวิจัยนี้ยังได้นำเสนอการวิเคราะห์พฤติกรรมรับแรงอัดซึ่งประกอบด้วย (1) การวิเคราะห์การถ่ายโอนความร้อนด้วยไฟไนต์เอลิเมนต์ 2 มิติ (2) คุณสมบัติเชิงกลของท่อเหล็กและคอนกรีตภายหลังเผาไฟ และ (3) แบบจำลองที่พิจารณาผลกระทบของการโอบรัดคอนกรีต และมีการตรวจสอบความเหมาะสมของการวิเคราะห์โดยการเปรียบเทียบความสัมพันธ์ระหว่างแรงอัดและความเครียดที่ได้จากการวิเคราะห์กับผลการทดสอบ

สาขาวิชา วิศวกรรมโยธา ลายมือชื่อนิสิต .....

ปีการศึกษา 2561 ลายมือชื่อ อ.ที่ปรึกษาหลัก .....

6070192021 : MAJOR CIVIL ENGINEERING

KEYWORD: Concrete-filled steel tube column, Fiber-reinforced polymer, ISO 834 standard fire, Analytical model

Dat Thanh Vu : COMPRESSION BEHAVIOR OF FIRE-DAMAGED CONCRETE-FILLED STEEL TUBULAR COLUMNS CONFINED WITH FIBER-REINFORCED POLYMER SHEETS. Advisor: Assoc. Prof. AKHRAWAT LENWARI, Ph.D.

This research investigates the axial compression behavior of fire-damaged circular concrete-filled steel tube (CFST) stub columns externally confined with fiber-reinforced polymer (FRP) sheets. A total of 38 CFST specimens were tested under axial compression to investigate the load capacity, ductility, stiffness and failure mode of fire-damaged CFST columns before and after strengthening with FRP sheets. The test variables include the level of fire damage (no damage and 2-hour ISO standard fire), compressive strength of infill concrete (24MPa and 55MPa), type of FRP sheets (carbon and glass), and the number of FRP layers (0, 1, and 2 layers). The test results showed that 55-MPa CFST columns are more damaged by fire than 24-MPa CFST columns. However, confinement effectiveness due to FRP wrapping is similar. The level of strength enhancement due to FRP for fire-damaged CFST columns is lower than undamaged ones. In contrast to undamaged CFST columns, FRP cannot improve the stiffness of fire-damaged ones. Furthermore, an increase in the number of FRP layers improves the load capacity of specimens but deteriorates the ductility. The glass fiber sheets provide competitive strength enhancement and superior in ductility enhancement than carbon fiber sheets. An analysis of compression behavior of FRP-confined fire-damaged CFST columns is also proposed. Three main components include (1) two-dimensional finite element heat transfer analysis, (2) Post-fire mechanical properties of steel tube and concrete, and (3) analytical model that incorporates the confinement effect. The validity of the proposed model is shown by comparing the predicted load-strain relationships with experimental results.

Field of Study:	Civil Engineering	Student's Signature .....
Academic Year:	2018	Advisor's Signature .....

ACKNOWLEDGEMENTS

First, and above all, I would like to express my sincerest gratitude to my academic supervisor Assoc. Prof. Akhrawat Lenwari. Thank you, Ajarn not only for your outstanding technical guidance but also for your trust, your comments, your counsel, your sharing stories, your life lessons, and for your time you put into discussing and revising my thesis work and my very first publications.

I would also like to thank the examiners of this thesis, Prof. Thanyawat Pothisiri, Prof. Thaksin Thepchatri, and Assist. Prof. Pitcha Jongvivatsakul for their time, their interest in reading and discussing this thesis work.

The work presented in this thesis has been funded by the ASEAN University Network/Southeast Asia Engineering Education Development Network (AUN/SEED-Net). The fire test was conducted at the Fire Safety Research Center (FSRC), Chulalongkorn University. Their support is gratefully acknowledged.

Last but not least, I dedicate this thesis to my family, and my friends, Chanachai, Voraphol, Joe, Kong, Tosporn, May, Linh Bui who always support and keep me going through difficult times during the implementation of this thesis.

Dat Thanh Vu

TABLE OF CONTENTS

Page

LIST OF TABLES

LIST OF FIGURES

LIST OF SYMBOLS

$A; B$	Parameters govern shape of stress-strain curve
A_c	Cross-section area of concrete core
A_{ck}	Cross-section area of concrete core of layer k
A_s	Cross-section area of steel tube
d	Diameter of CFST column, diameter of external confinement
E_c	Elastic modulus of concrete
E_{cp}	Post-fire residual elastic modulus of concrete
E_s	Elastic modulus of steel
E_{sp}	Post-fire residual elastic modulus of steel
E_{ssE}	Elastic modulus of external confinement (FRP)
f_c	Compressive strength of concrete
f_{cc}	Confined concrete stress
f_{ccp}	Confined peak concrete stress
f_{cp}	Post-fire residual compressive strength of concrete
f_r	Confining pressure on concrete core
f_{rE}	Confining pressure from external confinement (FRP)
f_{rs}	Confining pressure from steel tube
F_c	Load capacity by concrete core
F_s	Load capacity by steel tube
F_t	Load capacity of CFST column
f_y	Yield strength of steel
f_{yp}	Post-fire residual yield strength of steel

H	Height of specimen
i	Step of iterative process
k	Layer of discretized concrete
LS	Confinement effect parameter
m	Parameter on the effect of concrete strength
S	Center to center spacing of external confinement
T	Elevated temperature
T_0	Ambient temperature
v_s	Poison's ratio
ε_c	Strain corresponding peak strength of concrete
ε_{cc}	Strain corresponding peak strength of confined concrete stress
ε_{cp}	Strain corresponding of post-fire peak strength of concrete
ε_{cz}	Axial strain of concrete
$\varepsilon_{c\theta}$	Hoop strain of concrete
ε_{ssE}	Hoop strain of external confinement (FRP)
ε_{sz}	Axial strain of steel tube
$\varepsilon_{s\theta}$	Hoop strain of steel tube
ε_z	Axial strain of CFST columns
ε_θ	Hoop strain of CFST columns
σ_E	Hoop stress provided by external confinement (FRP)
σ_{ssE}	Yield stress of external confinement (FRP)
σ_{sy}	von Mises yield stress
σ_{sz}	Axial stress provided by steel tube
$\sigma_{s\theta}$	Hoop stress provided by steel tube

CHAPTER 1
INTRODUCTION

1.1. Motivation

Composite construction has now been developed significantly since its origins approximately 100 years ago when the idea that the concrete fire protection around columns might be able to serve some structural purpose or that the concrete bridge deck might, with advantage, be made to act in conjunction with the supporting steel beam was first proposed (Nethercot, 2003). Normally, "composite construction" within the aspect of civil engineering is known as the use of steel and concrete formed together into a component.

An initial application of composite columns was for fire protection requirements of the steel section and later on make use of the composite action for strength and stability (Uy, 1998) as shown in Figure 1.1a. Moreover, with the demand to achieve higher steel percentages than the conventional reinforced concrete structures and provide the time-saving for construction, the erection columns as shown in Figure 1.1b are also used widely.

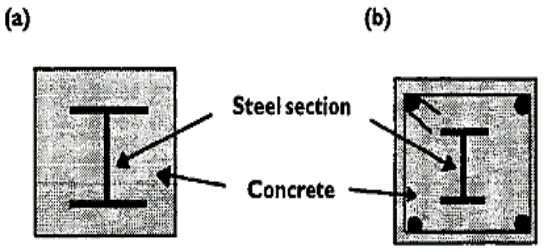

Figure 1.1 Encased composite section

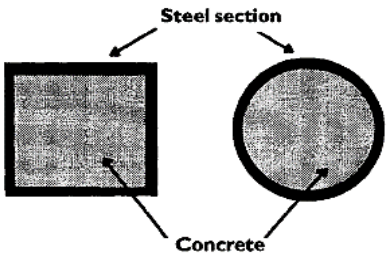

Figure 1.2 Concrete-filled steel tube

Concrete-Filled Steel Tube (CFST) columns as illustrated in Figure 1.2 have been developed much later but are still based on the fundamental principle that the steel and concrete are most effective in tension and compression respectively (Uy, 1998). CFST, nowadays, have been popularly used in building construction, especially in high-rise apartment buildings, because of the following major benefits:

- Higher strength than individual material (steel and concrete) standing alone (Uy, 2001). The local buckling of steel tube is much enhanced by infill concrete. The concrete, which is confined by steel, behave more perfectly (Nethercot, 2003). Also, the extra load bearing due to interaction between these two materials takes advantage for this type of columns.
- Greater ductility in cyclic loading experienced during earthquake. In Great Kanto Earthquake in 1923, the existing composite structures were relatively undamaged (Wakabayashi, 1987)
- Formwork omission can save construction time. Steel columns acts as a permanent and integral formwork.

Nevertheless, CFST columns have some disadvantages. They required large steel plate thickness (Uy, 1998). Also, one of the major concerns in high-rise structures is the possibility of a fire or the effect of elevated temperatures on structural members. In the tragic event of the colossal World Trade Center in September 2001 in New York, USA (Scheuerman A, 2002 Mar 12.) there is misconception. The main reason for collapse is the fire not the plane caused as we known nowadays. That tragic event makes us comprehend clearly about the considerable damages caused by fire. In the case of fire hazards, civil engineering structures in general and CFST columns in particular, strength and stiffness will be deteriorated quickly. In order to regain some structural properties and strengthen for post-fire construction members, there are a huge of treatments that can be applied. The implements of Fiber-Reinforced Polymer (FRP) materials have shown great potential method and have been popularly used (Teng et al, 2002).

In recently years, FRP materials have developed into economically and structurally viable construction materials for buildings and bridges. FRP composite materials typically used in structural engineering consist of glass, carbon, or aramid fibers encased in a matrix of epoxy, polyester, vinyl ester, or phenolic thermosetting resins with fiber concentration greater than 30% by volume (Bank, 2006). FRP materials have been effectively applied in retrofitting concrete columns because of their high strength-to-weight ratio, durability enhancement, and ease of application

(Mirmiran & Shahawy, 1997) or even local buckling prevention for CFST (Hu et al., 2011). Beside the use of FRP materials as a part of structure member, the applications of FRP confinements for member whose purpose is to enhance the damaged-member properties, have also received a huge concern.

When a CFST columns is exposed to devastating fire for a long period of time, its strength reduces considerably (Yao & Hu, 2015). FRP confinement or the use of FRP wrapping is an effective technique to enhance structural properties for fire-damaged CFST columns (Wang et al, 2018).

1.2. Significance

Fire dangers can be a threat to all structures and CFST columns are more popularly used in high-rise buildings. However, the available studies on the strengthening of fire-damaged CFST columns are still limited. This research is conducted to investigate the FRP strengthening effect and wrapped compression behavior of fire-damaged CFST short columns externally strengthened with FRP sheets. From this research, the behavior of FRP-confined fire-damaged CFST columns will be more understood. A mathematical model is also proposed to predict the behavior of the fire-damaged columns after being strengthened with FRP sheets.

1.3. Objectives

In this research, the main objectives are as follows,

1. To investigate the compression behavior of fire-damaged Concrete-Filled Steel Tube (CFST) columns.
2. To investigate the effectiveness of Fiber-Reinforced Polymer (FRP) sheets on strengthening fire-damaged CFST columns.
3. To review the existing analytical and empirical models on the compression behavior of fire-damaged CFST columns.
4. To propose a mathematical model to predict compression behavior of fire-damaged CFST columns confined with FRP sheets.

1.4. Scope

The scope of this research is given below,

1. The compressive behavior includes the load-deformation relationships, load-strain relationships, strength, ductility, stiffness, and failure modes.
2. The experiment is conducted on short columns (height of 300mm). The test variables include the level of fire damage (ambient and 2-hour ISO standard fire), compressive strength of infill concrete (24 and 55 MPa), type of FRP sheets (CFRP and GFRP), and number of FRP layers (0, 1 and 2 layers).
3. Sustained loads, damages of bond between steel and concrete caused by fire, and environmental effects are not considered in this research.

1.5. Expected output

After the completion of this research, the below results should be obtained:

1. Residual strength of the fire-damaged CFST columns before and after being confined with FRP sheets.
2. The effects of infill concrete strength and FRP wrapping scheme (CFRP 1-layer, GFRP 1-layer, CFRP 2-layer and hybrid) on the compression behavior of FRP-confined fire-damaged CFST columns.
3. Review of existing prediction models based on the experiment results from this research.
4. A mathematical model for compression behavior of FRP-confined fire-damaged CFST columns.

1.6. Methodology

The research method can be explained as follows,

1. Review the previous works on post-fire material properties and behavior of CFST columns, and FRP strengthening of the fire-damaged CFST columns.
2. Summarize the effects of relevant parameters in this research.
3. Conduct an experiment on the fire-damaged CFST columns to investigate the post-fire behavior of CFST columns.

4. Strengthen the fire-damaged CFST columns and conduct the compression test to investigate the behavior of fire-damaged CFST columns confined by FRP sheets.
5. Collect test results and determine the effectiveness of FRP on strengthening fire-damaged CFST columns.
6. Review the existing models that predict the residual strength and strength enhancement by FRP wrapping.
7. Discuss on the test and analytical results, and then conclude the effectiveness of these results.
8. Develop a mathematical model for compression behavior of FRP-confined fire-damaged CFST columns.

1.7. Research schedule

Tasks		2018									2019					
		4	5	6	7	8	9	10	11	12	1	2	3	4	5	6
1	Literature review															
2	**Thesis Proposal**															
3	Test preparation															
4	Casting of CFST specimens															
5	Preparations and experiment on fire test															
6	CFRP confinement for post-fire CFST columns															
7	Compression test on FRP-confined fire-damaged CFST columns															
8	Analysis of experimental results															
9	Analytical works															
10	Discussions and conclusions															
11	Technical papers and thesis writing															
11	**Thesis defense**															

CHAPTER 2

LITERATURE REVIEW

2.1. Axial compression behavior of undamaged CFST columns

Han et al. (2014) showed a comparison between a steel tubular column, a reinforced concrete tubular column and a concrete-filled steel tubular column without steel reinforcement, in the similar geometry of the circular hollow steel sections. Figure 2.1 shows that the concrete-filled steel tube has higher strength than the summation of the individual strength of steel tube and RC columns. Also, the ductility of the CFST columns are significantly enhanced when compared to those of the steel tube and concrete standalone.

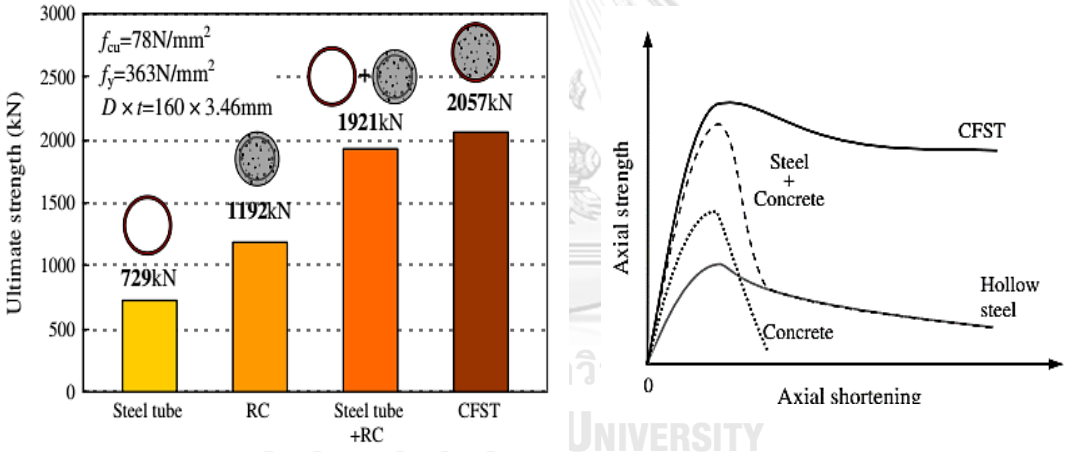

Figure 2.1 Axial compressive behavior of CFST columns (Han et al., 2014)

One of the vital advantages of CFST is the increased resistance to inward local buckling of the steel due to the presence of concrete. It was found that the post-local buckling strength was 150% of that of hollow steel columns (Uy, 1998). The ultimate load carrying capacity and stiffness of concrete are also enhanced because the concrete is subjected to the tri-axial state of stress caused by uniform continuous pressure from steel tube (Liu et al., 2003).

The materials used in CFST columns are also varietally developed and carried out in recent decades. O'Shea and Bridge (1994) showed that the use of high

strength concrete increases the columns stiffness and therefore reduces cross-section sizes. That would be very useful and effective especially for design of components subjected mainly to slenderness effects or lateral loadings. Ekmekyapar and Al-Eliwi (2016) revealed that the confinement performance is greater for columns with lower concrete strength. It means that composite action and confinement efficiency in CFST with normal strength infill concrete is better than high strength infill concrete. Besides, CFST with high strength infill concrete has some disadvantages because the degradation in strength and ductility will occur beyond the elastic stage due to outward buckling of steel tube (Lai & Ho, 2016)

For the research on the behavior of CFST stub columns under compression, previous works have mainly studied on the compressive strength. Few works have paid attention in compressive stiffness and deformation capacity (ductility). Wang et al. (2017) defined that the ductility is the axial strain corresponding to the ultimate strength, and stiffness as the secant stiffness corresponding the column strength of $0.4N_u$. Meanwhile, there is another definition for CFST stiffness and ductility (Lin & Tsai, 2003) defined as:

$$\mu_{95} = \frac{\varepsilon_{95}}{\varepsilon_y} \tag{2.1}$$

$$\varepsilon_y = \frac{\varepsilon_{75}}{0.75} \tag{2.2}$$

where ε_{75} and ε_{95} are the axial strains corresponding to the 75% and 95% of the peak axial load before and after the peak load, respectively. The idealized yield strain ε_y is extrapolated from ε_{75}. Kitada (1998) defined stiffness, strength and ductility as shown in Figure 2.2. P_y and P_u are the yield and ultimate strength. The limit displacements and yield displacement are $\delta_u, \delta_u^*, \delta_y^*, \delta_y$, respectively.

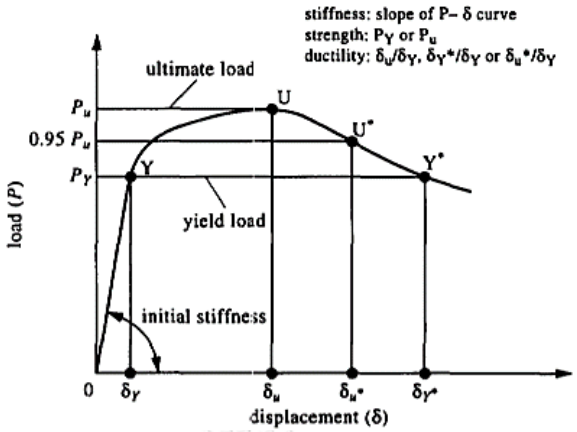

Figure 2.2 Definition of stiffness, strength and ductility (Kitada, 1998)

2.2. Axial compression behavior of fire-damaged CFST columns

Yao and Hu (2015) evaluated the strength reduction of steel in CFST columns after fire exposure (Figure 2.3). Generally, steel recovers most of its strength and stiffness after cooling down. However, the higher the maximum temperature attained in steel, the lower the steel residual strength is, particularly when the maximum temperature in steel exceeds 500°C. Abbas et al. (2017) revealed by the experiment of CFST in constant 600°C fire within 3 hours that the compressive strength of fire-damaged steel columns (without concrete infill) decreased slightly from 5.2% to 11.2% compared with the non-fired steel columns. This is because of the strength regain ability of steel after cooling down. In contrast, the strength degradation of concrete in CFST columns is pronounced. One of the differences between steel and concrete is that the strength of concrete cannot recover when temperature exceeds 200°C. Figure 2.4 shows the residual strength ratio of normal strength concrete (NSC) and high strength concrete (HSC) as a function of the exposure temperature.

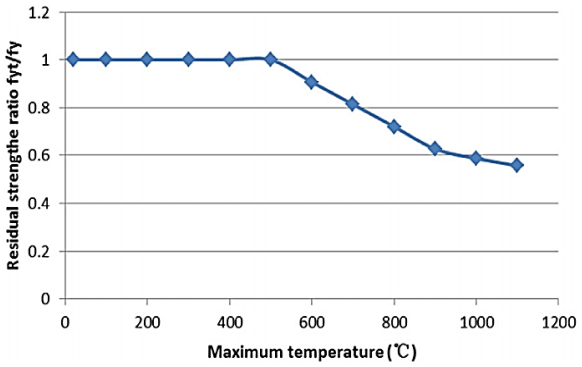

Figure 2.3 Residual strength ratio versus maximum temperature of steel. (Yao & Hu, 2015)

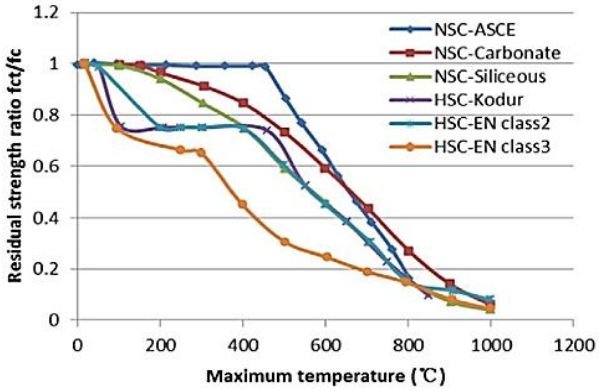

Figure 2.4 Residual strength ratio versus maximum temperature of concrete. (Yao & Hu, 2015)

HSC has lower permeability compared with NSC. This is thought to being more susceptible to spalling on heating. To overcome this, some methods are presented. One is the addition of polypropylene fibers, which melt at around 160^0C. Fibers can create pores which can relief the water vapor (Rush, 2013). Similar results are concluded in Yao and Hu (2015).

The effect of cross-section in the behavior of CFST columns has been also studied. Rush et al. (2015) showed that the square CFST sections may be more sensitive than the circular CFST in residual capacity perspective (ISO 834 fire curve, 5mm wall thickness) when exposed to the same elevated temperature. It is explained that because square columns experience comparatively less confinement than circular ones and are therefore less able to rely on the core concrete for

residual strength contributions. That hypothesis was also prior predicted by Han et al. (2002) with strain versus stress curves for both circular and square CFST columns with 5mm steel tube thickness (Figure 2.5). It is noteworthy that Han et al. (2002) proposed the same confined compressive strength for concrete in both cross sections. However, circular columns demonstrate a lower level of post-peak softening as a consequence of the superior lateral confinement versus square CFST section.

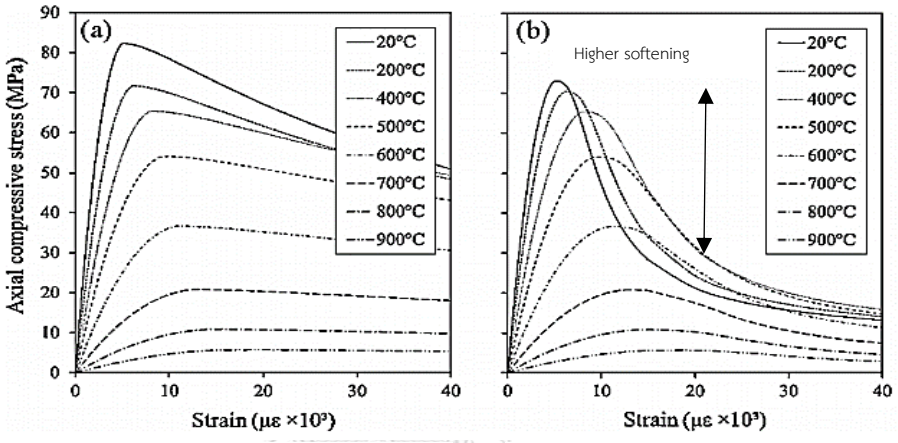

(a) Circular CFST columns (b) Square CFST columns

Figure 2.5 Residual stress-strain curves for core concrete (Han et al., 2002)

Only limited research is available on the residual capacity of fire-exposed CFST columns. The predicted Residual Strength Index (RSI) when exposed to ISO 834 fire curve were proposed by Han et al. (2002) in Figure 2.6. A more ductile behavior of fire-damaged CFST was also observed (Han et al., 2005). Rush et al. (2015) also revealed that, as expected, as the maximum temperatures experienced within the CFST sections increases, the residual axial failure load and axial stiffness of the CFST columns decreases.

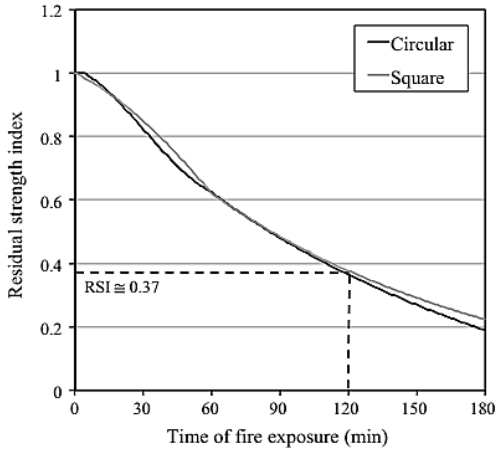

Figure 2.6 RSI for circular and square CFST column geometries when exposed to ISO 834 standard fire. (Han et al., 2002)

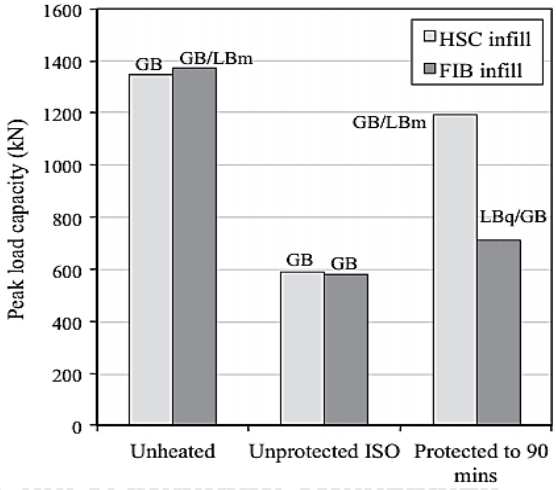

Figure 2.7 Effect of concrete infill type on load capacity (Rush et al., 2015)

Rush et al. (2015) investigated the type of infill concrete and concluded that high strength concrete (nominally compressive strength of 70Mpa at 28-day) and fiber-reinforced concrete (Poly Propylene fibers of 2kg/m^3) had no obvious effect or appears to be minimal (Figure 2.7) on the behaviors. However, fire duration time (Figure 2.8), cross-sectional diameter and slenderness ratio (Figure 2.9) have significant influence to the residual load capacity or RSI of post-fire CFST columns (Yao & Hu, 2015). Other parameters, such as steel ratio, load eccentricity ratio, width-to-depth ratio, have moderate influence on RSI.

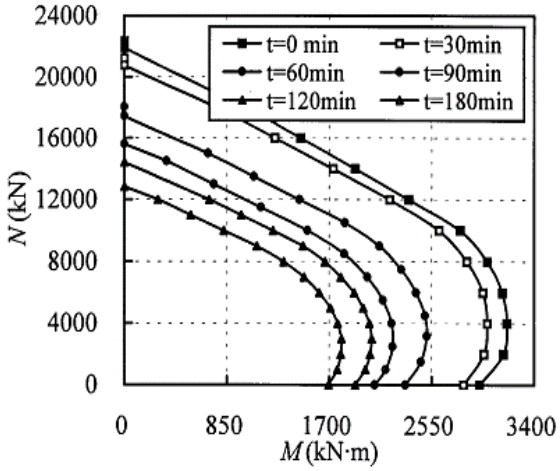

Figure 2.8 Influence of time duration on tube 600x600x14 (Yao & Hu, 2015)

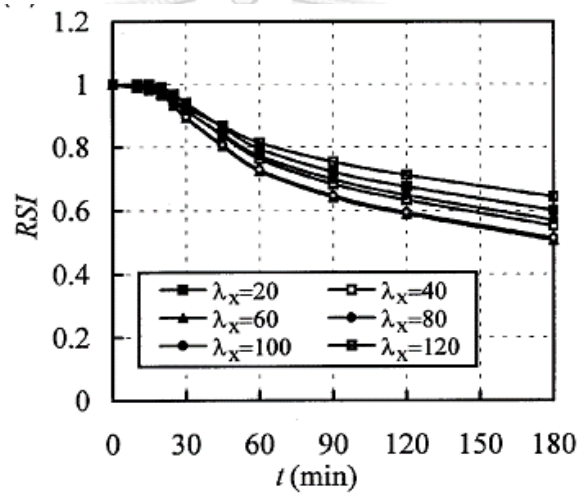

Figure 2.9 Influence of slenderness ratio (Yao & Hu, 2015)

The type of fire (Figure 2.10) is also important for the effect toward the behaviors of CFST columns. Rush et al. (2015) conducted an experiment with ISO-834 standard fire and smouldering fire and revealed that there were no obvious different effects on RSI (Figure 2.11). There is slight difference in the peak temperature between two types of fire exposure (regardless of the section shape). However, Yao and Hu (2015) based on the Fire Dynamics Simulator (FDS) concluded that behavior of the CFST columns under natural fire is different from traditional ISO-834 or ASTM-119 standard fire.

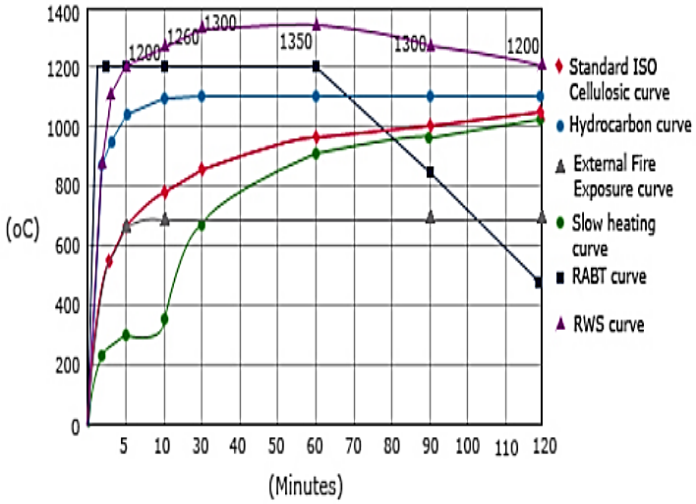

Figure 2.10 Different type of fire exposure curve (Source: http://www.sobhaprojects.com). Access on: 28 May 2018

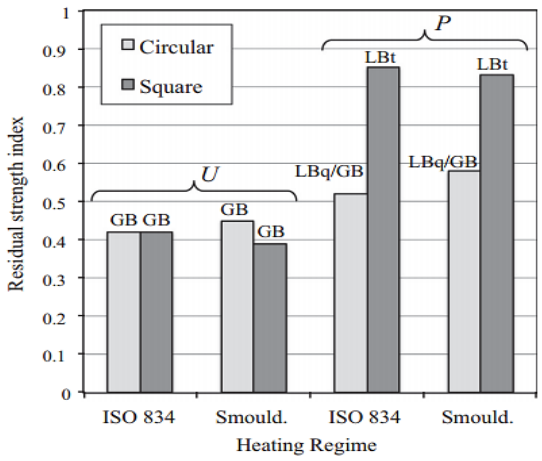

Figure 2.11 Effect of type of fire exposure on RSI (P: Protected by intumescent coating; U: unprotected; GB: failed by global buckling; LB: Local buckling; t: top; q: quarter height). (Rush et al., 2015)

Also by Rush et al. (2015), the fire evolution inside the concrete core by time were also performed. With the steel thickness of 10mm and 5mm in the 120mm diameter specimen, the reached temperature after 120 minutes under ISO-834 fire curve are 991°C, 979°C respectively for steel tube and 886°C, 841°C respectively for concrete core (measured by initial set-up thermometer). On the other hand, Milanović et al. (2016) proposed the ISO-834 fire evolution model for CFST columns

based on the SAFIR software with the certain cross sections (Figure 2.12) to predict level of temperature by time.

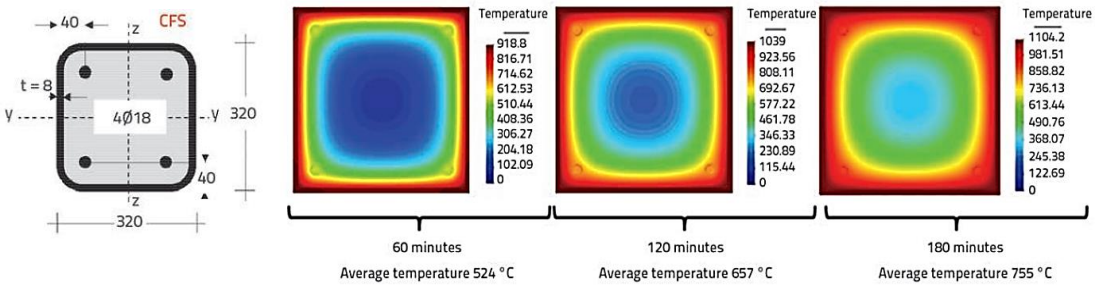

Figure 2.12 Predicted fire evolution by (Milanović et al., 2016)

When structures are exposed to fires, different methods are employed for cooling of the structures. Abbas et al. (2017) revealed that the annealing cooling method is slightly better than water-quenching for post-fire cooling of CFST columns. Water-quenching hardening slightly improves the strength of steel but relatively more damage caused to concrete because of the sudden escape of gases in water quenching. That is mainly responsible for more loss of strength as compared to the annealed columns. The result is similar comparing with the concrete columns (without steel tube) cooling method when the strength reduction in water quenching method is higher than air-cooled method (Lenwari et al., 2016). Abbas et al. (2017) revealed that the loss in residual load capacity of post-fire CFST is varying from 1.2% to 9.6%. This variation is because of the percentage of steel in columns (13.7% to 16.9%, herein experiment) which can be regained its strength and recovers portion of loss. Although the cooling methods affect the performance of post-fire CFST columns, studies have been limited in the available literatures.

2.3. Behavior of CFST columns confined by FRP wrapping

FRP has a variety of type that can be used widely. However, Carbon Fiber-Reinforced Polymer (CFRP) and Glass Fiber-Reinforced Polymer (GFRP) are the most popular applied in a major of civil engineering. Figure 2.13 shows a linear elastic stress-strain behavior of FRP composites before failure by rupture (Teng et al., 2012). For the strength enhancement, CFRP has the higher elastic modulus than GFRP. To enhance buckling resistance, the use of ultra-high modulus CFRP is more attractive.

In contrast, when ductility enhancement is the main aim, GFRP is more reasonable as it is cheaper, galvanic corrosion resistance, and offers a greater strain (>2%) (Teng et al., 2012).

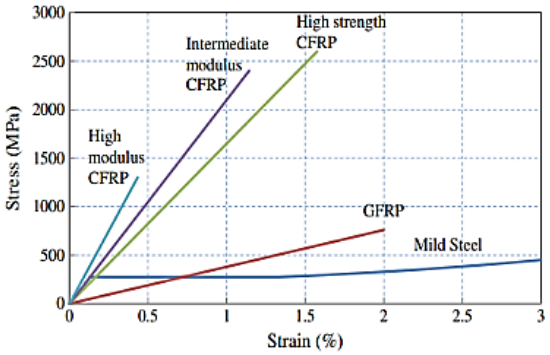

Figure 2.13 Typical FRP and mild stress-strain curves. (Teng et al., 2012)

Hu et al. (2011) conducted an experiment on FRP-confined CFST columns and observed that all specimens failed by explosive rupture of the FRP wrap in the midheight region as a result of the lateral expansion of the concrete, leading to a sudden and rapid load drop. The same result is also observed by Barrington et al. (2011). The study also revealed that hoop strains at failure may vary over the surface of a column. The values are higer than 57% of the coupon failure strain. Prabhu and Sundarraja (2013) conducted an experiment on square CFST columns with discontinous FRP strips (Figure 2.14). The outward buckling failure of unbonded region generally located at the bottom of the columns for 40mm strip spacing specimens and fiber rupture at the bottom for 30mm strip spacing specimens. However, the full wrapping arrangement of CFRP is much more effective than the partial wrapping for enhanching the load carrying capacity and stiffness of CFST columns (Dong et al., 2013).

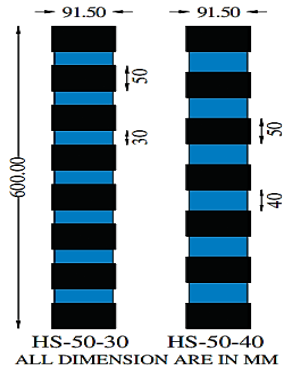

Figure 2.14 Prabhu's experiment specimens (Prabhu & Sundarraja, 2013)

The FRP confinement can be also applied on circular or square cross section of CFST columns. Tao et al. (2007b), with their experiments on both cross section geometries of FRP-confined CFST columns concluded the better performance with FRP wrapping of the circular columns than square ones. Tao et al. (2007b) also studied the compression behavior of CFST columns confined by CFRP with a circular and rectangular cross-section. For the circular columns, when the number of CFRP increased, the load capacity increased, but the ductility decreased. For rectangular columns, with the increasing of the CFRP layer number, load capacity had no obvious changes, but the ductility was improved. Hu et al. (2011) revealed that, with the additional confinement, the load carrying capacity can be increased by 60%, whereas the axial shortening capacity can be increased by up to 153%. On the other hand, with the limited of available literature on square CFST columns confined by FRP, Prabhu and Sundarraja (2013) showed that with CFRP strips, the axial capacity of the square CFST columns can be increased up to 1.5 times.

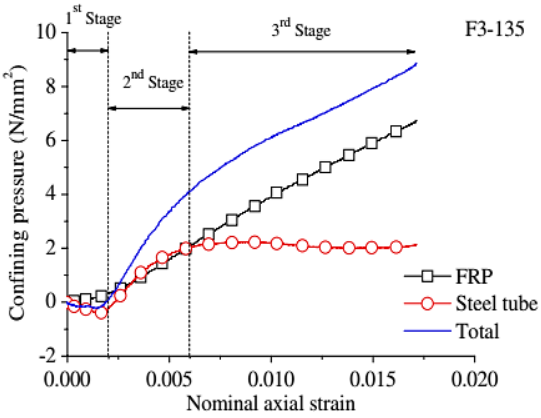

Figure 2.15 Confining pressure from FRP and steel in particular specimen. (Hu et al., 2011)

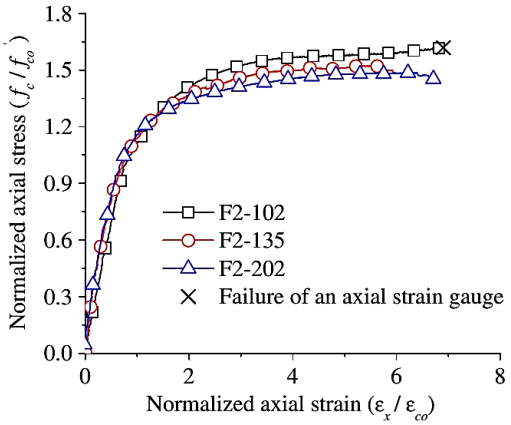

Figure 2.16 Effect of steel tube thickness on stress-strain behavior. (Hu et al., 2011)

Hu et al. (2011) proposed that the development of confining pressures can be divided into three stages (Figure 2.15). To clarify the effect of the steel tube thickness or diameter-to-thickness ratio (D/t) on the compression behavior, Hu et al. (2011) conducted an experiment with different D/t ratios (102, 135, 202) and concluded that specimens with a thicker steel tube generally have a greater confinement, just due to the steel tube confining effect. The role of CFRP confinement effect, otherwise, are similar in all groups (Figure 2.16) with the linear portion attribution in third stage (steel tube confining pressure is constant at this stage). The same conclusion was given by Lu et al. (2014). When the thickness of steel tube increased, the ultimate load increased. However, increasing the steel tube thickness had no obvious effect on the axial shortening at the ultimate load (Figure 2.17). In terms of confined concrete filled in thin wall steel tube, Hu et al. (2011) revealed that the FRP wraps are highly effective in improving the axial compressive behavior for both load-carrying capacity and ductility (Figure 2.18).

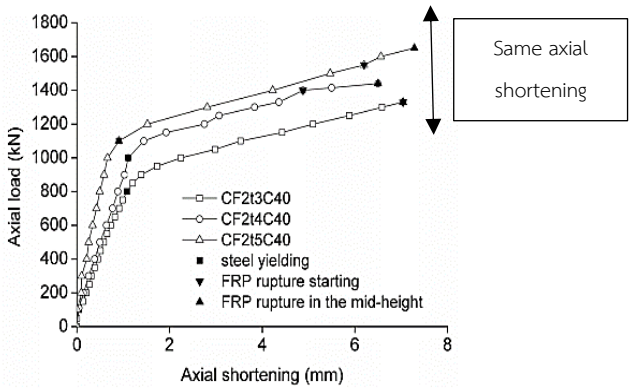

Figure 2.17 Lu's experiment results. (Lu et al., 2014)

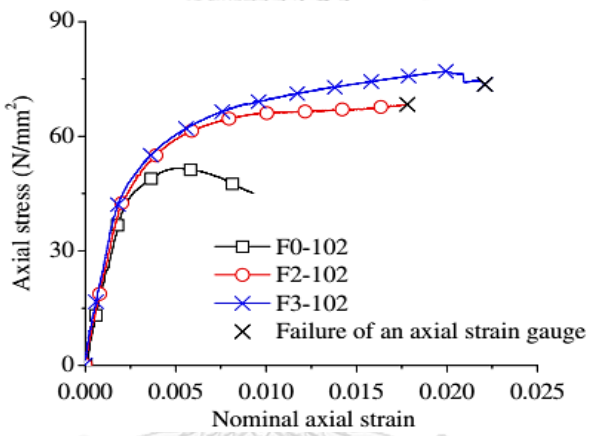

Figure 2.18 Axial stress-strain curves of confined concrete in thin wall CFST columns (D/t=102). (Hu, Yu, & Teng, 2011)

The strength of concrete also affects the compression behaviors of FRP-confined CFST columns. Lu et al. (2014) concluded that the ultimate load and the axial shortening at the ultimate load increased slightly when the concrete strength increased. Besides, Dong et al. (2013)'s experiment results showed that the ultimate loads of CFST columns filled with recycle aggregate concrete were comparable to ones filled with normal concrete after the 90-day curing period and similar compressive strength.

Beside the use of CFRP wrapping, GFRP wrapping was also used to enhance the load capacity and ductility of CFST columns. Some reasons are: GFRP can keep CFST column avoid suffering from galvanic corrosion problems, that might be a problem for CFRP directly bonded to steel, large ultimate strain which suitable for

ductility enhancement (Hu et al., 2011). Hu et al. (2011) also conducted an experiment and concluded that, GFRP is highly effective in enhanching the axial compressive behavior of CFST in terms of both load-carrying and ductility. The effect of FRP wraps is also more effective for CFST with thinner steel tube. The stiffness (elastic modulus) is also improved slightly (Ravindran & Hameed, 2016).

2.4. Behavior of fire-damaged CFST columns confined by FRP wrapping

Until now, there has been a very limited research works on the behavior of post-fire CFST columns strengthened by FRP confinement. Tao et al. (2007a) conducted an experiment with the ISO 834 standard fire and observed that the steel tube buckled first at 60% of the ultimate load, followed by a sudden failure as a result of the rupture of CFRP jackets at mid-height. Shahidan et al. (2016)'s experiment, with the ASTM-E119 standard fire, had the similar results and even observed the rupture not only on mid-height but also near top and bottom of specimens. Wang et al. (2018) conducted an experiment on twenty-one circular CFST short columns. Test variables are temperature levels and number of CFRP layers. The temperature levels are 600, 800, 1000 and 1100°C for one hour. It was concluded that, all of specimens experienced rupture of CFRP sheet and buckling of steel tube. The failure modes varied as the exposure temperature and the number of CFRP layers change (4 modes).

The strength enhancement was also studied by those studies. Tao et al. (2007a), with the enhancement indicated by SEI (Strength Enhancement Index), had the results of enhance percentage varied from 11.7% to 70.9% for either circular or square specimens (Figure 2.19). However, it is noted that the strengths of all damaged specimens have not been fully. On the other hand, Shahidan et al. (2016) concluded that wrapping more than one layer of FRP for severe fire-damaged specimens yielded result similar to specimens repaired with single layer of FRP (Figure 2.20). In Wang et al. (2018)'s experiment, the distintive improvements were indicated by 62.41%, 43.83%, 85.47%, and 64.38% when the 4-CFRP layer (thickness of 0.167mm per layer) specimens subjected to temperature levels of 600, 800, 1000, 1100°C, respectively.

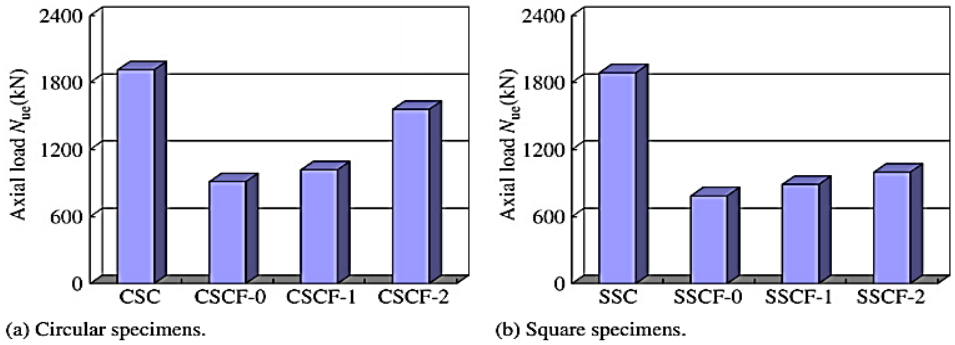

Figure 2.19 Tao's experimental results in ultimate load (Tao et al., 2007a)

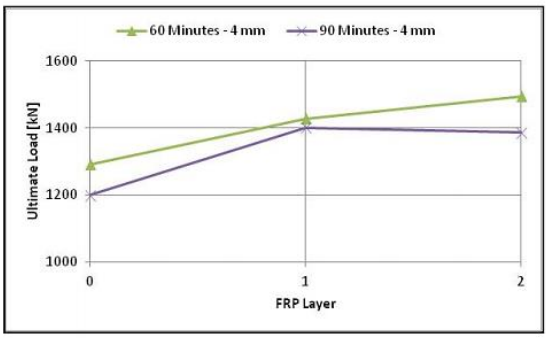

Figure 2.20 Effect of FRP on ultimate load. (Shahidan et al., 2016)

In spite of having the excellent deformation resistance after being strengthened with CFRP sheets, the ductility deteriorated with the increase of the number of CFRP layers (Wang et al., 2018). It can be explained that all strains of measuring points on the external surface of steel tubes go into the plastic range. The research also showed that the measured strains on the CFRP surface are gennerally higher than the ones on the surface of steel tube (Figure 2.21). Tao et al. (2007a)'s experiment also provided the same results that the ductility of the specimens decreases with the increasing number of CFRP layers (Figure 2.22). It was explained by the attribution of the abrupt rupture of CFRP jackets. The more CFRP jacket used, the more abrupt the failure.

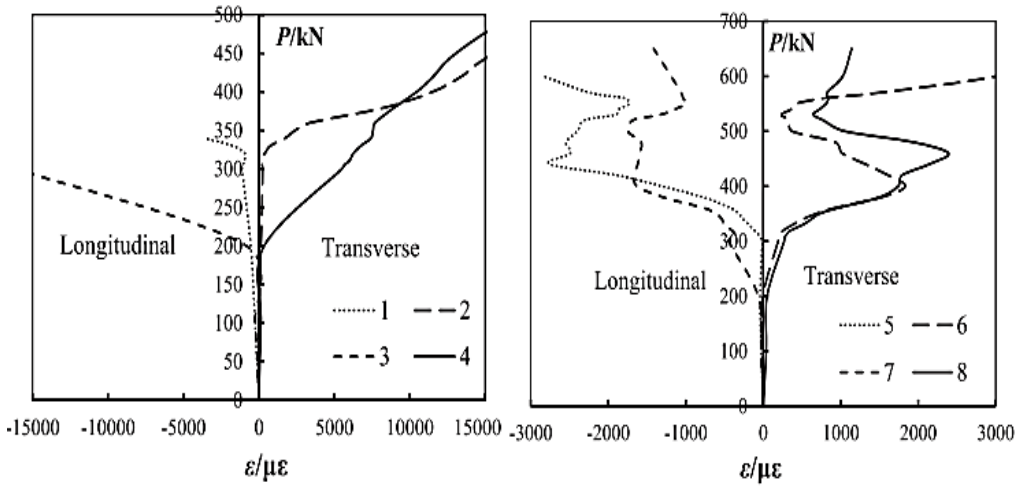

Figure 2.21 Axial strain-load curves of specimens exposed to 800°C and 1 CFRP layer; (1-4: Strain gauge on CFRP surface; 5-8: Strain gauge on steel surface). (Wang et al., 2018)

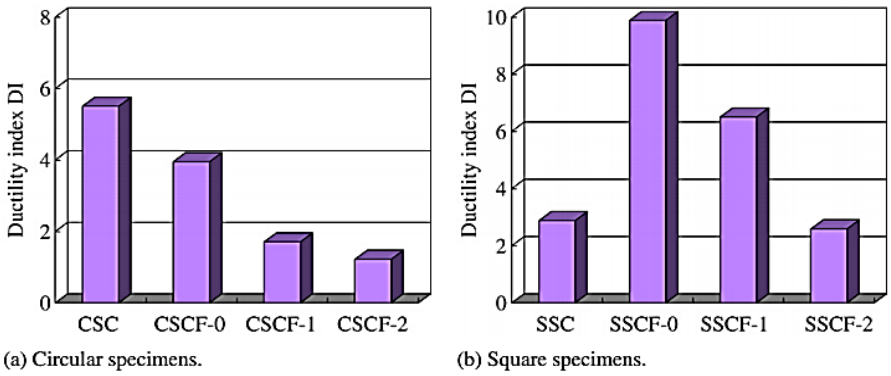

Figure 2.22 Ductility of specimens in Tao's experiment. (Tao et al., 2007a)

It is a primary importance in the surface preparation before wrapping CFRP into steel surface. In the available experiments on the FRP confine the post-fire CFST columns, it was not mentioned in details about the steps to prepare after fire exposure and before bonding. Tao et al. (2007a) just went directly to wrap CFRP by hand lay-up method with the sheet overlapped the starting end by 150 mm. Wang et al. (2018) tried to fully remove the contaminating practices by scrupulously polishing and degreasing methods. For the square geometry, the rounded corner shape specimens should be used to reduce the decrease in strength and to prevent

the tearing of the CFRP sheets. As can be observed from Tao et al. (2007a)'s experiment results, the failure of square specimens were the CFRP rupture at the corner even it was designed to have the overlapping wrap at this location (Figure 2.23). Teng et al. (2012) mentioned on two existing approaches of steel surface treatment as known as chemical bonding and mechanical bonding. However, the most popular approach is combined one that includes solvent cleaning and then mechanical abrasion. Another deep study on effective bonding by Teng et al. (2011) revealed that grit-blasting prior to bonding is the most effective approach to avoid adhesion failure.

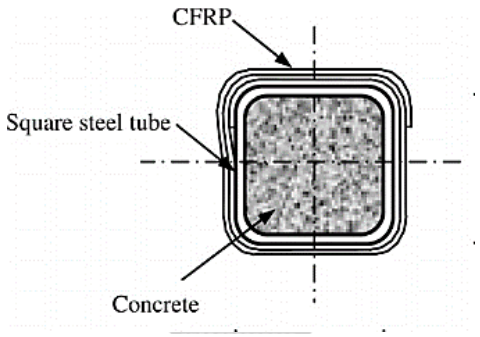

Figure 2.23 Square CFST experimental specimen (Tao et al., 2007a)

The use of FRP wraps to strengthen fire-damaged CFST columns expose may be an effective and economic advantages. However, limited research has been reported and lack of study related to the effective enhancement by FRP for between fire-damaged normal strength CFST (NSCFST) and high strength CFST (HSCFST). Besides, the implement of GFRP's advantage in ductility enhancement has not been much concerned although there are the disadvantages in previous studies when using CFRP that, the more CFRP layers, the ductility is easier to be deteriorated.

CHAPTER 3

THEORETICAL BACKGROUND

3.1. Heat transfer analysis (Ding & Wang, 2008)

Ding and Wang (2008) employed the commercial finite element model ANSYS to analyze the heat transfer and thermal behavior of CFST columns in fire. Because of the length of a column is assumed to be uniform, the temperature distribution within column is performed by 2D model for the cross-section. The 2-D solid thermal element PLANE55 was used to mesh the cross-section of the CFST columns (Figure 3.1), the surface is simulated by a layer of element SURF151. SURF151 is a 2-D surface element, adopted to perform the effect of thermal convection and radiation from surrounding environment to the section surface.

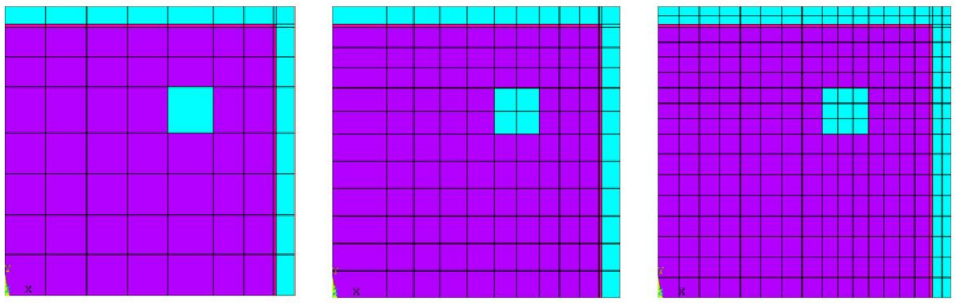

Figure 3.1 2-D solid element mesh of cross-section (Ding & Wang, 2008)

The results of this model are shown in Figure 3.2 by with points in different positions and types of mesh (mesh A to C in the order of “coarse” increase in mesh).

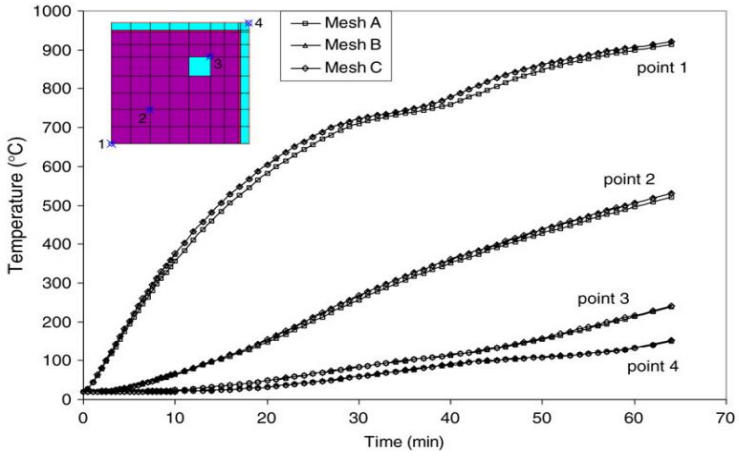

Figure 3.2 Results of model between points and mesh (Ding & Wang, 2008)

3.2. Compressive strength equations for CFST columns

3.2.1 Eurocode-4: Design of composite steel and concrete structures

The plastic resistance of concrete-filled composite section $(N_{pl,Rd})$ is calculated by adding the resistance of constituent steel and concrete materials as follows,

$$N_{pl,Rd} = A_s f_y + A_c f_c \tag{3.1}$$

where

A_s, A_c are area of steel tube and concrete.

f_y, f_c are yield strength of steel and compressive strength of concrete.

Note that square and rectangular tubes offer little confinement because the walls in these tubes resist the concrete pressure by plate bending, instead of generated hoop stress in circular section (Ekmekyapar & Al-Eliwi, 2016). For circular columns, EC4 presents the following formulation which also incorporates the confinement effect

$$N_{pl,Rd} = \eta_a A_s f_y + A_c f_c \left(1 + \eta_c \frac{t}{D}\frac{f_y}{f_c}\right) \tag{3.2}$$

where

Steel reduction factor η_a and concrete enhancement factor η_c

$$\eta_a = 0.25(3 + 2\lambda) \leq 1.0$$

$$\eta_c = 4.9 - 18.5\lambda + 17\lambda^2 \geq 0$$

λ is relative slenderness ratio

$$\lambda = \sqrt{\frac{N_{pl,Rd}}{N_{cr}}}$$

N_{cr} is the Euler critical load

$$N_{cr} = \frac{\pi^2 (EI)_e}{L^2}$$

$(EI)_e$ refers to the effective stiffness of member

$$(EI)_e = E_s I_S + K_e E_c I_c$$

E_s, E_c are the elastic modulus of steel and concrete.

K_e is a correction factor (0.6).

3.2.2 AISC 360-16: Specification for Structural Steel Buildings

For axially loaded CFST columns, AISC 360-16 calculates the compressive load capacity based on slenderness of member are as follows,

$$P_n = P_{n0}\left(0.658^{\frac{P_{n0}}{P_e}}\right) \qquad \frac{P_{n0}}{P_e} \leq 2.25 \qquad (3.3)$$

$$P_n = 0.877P_e \qquad \frac{P_{n0}}{P_e} > 2.25$$

where

$P_e = \pi^2(EI_{eff}) \,/\, L_c^2$ is elastic critical buckling load.

$P_{n0} = P_p$ for compact section CFST (used in this research)

$$P_p = F_y A_s + C_2 f'_c\left(A_c + A_{sr}\frac{E_s}{E_c}\right) \qquad (3.4)$$

$C_2 = 0.85$ for rectangular sections.

$C_2 = 0.95$ for round sections.

$EI_{eff} = E_s I_s + E_s I_{sr} + C_3 E_c I_c$ is the effective stiffness of composite section.

$C_3 = 0.45 + 3\left(\frac{A_s + A_{sr}}{A_g}\right) \leq 0.9$ is coefficient for calculation of effective rigidity of filled composite.

I_s is moment of inertia of steel shape about the elastic neutral axis of the composite section.

I_{sr} is moment of inertia of reinforcing bars about the elastic neutral axis of the composite section.

I_c is moment of inertia of the concrete section about the elastic neutral axis of the composite section.

f'_c is specified compressive strength of concrete.

Ekmekyapar and Al-Eliwi (2016) revealed that as the column's slenderness increases predictions of EC4 and AISC 360-16 became closer. Although both codes provide conservative results beyond a relative slenderness of 1.0, AISC performs a little better and has predictions closer to their test results.

3.3. Compressive strength models of fire-damaged CFST columns

In this section, models and approaches to estimate the residual strength of concrete and CFST columns after fire exposure are introduced:

3.2.1 Residual material properties of CFST columns after exposure to high temperature (Han & Huo, 2003)

The residual yielding strength of steel $f_{sy}(T)$ after exposure to high temperature T is as follow,

$$f_{sy}(T) = \begin{cases} f_{sy} & T \leq 400°C \\ f_{sy}.[1 + 2.33 \times 10^{-4}(T - 20) - 5.88 \times 10^{-7}(T - 20)^2] & T > 400°C \end{cases} \quad (3.5)$$

The residual compressive strength of confined concrete $\sigma_0(T)$ and corresponding strain $\varepsilon_{cc}(T)$ after heated to temperature T and then cooled down to the ambient temperature of 20°C are

$$\sigma_0(T) = \frac{\sigma_0}{1 + 2.4(T - 20)^6 \times 10^{-17}} \quad (3.6)$$

$$\varepsilon_{cc}(T) = [1 + (1500 \times T + 5 \times T^2) \times 10^{-16}]\varepsilon_{cc} \quad (3.7)$$

where σ_0 and ε_{cc} are the compressive strength and corresponding strain at the ambient condition, respectively.

3.2.2 Simplified approach for fire-damaged CFST columns by Yao and Hu (2015)

This approach involves the following steps

a. Estimation of the maximum temperatures

The temperatures are measured directly by the maximum temperature of the furnace or obtained from equivalent temperature based on the finite element analysis

b. Estimation of the residual strength of steel tube and core concrete

Generally, steel can recover its strength after cooling down. However, the higher the maximum temperature attained in steel, the lower steel residual strength

is. The relationship between steel residual strength ratio and maximum temperature was proposed as shown in (Figure 3.3)

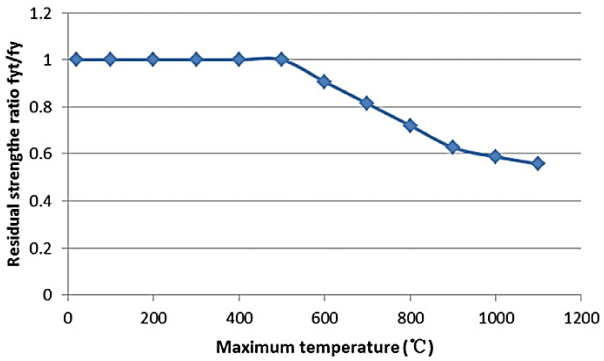

Figure 3.3 Residual strength ratio versus temperature of steel (Yao & Hu, 2015)

Figure 3.4 shows the residual strength ratio of variety types of concrete. The strength of concrete cannot recover when temperature exceeds 200°C.

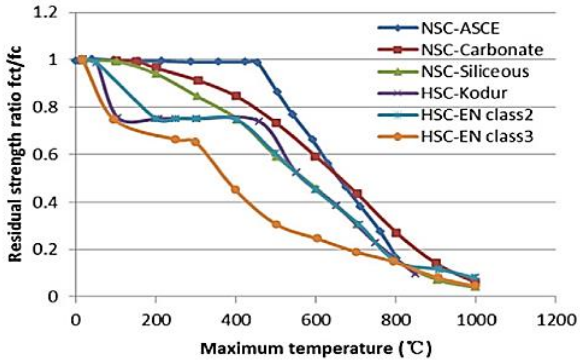

Figure 3.4 Strength ratio versus temperature of concrete (Yao & Hu, 2015)

The residual compressive strength f'_{cr}, corresponding peak strain ε_{or}, and residual elastic modulus of unconfined concrete after heated to temperature T (up to 800°C) can be also obtained by (Chang et al., 2006)

$$f'_{cr}/f'_c = \begin{cases} 1.01 - 0.00055T & 20°C \le T \le 200°C \\ 1.15 - 0.00125T & 200°C \le T \le 800°C \end{cases} \quad (3.8)$$

$$\varepsilon_{or}/\varepsilon_o = \begin{cases} 1.00 & 20°C \le T \le 200°C \\ (-0.1f'_c + 7.7)\left[\frac{\exp(-5.8 + 0.01T)}{1 + \exp(-5.8 + 0.1T)} - 0.0219\right] + 1.0 & 200°C \le T \le 800°C \end{cases} \quad (3.9)$$

$$E_{cr}/E_c = \begin{cases} -0.00165T + 1.033 & 20°C \le T \le 125°C \\ \frac{1}{1.2 + 18(0.0015T)^{4.5}} & 125°C \le T \le 800°C \end{cases} \quad (3.10)$$

where f'_c, ε_o and E_c are the compressive strength, corresponding strain and elastic modulus at the ambient condition, respectively.

Another formula proposed by Du et al. (2014) to calculate the relative compressive strength for polypropylene fiber reinforced concrete is

$$\frac{f_{cu}^T}{f_{cu}} = 0.25 + \frac{0.76}{1 + \left(\frac{T}{545}\right)^{2.57}} \qquad 20°C \le T \le 1000°C \quad (3.11)$$

c. Computation of the residual load capacity of post-fire CFST columns

The residual capacity of CFST columns could be estimated by applying the design equations under ambient conditions as recommended in the Eurocode and ACI code as follows,

$$N_r = A_c f_{ct} + k_{st} A_s f_{yt} \quad (3.12)$$

where N_r is the residual strength of post-fire CFST columns, A_c is the area of concrete cross-section, A_s is the area of steel tube cross-section, k_{st} is the reduction coefficient due to the spalling of concrete (assumed to be 1 for CFST columns), f_{ct} and f_{yt} is the residual strength of concrete and steel measured by above steps.

Some limitations of the proposed approach are summarized as follows: Columns slenderness ratio $\lambda \le 90$; cross area $0.02\ m^2 \le A_c \le 0.16\ m^2$.

Validation of Yao and Hu (2015)'s approach was by comparing predictions with the test results. Mean value of **0.913** and COV of **0.126** was obtained.

3.3. Compressive strength models for CFST columns confined by CFRP sheets

This section introduces available models to predict the compressive behavior of FRP-confined CFST columns.

3.3.1 Prediction model by Tao et al. (2007b)

The strength of FRP-confined CFST columns, N_u is proposed to be

$$N_u = (1 + 1.02\xi_s)f_c' A_{sc} + 1.15\xi_{frp} f_c' A_c \quad (3.13)$$

where

$\xi_s = A_s f_y / A_c f_c'$ is confinement factor between steel tube and concrete core.

$\xi_{frp} = A_{frp} f_{frp} / A_c f_c'$ is confinement factor between concrete core and CFRP jacket.

A_s, A_{frp}, A_c are the cross-sectional areas of steel tube, CFRP jacket and core concrete, respectively.

The ultimate loads (N_{uc}) obtained from above equations were compared with the experimental values (N_{ue}). It was shown that the mean ratio (N_{uc}/N_{ue}) and COV (coefficient of variation) are **0.839** and **0.037**.

Limitations: Equations are based on the experiment of the CFST columns with height of 450mm and 750mm; the dimensions are 150mm, 250mm for circular CFST columns and 100x250mm for rectangular CFST columns. The steel tube has the thickness of 3mm and yield strength of 337 MPa. The compressive strength of infill concrete at 28-day is 46 MPa. CFRP with the thickness of 0.17mm is used.

3.3.2 Prediction model by Liu and Lu (2010)

The load bearing capacity of FRP-confined CFST columns is expressed as:

$$N_u = A f_c A_c + B f_y A_s + 0.5 k_f f_f A_f \quad (3.14)$$

where

f_c is axial compressive strength of unconfined concrete.

f_y is yield strength of steel.

f_f is transverse tensile strength of CFRP.

k_f is effective confinement coefficient suggested for CFRP are 0.7, 0.68, 0.59 for concrete strength are C40, C50, and C60, respectively.

k_s is stress efficient coefficient suggested for CFST=0.52, CFST wrapped CFRP=0.3.

A_s, A_f, A_c are cross-sectional areas of the steel tube, CFRP jacket, and the core concrete, respectively.

$$A = \frac{1}{2m_c} + \sqrt{\left(1 - \frac{1}{2m_c}\right)^2 + \alpha_1(m_c - 1)}$$

$m_c = \frac{f_c}{f_t}$ with f_t is the concrete tensile strength.

$\alpha_1 = (0.5k_s\xi_s + 0.5k_f\xi_f)$

$\xi_s = A_s f_y / A_c f_c$ is coefficient factor of steel tube.

$\xi_f = A_f f_{fu} / A_c f_c$ is coefficient factor of CFRP wrap.

$B = 0.5\sqrt{4 - 3k_s^2}$

To validate the calculation method for bearing capacity of CFRP-CFST columns, a comparison between calculated results and test results are shown. The mean ratio value of **1.028** is obtained with a COV of **0.020**.

Limitations: Equations are based on the experiment of the circular CFST short columns with height of 400mm; diameter is 120mm. The steel tube has the thickness of 3mm, 4mm and 5mm with the yield strength of 248 MPa. The compressive strength of infill concrete at 28-day is 44.9 MPa. The tensile strength of CFRP sheets and GFRP sheets are 3550 MPa and 2930 MPa, respectively.

3.3.3 Prediction model by Lu et al. (2014)

The load capacity of CFRP-confined CFST columns depends on strength contributions of the steel tube (N_s), concrete core (N_c), unconfined concrete strength (N_{c0}), and strength enhancement by steel tube confinement (N_{cs}), the strength enhancement by FRP confinement for unconfined concrete (N_{cf})

$$N_u = N_s + N_{c0} + N_{cs} + N_{cf}, \text{ or}$$
$$N_u = (1 + 1.8\xi_s + 1.15\xi_f) f_c A_c \quad (3.15)$$

where

$\xi_s = A_s f_y / A_c f_c$ is coefficient factor of steel tube.

$\xi_f = A_f f_{fu} / A_c f_c$ is coefficient factor of CFRP wrap.

f_c is axial compressive of concrete without confinement.

The mean ratio value of **1.025** is obtained with a COV of **0.026**.

Limitations: Equations are based on the experiment of the circular CFST short columns with height of 400mm; length-to-diameter ratios range between 3.0 and 3.5. The steel tube has the thickness of 3mm, 4mm and 5mm and yield strength of 248 MPa. The compressive strength of infill concrete at 28-day are 40 MPa, 50 MPa and 60 MPa. CFRP with the thickness of 0.17mm and tensile strength of 3550 MPa, GFRP with the thickness of 0.169mm and tensile strength of 2930 MPa, are used.

3.4. Theoretical axial stress-strain model for circular FRP-confined CFST columns (Lai & Ho, 2016)

A perfect bonding between the concrete and steel is assumed. Therefore,

$$\varepsilon_{cz} = \varepsilon_{sz} = \varepsilon_z$$
$$\varepsilon_{c\theta} = \varepsilon_{s\theta} = \varepsilon_\theta \quad (3.16)$$

where:

ε_{cz} and ε_{sz} are the axial strains of the concrete and steel tube.

$\varepsilon_{c\theta}$ and $\varepsilon_{s\theta}$ are the hoop strains of the concrete and steel tube.

ε_z and ε_θ are the axial and hoop strains of the CFST column.

The relationship between axial strain and hoop strain is

$$\varepsilon_z = LS\left(\frac{f_{cp}}{30}\right)^m \left\{ \varepsilon_{cp}\left[1 + 0.75\left(\frac{-\varepsilon_\theta}{\varepsilon_{cp}}\right)\right]^{0.7} - \varepsilon_{cp}\exp\left[7\left(\frac{\varepsilon_\theta}{\varepsilon_{cp}}\right)\right] + 0.07(-\varepsilon_\theta)^{0.7}\left[1 + 26.8\left(\frac{f_r}{f_{cp}}\right)\right]\right\} \quad (3.17)$$

where

$\mathrm{LS} = \frac{\mathrm{LS_2}-\mathrm{LS_1}}{\mathrm{H}-\mathrm{d}}(\mathrm{S}-\mathrm{d}) + \mathrm{LS_1}$ is the parameter reflecting the effect of external confinement, $\mathrm{LS_2} = 0.6466$ for unconfined CFST columns and $\mathrm{LS_1} = 0.6650$ for FRP-confined CFST columns.

m is the parameter considering effect of concrete strength as follow,

$$\mathrm{m} = \begin{cases} 0 & \mathrm{f_{cp}} \leq 30 \\ -0.05 & \mathrm{f_{cp}} > 30 \end{cases} \quad (3.18)$$

S is the center-to-center spacing of external confinements; d is diameter of external confinement; H is the total height of specimen. In this case, $\mathrm{S} = \mathrm{d}$.

$\mathrm{f_r}$ is the confining pressure from steel tube to the confined concrete.

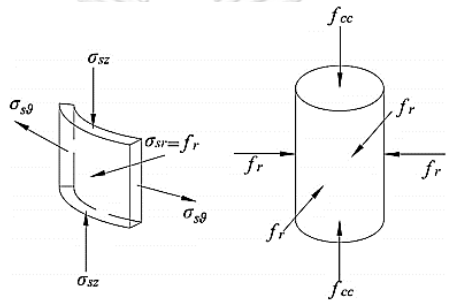

Figure 3.5 Stress state of steel tube and concrete (Lai & Ho, 2016)

In the confined CFST column, the core concrete is confined by both steel tube and external confinement (FRP wrap). Thus, $\mathrm{f_r}$ is equal to the sum of the confining stress from the steel tube $(\mathrm{f_{rs}})$ and external confinement $(\mathrm{f_{rE}})$ as follows

$$\mathrm{f_r} = \mathrm{f_{rs}} + \mathrm{f_{rE}} \quad (3.19)$$

where

$\mathrm{f_{rs}}$ is the confining stress from steel tube

$$\mathrm{f_{rs}} = -\frac{2\mathrm{t}}{\mathrm{D_0} - 2\mathrm{t}}\sigma_{\mathrm{s\theta}} \quad (3.20)$$

$\mathrm{f_{rE}}$ is the confining stress from external confinement

$$\mathrm{f_{rE}} = -\frac{2\mathrm{t_{FRP}}}{\mathrm{D_0} - 2\mathrm{t}}\sigma_{\mathrm{E}} \quad (3.21)$$

$\sigma_{\mathrm{s\theta}}$ is the hoop stress provided by steel tube; $\mathrm{t_{FRP}}$ is the thickness of FRP wrap. σ_{E} is the stress provided by external confinement (FRP); $\varepsilon_{\mathrm{ssE}}$, $\mathrm{E_{ssE}}$, σ_{ssE}

are the average hoop strain, elastic modulus and yield stress of FRP respectively.

σ_E is the stress provided by FRP

$$\sigma_E = \begin{cases} \varepsilon_{ssE} E_{ssE} & E_{ssE} \le \sigma_{ssE} \\ \varepsilon_{ssE} \sigma_{ssE} & E_{ssE} > \sigma_{ssE} \end{cases} \quad (3.22)$$

The three-dimensional stress-strain relationship of the steel tube can be evaluated using the hoop-axial strain relationships from Prandtl-Reuss theory (Eringen, 1983). However, for CFST with thin-walled steel tube, it is able to ignore the small radial stress (σ_{sR}) of the steel tube. Therefore, the steel tube stress can be assumed to be in plane stress. The 2-dimensional hoop-axial strain relationships (incremental form) are given by

Elastic stage:

$$\begin{Bmatrix} d\sigma_{sz}^{i} \\ d\sigma_{s\theta}^{i} \end{Bmatrix} = \frac{E_s}{1-v_s} \begin{bmatrix} 1 & v_s \\ v_s & 1 \end{bmatrix} \begin{Bmatrix} d\varepsilon_{sz}^{i} \\ d\varepsilon_{s\theta}^{i} \end{Bmatrix} \quad (3.23)$$

Plastic stage:

$$\begin{Bmatrix} d\sigma_{sz}^{i} \\ d\sigma_{s\theta}^{i} \end{Bmatrix} = \frac{E_s}{S_z^2 + S_\theta^2 + 2v_s S_z S_\theta} \begin{bmatrix} S_\theta^2 & -S_z S_\theta \\ -S_z S_\theta & S_z^2 \end{bmatrix} \begin{Bmatrix} d\varepsilon_{sz}^{i} \\ d\varepsilon_{s\theta}^{i} \end{Bmatrix} \quad (3.24)$$

where

$$S_z = \frac{1}{3}(2\sigma_{sz}^{i-1} - \sigma_{s\theta}^{i-1}) \quad (3.25)$$

$$S_\theta = \frac{1}{3}(2\sigma_{s\theta}^{i-1} - \sigma_{sz}^{i-1}) \quad (3.26)$$

The von Mises yield criterion is used for the steel tube

$$\sigma_{sz}^2 - \sigma_{sz}\sigma_{s\theta} + \sigma_{s\theta}^2 = \sigma_{sy}^2 \quad (3.27)$$

Axial load of the CFST column is

$$F_t = F_c + F_s \quad (3.28)$$

$$F_c = f_{cc} A_c \quad (3.29)$$

$$F_s = \sigma_{sz} A_s \quad (3.30)$$

where

A_s and A_c are areas of steel tube and confined concrete.

σ_{sz} is the axial stress of steel tube.

f_{cc} is the confined fire-damaged concrete stress, f_{ccp} and ε_{cc} are the confined peak concrete stress and the corresponding axial strain of concrete under a constant confining pressure f_r, calculated as below

$$\frac{f_{cc}}{f_{ccp}} = \frac{A\left(\frac{\varepsilon_z}{\varepsilon_{cc}}\right) + B\left(\frac{\varepsilon_z}{\varepsilon_{cc}}\right)^2}{1 + (A-2)\left(\frac{\varepsilon_z}{\varepsilon_{cc}}\right) + (B-1)\left(\frac{\varepsilon_z}{\varepsilon_{cc}}\right)^2} \tag{3.31}$$

$$\varepsilon_{cc} = \varepsilon_{cp}\left[1 + \frac{(17 - 0.06f_{cp})f_r}{f_{cp}}\right] \tag{3.32}$$

$$\frac{f_{ccp}}{f_{cp}} = 1 + 4.1\left(\frac{f_r}{f_{cp}}\right) \tag{3.33}$$

where A and B are parameters that govern the shape of the stress-strain curve (Kwan et al., 2015), Appendix A.

3.5. Compressive strength equation for fire-damaged concrete columns and CFST columns confined with FRP sheets

There are limited available models to predict the ultimate strength of the FRP-confined fire-damaged CFST columns.

3.4.1 Compressive strength of FRP-confined fire-damaged concrete columns (Lenwari et al., 2016)

The ACI equations (ACI, 2008) were adopted to predict the compressive strength of FRP-confined fire-damaged concrete, $f'_{cc\theta}$ and corresponding strain $\varepsilon_{ccu\theta}$

$$f'_{cc\theta} = f'_{c\theta} + 3.3\varphi_f f_l \tag{3.34}$$

$$\varepsilon_{ccu\theta} = \varepsilon'_{c\theta}\left[1.50 + 12k_b\frac{f_l}{f'_{c\theta}}\left(\frac{\varepsilon_{fe}}{\varepsilon'_{c\theta}}\right)^{0.45}\right] \tag{3.35}$$

$\varphi_f = 0.95$ is FRP strength reduction factor.

f_l is maximum confinement pressure:

$$f_l = \frac{2E_f n t_f \varepsilon_{fe}}{D} \tag{3.36}$$

$f'_{c\theta}, \varepsilon'_{c\theta}$ are unconfined compressive strength and corresponding strain of fire-damaged concrete.

D is diameter of cross section.

E_f, t_f, n are elastic modulus, thickness and number of FRP sheet.

ε_{fe} is the effective strain in the FRP at failure

$$\varepsilon_{fe} = k_e \varepsilon_{fu} \tag{3.37}$$

$k_e = 0.55$ is strain efficiency factor.

ε_{fu} is design rupture strain of FRP.

$k_b = 1.00$ is efficiency factor for circular cross section.

With the verifications with the conducted experimental results, Lenwari et al. (2016) concluded that the ACI equations are less accurate to predict the compressive strength of FRP-confined fire-damaged concrete columns.

3.4.2 Compressive strength of FRP-confined fire-damaged CFST columns (Wang et al., 2018)

The proposed equation in this research is

$$N_u = K_r \times N_{u0} \tag{3.38}$$

where N_{u0} is the calculated ultimate strength of CFST specimens without heat treatment and CFRP strengthening

$$N_{u0} = A_{sc} \times f_{scy} \tag{3.39}$$

$$f_{scy} = (1.14 + 1.02\xi) \times f_{ck}$$

$$A_{sc} = A_s + A_c$$

$$\xi = \alpha \times f_y / f_{ck}$$

A_s, A_c are the cross-sectional areas of steel tube and concrete, respectively, f_y is the yield strength of steel tube, f_{ck} is the compressive strength of concrete, determined by 67% of the compressive strength (f_{cu}) of the cubic blocks.

K_r is the corrected coefficient

$$K_r = G(\beta) \times G(\gamma) \tag{3.40}$$

where $G(\beta)$ is the function of β, where β is the dimensionless CFRP layers coefficient. $G(\gamma)$ is the function of γ, where γ is the dimensionless temperature-coefficient. The definition of β and γ are shown as follows:

$$\beta = \frac{A_{frp} \times f_{frp}}{A_{sc} \times f_{scy}}; \gamma = \frac{T}{T_0} \tag{3.41}$$

T is the peak furnace temperature (°C), T_0 is the temperature of 20°C, A_{sc} and A_{frp} are the cross-sectional areas of CFST short columns and the cross-section area of CFRP sheets attached to the external surface of post-heated CFST specimens. f_{frp} is the tensile strength of CFRP sheets in the hoop direction, and f_{scy} is the compressive strength of the circular CFST short columns.

Finally, $G(\beta)$ and $G(\gamma)$ are defined to be

$$G(\beta) = 1.032 \times e^{0.242\beta}, \quad 0 \leq \beta \leq 1.080 \tag{3.42}$$

$$G(\gamma) = 0.86 \times [1.246 - 0.079 \times \log(20\gamma)], \quad 1 \leq \gamma \leq 55 \tag{3.43}$$

The mean ratio value of **1.033** is obtained with a COV of **0.014**. The limit of this approach is just for short term of fire exposure (1hr). It will be lack of accuracy when expose to longer period of time on fire (3hr).

Limitations: The equations are based on the experiment of short CFST columns (height of 250mm), circular section with diameter of 89mm. The yield strength of steel and compressive strength of infill concrete are 235 MPa and 30 MPa, respectively. Carbon-fibers (CFRP) sheets with the thickness of 0.167 mm are used. The levels of temperature are 600 °C, 800 °C, 1000 °C and 1100 °C and subjected in 1 hour. After the heating period, the specimens are cooled down by kept in a dry condition at ambient temperature.

CHAPTER 4

EXPERIMENTAL PROGRAM

The experimental program is divided into 4 main steps as shown in Figure 4.1:

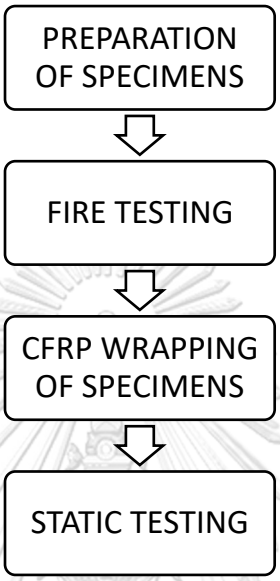

Figure 4.1 Experimental program steps

4.1. Preparation of test specimens

4.1.1 Material properties

All steel tubes were 300mm in height, Grade HS 41, (TIS 107). The ready-mix concretes have the designed compressive strength of 24 MPa for normal strength concrete (NSC) and 55 MPA for high strength concrete (HSC). CFRP and GFRP are SikaWrap®-230 C45 and SikaWrap®-430G, respectively, all materials are tested for mechanical properties as shown in **Table 4.1** to **Table 4.3**.

Table 4.1 Concrete and steel tube properties

Type	Grade/ Name	Tensile strength (Mpa)	Compressive strength (Mpa)		Elastic modulus (Mpa)	Test standard
			Nominal	Tested		
Steel	TIS 107-HS41	400 (yield)	n/a	n/a	201000	Nominal
Concrete	Normal Strength (NSC)	n/a	24	27.8	n/a	ASTM C39
	High Strength (HSC)	n/a	55	53.4	n/a	ASTM C39

Table 4.2 FRP properties (Data from Sika 430G and Sika wrap 230 C45 specifications)

Type	Grade/ Name	Thickness (mm)	Tensile strength (Mpa)	Strain at failure	Elastic modulus (Mpa)	Materials name
CFRP	SikaWrap® 230 C45	0.129	3500	1.7 %	238000	Carbon Fiber
GFRP	SikaWrap® 430G	0.170	2250	3.1 %	70000	Glass Fiber
Adhesive	Sikadur® 330	-	30 (7 days)	0.9 %	4500	Epoxy

Table 4.3 Fiber material properties (Coupon test – Appendix C)

Type	Grade/ Name	Thickness (mm)	Tensile strength (Mpa)	Strain at failure	Elastic modulus (Mpa)	Test standard	Remark
CFRP	SikaWrap® 230 C45	0.129	4279	0.9 %	276075	ASTM D3039	Failure at grip
GFRP	SikaWrap® 430G	0.170	3158	1.5 %	101855	ASTM D3039	Failure at grip

* Discuss that the material strength of FRP from specs is used instead of the coupon test data because there was a failure near grips.

4.1.2 Details of CFST specimens

A total of 38 circular CFST specimens were tested as shown in **Table 4.4**. The steel tube has the wall thickness of 2.5mm. All columns are 300 mm ($\pm$ 5mm) in height and has nominal diameter/size of 165 mm (Figure 4.2). Total of twenty (20) specimens were exposed to ISO-834 standard fire test for 2 hours. After fire exposure, the furnace was switched off and cooled down at ambient temperature in 14 hours. The specimens were then moved out the furnace and kept in a dry condition at ambient temperature for 1 month before confined with 0, 1 and 2 layers of CFRP and GFRP sheets. The similar series are conducted similar but no fire-damaged. The specimen designation starts with the nominal concrete compressive strength (55 or 21), next is the condition character of fire (F) and ambient (A), the next two characters are the wrap condition, CFRP (C) and GFRP (G), the last number is the number of specimens. For example, 55FCC-1 means the CFST column filled with HSC concrete (nominal 55MPa) in fire-damaged condition (F) and then wrapped with two layers of CFRP (CC).

To investigate the compressive strength of concrete, six standard cylinders with size of 150×300 cm were tested according to ASTM C39. Three specimens for HSC (nominal 55 MPa), three specimens for NSC (nominal 24 MPa). The results of concrete compressive strength tests in the ages of 122 days are shown in detail in Appendix B.

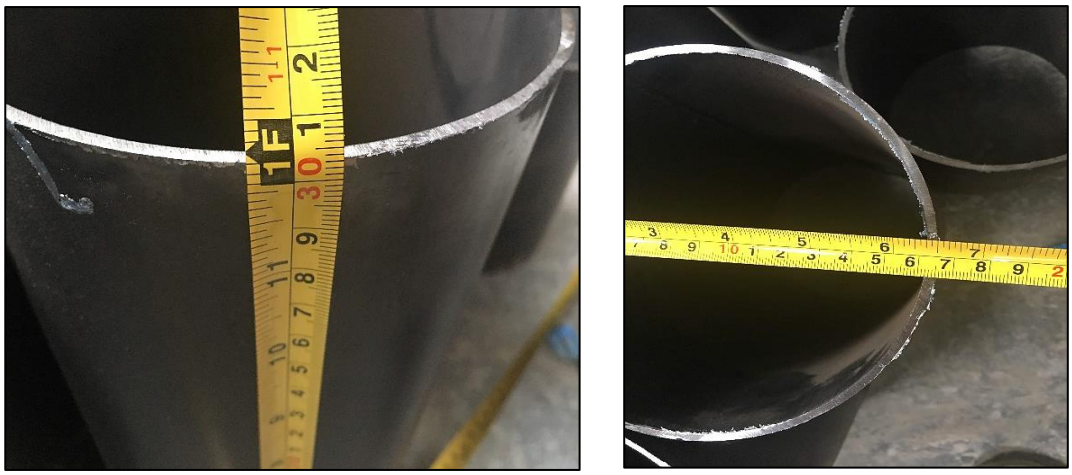

Figure 4.2 Measurement of steel tube's height and diameter

Table 4.4 Specimen details

No	Specimen group	Specimen	D x t_s (mm x mm)	L (mm)	f_y (Mpa)	f_c' (Mpa)	Heating	CFRP wrap (layer)	GFRP wrap (layer)	Specimen age at heating (days)	Specimen age at FRP wrap (days)	Specimen age at static test (days)
1	21A	1	165 x 2.5	300	400	27.8	-	-	-	-	-	121
		2	165 x 2.5	300	400	27.8	-	-	-	-	-	121
2	21AC	1	165 x 2.5	300	400	27.8	-	1	-	-	100	120
		2	165 x 2.5	300	400	27.8	-	1	-	-	100	121
3	21AG	1	165 x 2.5	300	400	27.8	-	-	1	-	100	121
4	21ACC	1	165 x 2.5	300	400	27.8	-	2	-	-	100	120
		2	165 x 2.5	300	400	27.8	-	2	-	-	100	121
5	21AGC	1	165 x 2.5	300	400	27.8	-	1	1	-	100	121
		2	165 x 2.5	300	400	27.8	-	1	1	-	100	121
6	21F	1	165 x 2.5	300	400	27.8	ISO-2 hour	-	-	72	-	121
		2	165 x 2.5	300	400	27.8	ISO-2 hour	-	-	72	-	121
7	21FC	1	165 x 2.5	300	400	27.8	ISO-2 hour	1	-	72	100	115
		2	165 x 2.5	300	400	27.8	ISO-2 hour	1	-	72	100	121
8	21FG	1	165 x 2.5	300	400	27.8	ISO-2 hour	-	1	72	100	121
		2	165 x 2.5	300	400	27.8	ISO-2 hour	-	1	72	100	121
9	21FCC	1	165 x 2.5	300	400	27.8	ISO-2 hour	2	-	72	100	120
		2	165 x 2.5	300	400	27.8	ISO-2 hour	2	-	72	100	121
10	21FGC	1	165 x 2.5	300	400	27.8	ISO-2 hour	1	1	72	100	121
		2	165 x 2.5	300	400	27.8	ISO-2 hour	1	1	72	100	121
11	55A	1	165 x 2.5	300	400	53.4	-	-	-	-	-	121
		2	165 x 2.5	300	400	53.4	-	-	-	-	-	121
12	55AC	1	165 x 2.5	300	400	53.4	-	1	-	-	100	120
		2	165 x 2.5	300	400	53.4	-	1	-	-	100	121
13	55AG	1	165 x 2.5	300	400	53.4	-	-	1	-	100	121
14	55ACC	1	165 x 2.5	300	400	53.4	-	2	-	-	100	120
		2	165 x 2.5	300	400	53.4	-	2	-	-	100	121
15	55AGC	1	165 x 2.5	300	400	53.4	-	1	1	-	100	121
		2	165 x 2.5	300	400	53.4	-	1	1	-	100	121
16	55F	1	165 x 2.5	300	400	53.4	ISO-2 hour	-	-	72	-	121
		2	165 x 2.5	300	400	53.4	ISO-2 hour	-	-	72	-	121
17	55FC	1	165 x 2.5	300	400	53.4	ISO-2 hour	1	-	72	100	120
		2	165 x 2.5	300	400	53.4	ISO-2 hour	1	-	72	100	121
18	55FG	1	165 x 2.5	300	400	53.4	ISO-2 hour	-	1	72	100	121
		2	165 x 2.5	300	400	53.4	ISO-2 hour	-	1	72	100	121
19	55FCC	1	165 x 2.5	300	400	53.4	ISO-2 hour	2	-	72	100	120
		2	165 x 2.5	300	400	53.4	ISO-2 hour	2	-	72	100	121
20	55FGC	1	165 x 2.5	300	400	53.4	ISO-2 hour	1	1	72	100	121
		2	165 x 2.5	300	400	53.4	ISO-2 hour	1	1	72	100	121

4.1.3 Instrumentation and concrete casting

Before the step of casting concrete, the steel tubes which planned to be heated, were drilled vent holes and set up thermocouples (TCs) (Figure 4.3), details will be in next part. To avoid the damage on the TCs, the rod and rubber hammer were used to vibrate and distribute concrete uniformly inside the steel tube. Masonry trowel was used to make the smooth surfaces of the infilled concrete (Figure 4.4). All steps were done carefully to ensure that the equal quality between every specimen. After the casting concrete procedure 24 hour, all specimens were cured by plastic method and kept at the same conditions. The label name of each specimens was also made to avoid mistakes for the next steps of the experiment (Figure 4.5).

Figure 4.3 Steel tube vent holes and Thermocouples set up

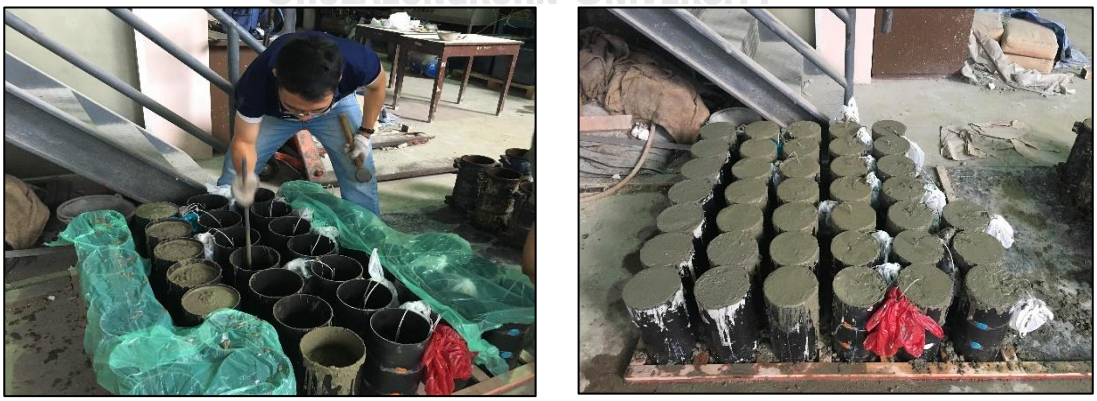

a) Concrete distribution by rod b) Concrete surface after casting

Figure 4.4 Concrete casting for specimens

Figure 4.5 Plastic sheet curing and specimen label marking

4.2. Fire test: Preparation, test and observations

In order to strictly avoid the spalling of the infilled concrete and furnace suddenly stop, vent holes and pre-dry process were implemented carefully (Figure 4.6). With the aim release the water of infilled concrete before and in the process of heating, the ability of spalling occurs minimized. Pre-dry process was applied for 24-hour at the temperature of 100°C at the age of 60, after the concrete casting. For each specimen, there are 4 vent holes with 10mm diameter in the position of 1/3 and 2/3 height of specimen, in the opposite side also. These holes were filled by epoxy after the heating process. The effective of these methods was proven by the fact that, after heating process, there was no occurrence of spalling and explosion. The furnace ran smoothly when the inside sensor did not detect any danger throughout the fire test.

a) Specimens in electrical oven b) Vent holes of specimens

Figure 4.6 Pre-dry process

In order to measure the temperature history, thermocouples (TCs) were used. The average furnace temperature was obtained from 9 TCs type-K installed at three level of 0.5, 1.5, and 2.5m above the furnace floor. Temperature within each column was recorded by 2 type-K thermocouples, one is welded at the outer steel surface, another is embedded in the center of concrete infilled (Figure 4.7).

Figure 4.7 Outer steel tube and middle concrete embedded thermocouples

At the age of 72 days after concrete casting, twenty fire-damaged CFST specimens and four plain concrete cylinders were put into the furnace for fire test. The procedure was conducted at the Fire Safety Center Research (FSRC), Chulalongkorn University. Dimensions of furnace are 3000 x 3000 x 1000 mm (Figure 4.8). The furnace heating was controlled as designed as ISO-834 standard fire for two

hours. Inside the furnace, the specimens were arranged to ensure the uniform distribution of heating from the gas oven. In order to avoid the directly exposed to the furnace oven, the closest specimens were positioned 0.8m away from the oven (Figure 4.9). Finally, the test was started, after checking and inspecting carefully for TCs protection, gas remaining, ceramic cover. All of fire test procedure was prepared within almost three months.

Figure 4.8 Fire furnace at the FSRC, Chulalongkorn University

Figure 4.9 Specimen arrangements inside the fire furnace

After heating stage of 2 hours in ISO-834 standard fire condition and 24 hours of cooling down stage, the furnace was opened. Noted that the data were recorded for the entire testing period (heating up and cooling down stage). The observations of the specimens after fire test are as below,

For the plain cylinder concrete specimens, it was observed that all of specimens were collapsed after fire test for both NSC and HSC (Figure 4.10, Figure 4.11).

For CFST specimens, although the top was covered by ceramic, but it was still damaged by high temperature, some of ingredients turn white. On the steel tube surface, it has the thin oxide layers are peeled out (Figure 4.12). Besides, black color was also observed proved that the temperature of steel surface temperature reached to 1000°C.

Generally, HSC was observed more seriously damaged than NSC.

Figure 4.10 Post-heated plain NSC cylinder

Figure 4.11 Post-heated plain HSC cylinder

Figure 4.12 Post-heated infilled concrete and steel tube of CFST column

All specimens (except collapsed cylinder plain concrete) were then removed from the furnace, cleaned by metal brush for the concrete top and steel tube surface (Figure 4.13), before prepared for the next steps of the experiment (Figure 4.14).

Figure 4.13 Top concrete and steel surface cleaned

Figure 4.14 Post-heated specimens; prepare for the next steps of experiment

4.3. FRP wrapping procedure

After 28 days from the fire test (100 days age of concrete), the specimens were strengthened by FRP wraps. CFRP and GFRP (properties are mentioned above) were cut from the complete roll to the designed size (Figure 4.15). Before wrapping, the steel surface of CFST columns was well-prepared by grinding, alcohol cleaning, in order to remove entirely of rust, dust and especially the oxide layers from the surface (Figure 4.16) to guarantee the simultaneously working between steel tube and FRP sheets. The epoxy Sikadur® 330 was mixed with the portion as instructed by the supplier (Sika) by mixer in 2 minutes for each epoxy batch. All pre-procedures were prepared carefully before wrapping to ensure for the quality of the strengthening.

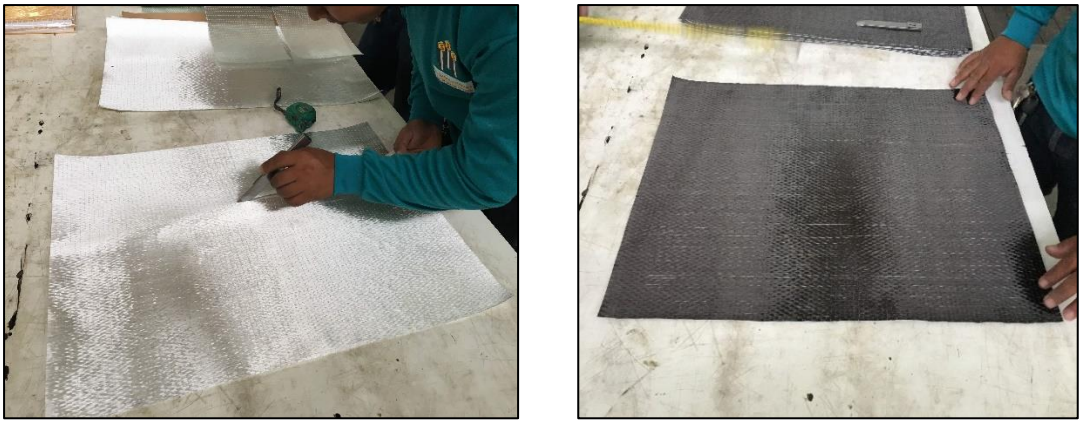

Figure 4.15 GFRP and CFRP sheets cut as designed size (300 x 670 mm)

Figure 4.16 Prepared tube surface and adhesive mixing

After the careful preparation, the wrapping procedure was conducted with 4 types of wrap: CFRP-1 layer, CFRP-2 layer, GFRP-1 layer, CFRP-GFRP (hybrid). The overlap length is 150mm. Adhesive was used for both size of sheets. For the specimens with two layers, the second layer were wrapped starting from the opposite side of the ending of the first layer. Two layers were wrapped in counter direction (Figure 4.17). After wrapping, all specimens were left to cure at the room temperature conditions.

Figure 4.17 FRP wrapping procedures

Figure 4.18 FRP-confined CFST columns (fire-damaged and unfire-damaged)

Figure 4.19 FRP wrap curing at the room temperature condition

4.4. Static test: Preparation, test and observations

A 5000kN capacity testing machine (Amsler) was used for static test of all CFST column specimens. Three strain gages (SG) were installed to measure the strain at the middle point of specimen (2 for axial strain and 1 for transverse strain) (Figure 4.20). All of specimens were cap with the Plaster at both ends to ensure for the smooth surface at top and bottom, in order to guarantee for the uniform load were applied throughout the cross-section specimens (Figure 4.21). LVDTs were also used to measure the globle displacement of specimens and the displacement of machine head. LVDT were set up following ASTM C-469 by the use of Compressor Meter (Figure 4.22). The loading rate was controlled at closer at 1.25mm/min (ASTM C-39). Before placed in the testing machine, the prepared specimens were checked for balance to ensure the axial load into the specimen (Figure 4.23).

Figure 4.20 Axial and transverse SGs for specimen strain measurements

Figure 4.21 Specimen capping for both ends

Figure 4.22 Axial, transverse LVDTs set up by Compressormeter (ASTM C469)

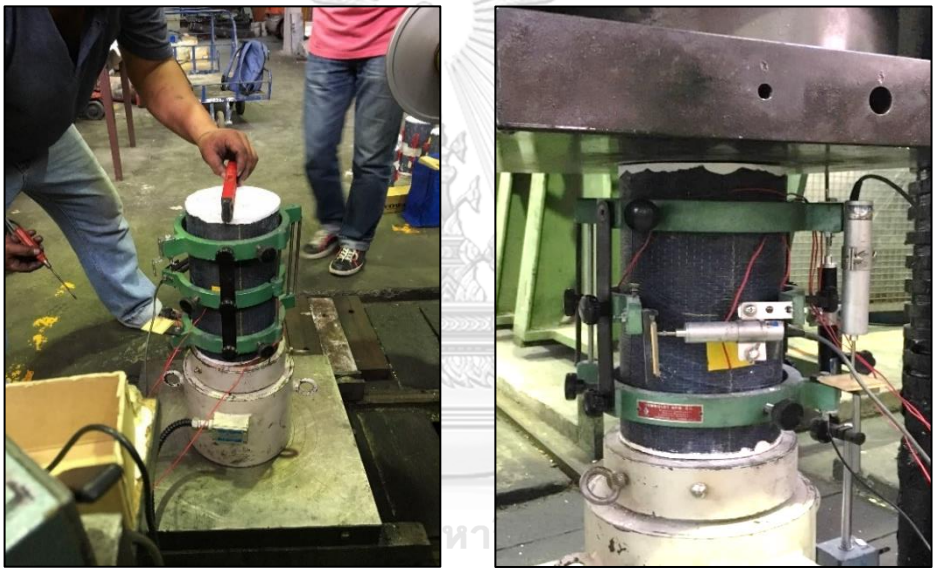

Figure 4.23 Balance checking and complete set up for static test

All test data including strain, load and displacement values were recorded simultaniously by the data logger until failure. After the static test, **three types** of failure were observed (Figure 4.24): FRP rupture, buckling at middle height, and buckling at top of the columns. FRP rupture is the failure for most cases (all of FRP wrap specimens and some unwraped specimens). Local bucklings (at middle and top) were observed in only unwraped specimens.

1. FRP rupture (CFRP rupture)		
FRP rupture (GFRP + hybrid rupture)		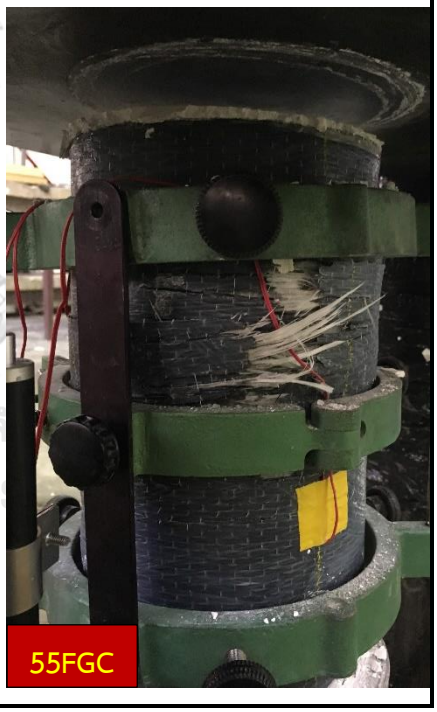

2. Buckling at middle		
3. Buckling at top		

Figure 4.24 Failure modes of specimens

CHAPTER 5
EXPERIMENTAL RESULTS AND DISCUSSION

5.1. Measured temperature and fire-test result discussion

Figure 5.1 shows the position of all specimens inside the furnace. The positions will affect to the temperature variations between specimens (the closer to the burners, the higher in temperature). The specimens were arranged to avoid the direct heat from the burners.

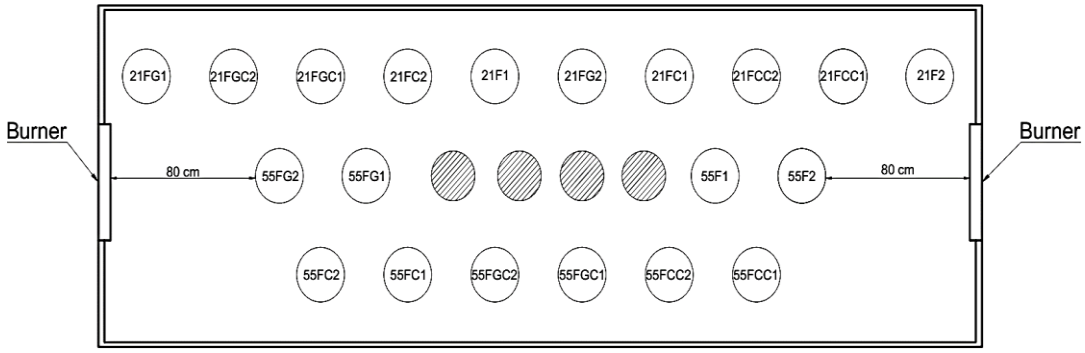

Figure 5.1 Specimen positions inside the furnace

Thermocouples were installed for all 20 fire exposed specimens (total of 40 TCs). Because the working channel (CH) from furnace was not enough (23 CH working), so the history temperature data was just recorded from 23 TCs (10 CH-steel tube TCs, 13 CH-concrete core TCs) as shown in Figure 5.2 and Figure 5.3. The values of specimen peak temperature are summarized in Table 5.1.

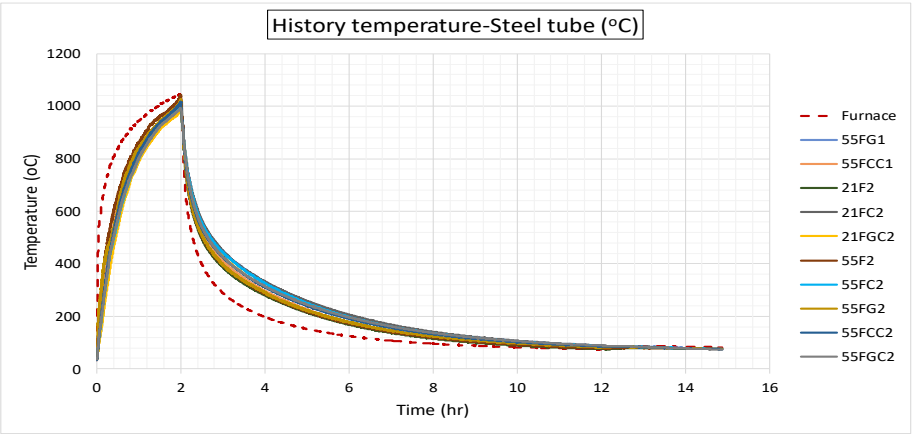

Figure 5.2 Recorded steel tube temperature histories

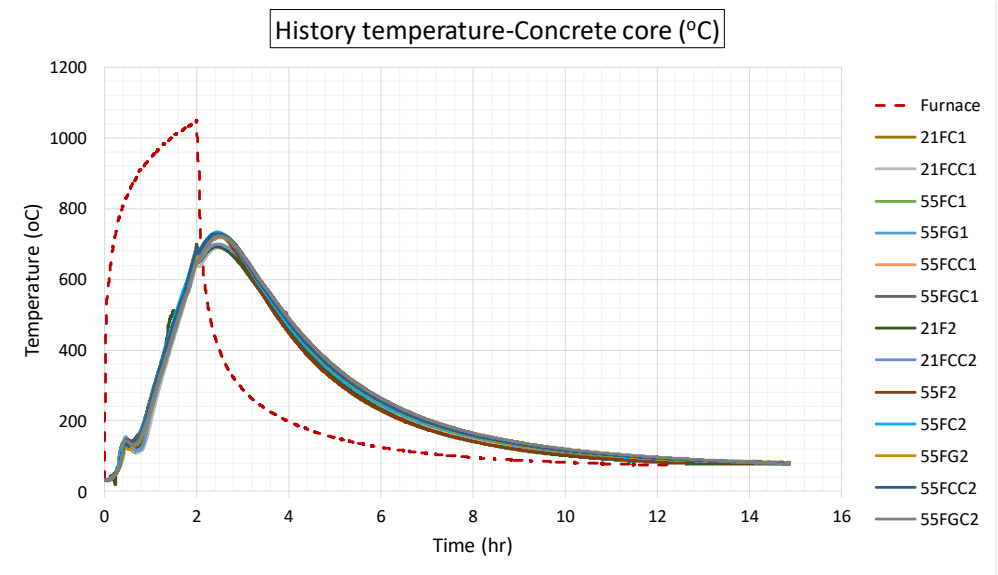

Figure 5.3 Recorded center concrete core temperature histories

Table 5.1 Peak temperature of fire-exposed specimens

No	Specimen group	Specimen	Heating	Specimen age at heating (days)	Steel tube peak temperature (°C)	Concrete core peak temperature (°C)
6	21F	1	ISO-2 hour	72	-	-
		2	ISO-2 hour	72	**989**	**693**
7	21FC	1	ISO-2 hour	72	-	**698**
		2	ISO-2 hour	72	**1027**	-
8	21FG	1	ISO-2 hour	72	-	-
		2	ISO-2 hour	72	-	-
9	21FCC	1	ISO-2 hour	72	-	**690**
		2	ISO-2 hour	72	-	**700**
10	21FGC	1	ISO-2 hour	72	-	-
		2	ISO-2 hour	72	**982**	**686**
16	55F	1	ISO-2 hour	72	-	-
		2	ISO-2 hour	72	**1045**	**724**
17	55FC	1	ISO-2 hour	72	-	**718**
		2	ISO-2 hour	72	**996**	**733**
18	55FG	1	ISO-2 hour	72	**1004**	**728**
		2	ISO-2 hour	72	**1026**	**719**
19	55FCC	1	ISO-2 hour	72	**1016**	**733**
		2	ISO-2 hour	72	**1017**	**730**
20	55FGC	1	ISO-2 hour	72	-	**727**
		2	ISO-2 hour	72	**993**	**723**

Furnace: The furnace temperature on heating phase follows perfectly with ISO-834 standard fire (Figure 5.4), so the heating condition is guaranteed. The recorded peak temperature of the furnace is 1054°C.

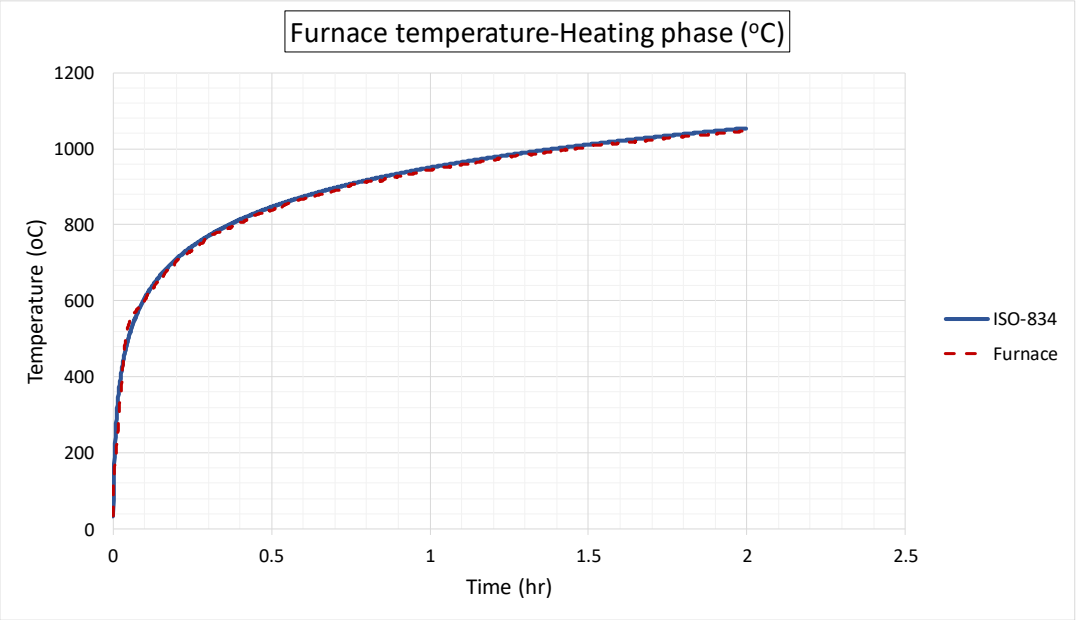

Figure 5.4 Furnace temperature during heating phase

Steel tube: Total of 10 specimens are obtained for the steel tube temperature, which the highest and lowest are 1045°C and 982°C. The temperature difference is ~63°C (6%) between those ones.

Concrete core: Total of 13 specimens are obtained for the concrete core temperature, which is 733°C for the highest and 686°C for the lowest. The temperature difference is ~47°C (6.4%) between those ones.

With this small variation in temperature data for both steel tube and core concrete, the test has shown the good and reliable results.

As can be seen, the peak temperature for HSC infilled CFST is generally higher than NSC infilled CFST. That also performed the reason for the more seriously damaged in HSC infilled CFST than NSC infilled CFST. Both NSC and HSC infilled CFST also observed the “discontinuity” in concrete history temperature (at 100°C-170°C)

may be because of the water vaporization at that boiling point, which has the higher than the normal boiling point due to the pressurization of water within the pores.

It is noted that, the temperature in concrete increases for a period during cooling phase, as expected, due to the thermal wave continuing to move through the cross section (low conductivity in concrete). The amount of increased temperature is approximately 74°C in nearly 28mins after the peak furnace temperature reached.

In the cooling phase, the temperature in steel is more rapidly decreased in temperature than the concrete core, obviously. While the steel tube temperature needs around 10 more hours of decreasing in natural condition to get the furnace temperature, the concrete core needs around 12 hours. (The data recorded was switched off after 15 hours of operation).

5.2. Static test results

Strengthening ratio index is defined as the percentage increase in ultimate load/ ductility/ stiffness (composite modulus)

$$\mathrm{SEI} = (\mathrm{N_{eS}} - \mathrm{N_{eU}})/\mathrm{N_{eU}} \tag{5.1}$$

$$\mathrm{DEI} = (\mathrm{DI_{eS}} - \mathrm{DI_{eU}})/\mathrm{N_{eU}} \tag{5.2}$$

$$\mathrm{EEI} = (\mathrm{E_{eS}} - \mathrm{E_{eU}})/\mathrm{N_{eU}} \tag{5.3}$$

where $\mathrm{N_{eS}}/\mathrm{D_{eS}}/\mathrm{E_{es}}$ and $\mathrm{N_{eU}}/\mathrm{D_{eU}}/\mathrm{E_{eU}}$ are maximum value of loads/ductility index/elastic modulus for strengthened and un-strengthened specimens, respectively.

Figure 5.5 shows that the load capacity and the general different percentage between 2 series are small (0.2%-12.4%). It also shows that the experimental work results and data are good and reliable. Except one specimen showed the high difference between two series (34.7%) because of the purpose of adjustment in the first tested specimen (specimen 21FC1).

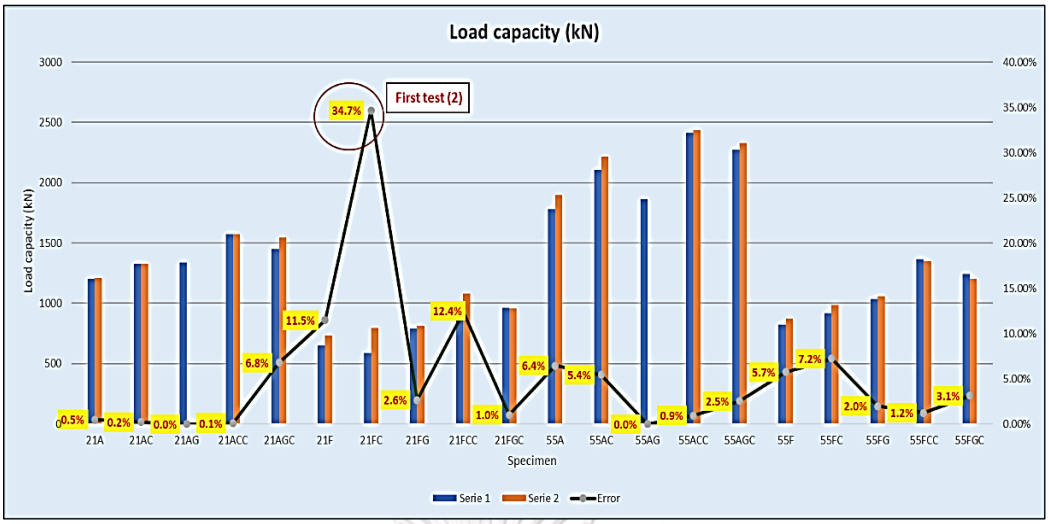

Figure 5.5 Load capacity results and differences (%) between two series

All test results are shown in Table 5.2, and from Figure 5.6 to Figure 5.9 (compression behavior-first group), and Appendix D.

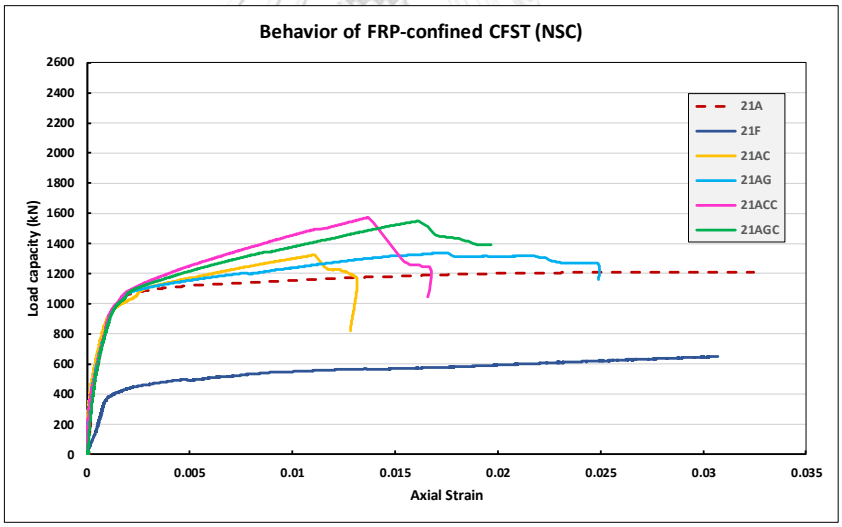

Figure 5.6 Load-Strain FRP-confined CFST (NSC)

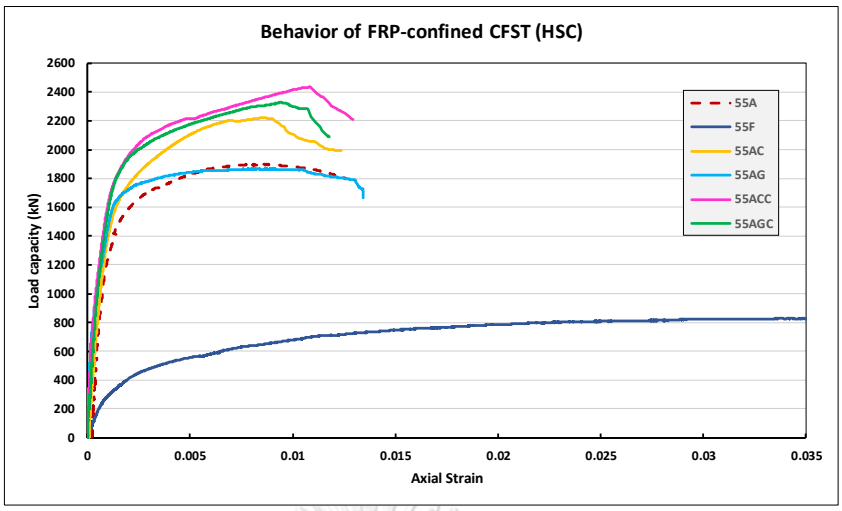

Figure 5.7 Load-Strain FRP-confined CFST (HSC)

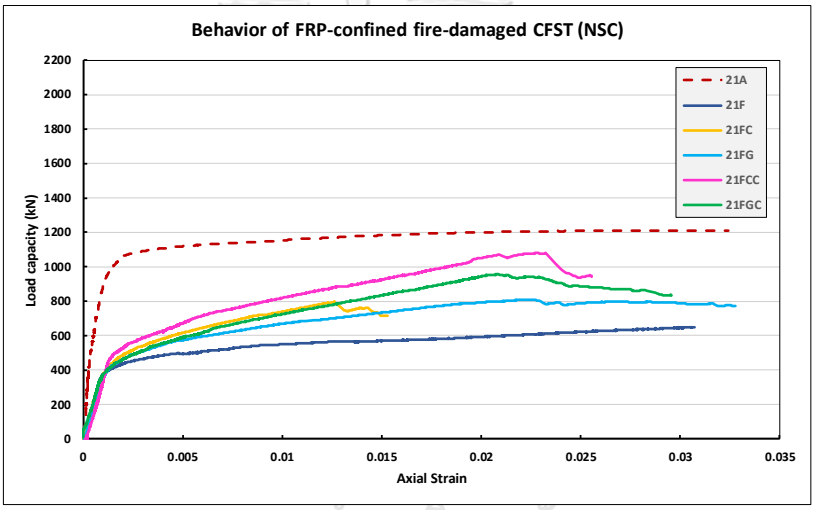

Figure 5.8 Load-Strain FRP-confined fire-damaged CFST (NSC)

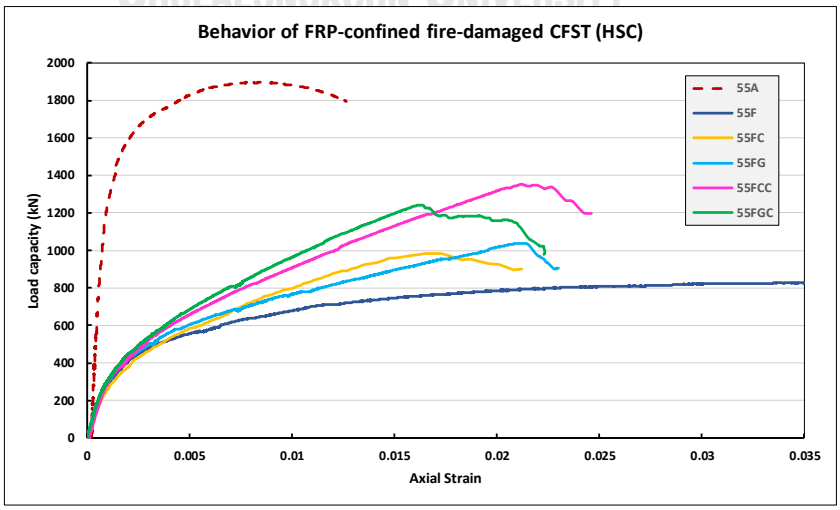

Figure 5.9 Load-Strain FRP-confined fire-damaged CFST (HSC)

Table 5.2 Summary of test results

No	Specimen group	Specimen	Type of Failure	Load capacity (kN)	Mean	Standard Deviation	SEI (%)	Ductility μ_u	Mean	Standard Deviation	DEI (%)	Ductility μ_{pl}	Mean	Standard Deviation	DEI (%)	Modulus (10^4 Mpa)	Mean	Standard Deviation	EEI (%)
1	21A	1	Buckling (mid)	1204	1207	4.17	-	25.3	25.79	0.63	-	119.9	105.56	20.35	-	2.29	2.47	0.26	-
		2	Buckling (mid)	1210				26.2				91.2				2.66			
2	21AC	1	FRP rupture	1325	1326	2.05	9.9%	11.0	15.04	-	-41.7%	55.6	55.65	-	-47.3%	2.62	2.62	-	6.0%
		2	FRP rupture	1328				-				-				-			
3	21AG	1	FRP rupture	1338	1338	0.00	10.8%	18.6	18.56	-	-28.0%	78.8	78.79	-	-25.4%	2.51	2.51	-	1.7%
4	21ACC	1	FRP rupture	1575	1574	0.91	30.4%	12.4	12.60	0.35	-51.1%	60.6	66.52	8.43	-37.0%	2.61	2.80	0.27	13.4%
		2	FRP rupture	1573				12.8				72.5				2.99			
5	21AGC	1	FRP rupture	1447	1496	69.51	24.0%	-	13.58	-	-47.3%	-	70.82	-	-32.9%	2.95	2.91	0.05	17.7%
		2	FRP rupture	1546				13.6				70.8				2.87			
6	21F	1	Buckling (top)	650	692	59.61	-42.6%	35.1	35.06	-	35.9%	35.5	35.50	-	-66.4%	1.66	1.66	-	-33.1%
		2	Buckling (mid)	735				-				-				-			
7	21FC	1	FRP rupture	-	794	-	-34.2%	4.5	20.16	-	-21.8%	-	15.13	-	-85.7%	1.61	1.77	0.22	-28.5%
		2	FRP rupture	794				10.3				15.1				1.92			
8	21FG	1	FRP rupture	790	800	14.71	-33.7%	22.6	22.49	0.20	-12.8%	20.8	20.10	0.97	-81.0%	1.73	1.74	0.01	-29.8%
		2	FRP rupture	810				22.3				19.4				1.74			
9	21FCC	1	FRP rupture	945	1012	94.33	-16.1%	-	16.92	-	-34.4%	-	18.44	-	-82.5%	-	1.83	-	-25.9%
		2	FRP rupture	1079				16.9				18.4				1.83			
10	21FGC	1	FRP rupture	966	961	6.86	-20.4%	21.1	19.86	1.76	-23.0%	22.4	23.31	1.28	-77.9%	1.99	1.87	0.16	-24.3%
		2	FRP rupture	956				18.6				24.2				1.76			
11	55A	1	Buckling (mid)	1781	1838	81.11	-	4.6	4.67	0.04	-	14.7	14.46	0.33	-	4.08	4.29	0.30	-
		2	Buckling (mid)	1895				4.7				14.2				4.50			
12	55AC	1	FRP rupture	2104	2161	80.82	17.6%	4.9	5.24	0.51	12.3%	19.8	16.44	4.75	13.7%	4.83	4.87	0.06	13.6%
		2	FRP rupture	2219				5.6				13.1				4.91			
13	55AG	1	FRP rupture	1863	1863	0.00	1.3%	6.6	6.59	-	41.2%	35.3	35.33	-	144.4%	4.53	4.53	-	5.7%
14	55ACC	1	FRP rupture	2412	2423	15.70	31.8%	13.2	13.23	0.01	183.6%	68.0	60.89	10.11	321.2%	4.95	5.53	0.82	28.9%
		2	FRP rupture	2435				13.2				53.7				6.11			
15	55AGC	1	FRP rupture	2271	2300	40.66	25.1%	12.1	11.70	0.56	150.8%	48.8	47.05	2.42	225.5%	5.44	5.91	0.68	38.0%
		2	FRP rupture	2328				11.3				45.3				6.39			
16	55F	1	Buckling (mid)	825	849	33.38	-53.8%	19.9	20.68	1.14	343.2%	45.6	44.49	1.52	207.7%	1.54	1.59	0.06	-63.0%
		2	Buckling (top)	873				21.5				43.4				1.63			
17	55FC	1	FRP rupture	919	952	46.88	-48.2%	9.9	16.07	1.46	244.4%	16.1	19.75	5.11	36.6%	1.70	1.52	0.26	-64.6%
		2	FRP rupture	985				12.0				23.4				1.33			
18	55FG	1	FRP rupture	1038	1048	14.50	-43.0%	17.9	18.45	0.81	295.5%	29.5	27.07	3.44	87.2%	1.62	1.50	0.17	-65.0%
		2	FRP rupture	1059				19.0				24.6				1.38			
19	55FCC	1	FRP rupture	1367	1359	11.74	-26.1%	12.6	12.16	0.63	160.6%	25.5	23.53	2.80	62.8%	1.48	1.50	0.02	-65.1%
		2	FRP rupture	1351				11.7				21.5				1.51			
20	55FGC	1	FRP rupture	1242	1222	27.44	-33.5%	9.0	8.96	0.08	92.1%	21.1	19.23	2.64	33.0%	1.55	1.52	0.04	-64.6%
		2	FRP rupture	1203				8.9				17.4				1.49			

5.2.1 Load capacity

Figure 5.10 and Figure 5.11 show that the HSC infilled CFST is more seriously damaged than NSC infilled CFST in the same situation of fire-damaged, 53.8% and 42.6% respectively.

Specimens with carbon two-layers (CC) have the highest load capacity in both NSC and HSC infilled CFST columns for heated and non-heated specimens also, obviously. The more layers, the more load capacity is improved. Hybrid wrap (GC) is slightly less effective (3 to 10%) than CC. For one layer, generally, one carbon (C) and one glass (G) shows the same amount of effectiveness for all situations in NSC infilled. However, in HSC-infilled, G shows the better improvement for heated specimens, while C shows the better improvement for non-heated specimens.

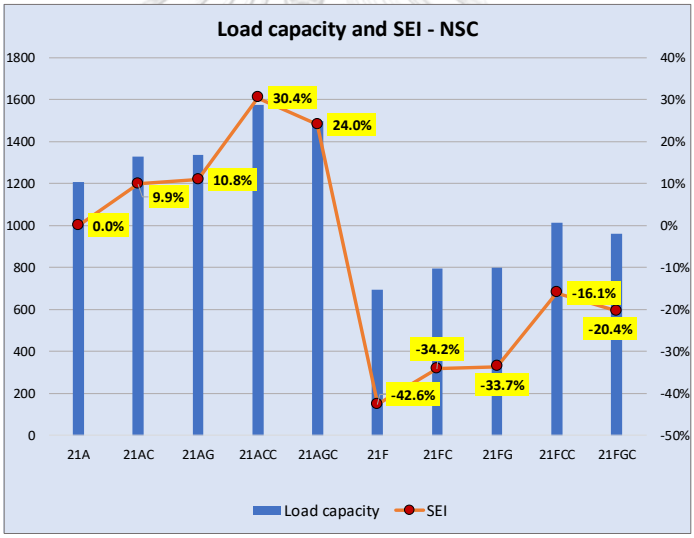

Figure 5.10 Load capacity results and SEI (%)-NSC infilled CFST

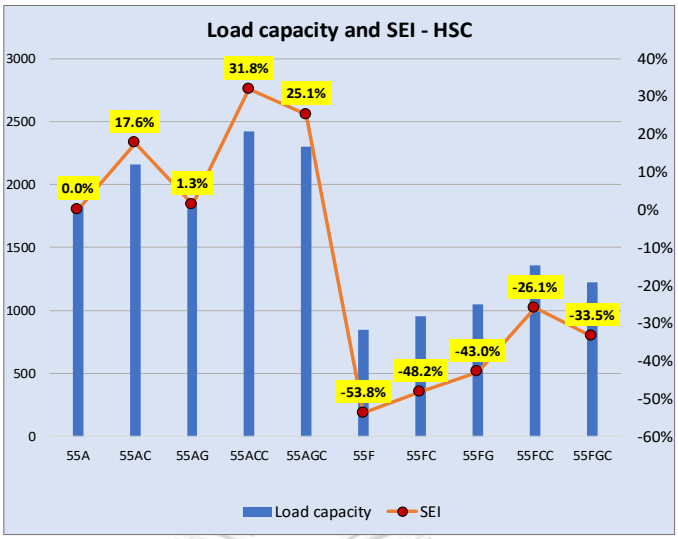

Figure 5.11 Load capacity results and SEI (%)-HSC infilled CFST

The use of FRP, even with two layers, cannot fully restore the load capacity of the fire-damaged CFST columns as the undamaged specimens ability.

The confinement effect by FRP for fire-damaged specimens is less effective than the undamaged ones for both NSC and HSC infilled. For NSC infilled CFST columns, the load capacity increases around 10.4%, 27.2% for the undamaged with 1 and 2 FRP layers, respectively while 8.7%, 24.4% for fire-damaged specimens. It means

Using FRP to increase the load capacity for undamaged CFST is slightly better than using FRP as a method to improve the load capacity of fire-damaged CFST columns.

For the confinement effect between NSC and HSC infilled, the comparable results are shown for both undamaged and fire-damaged specimens. It also means that the effectiveness of using FRP wrap in load enhancement is similar when applying for both NSC and HSC infilled CFST columns, undamaged and fire-damaged conditions.

5.2.2 Axial ductility

The ductility index (DI) used in this study is the ultimate ductility (μ_u), the definition is as below,

$$\mu_u = \frac{\varepsilon_u}{\varepsilon_y} \tag{5.4}$$

where the ultimate strain (ε_u) is the strain corresponding to the ultimate load (P_u), and yield strain (ε_y) is the strain corresponding to $0.4P_u$ (ASTM C-469).

The Ductility Index (DI) results and DEI (5.2) results are shown in Figure 5.12 and Figure 5.13.

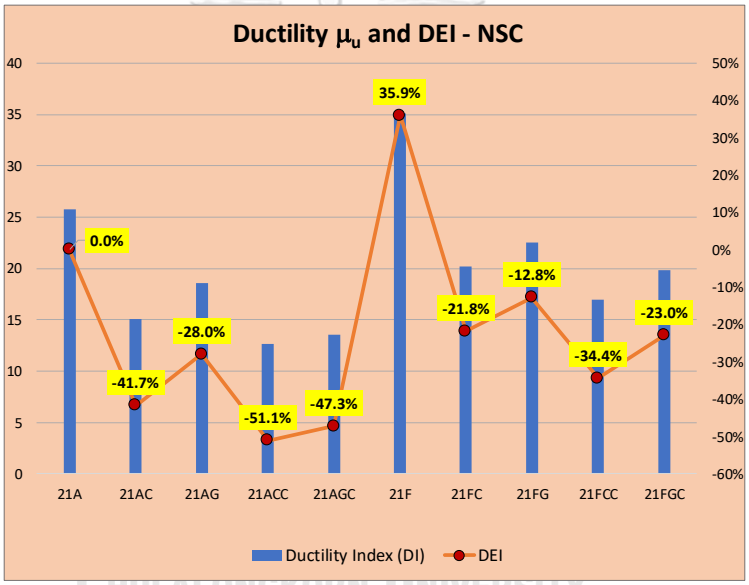

Figure 5.12 Ductility Index results and DEI (%)-NSC infilled CFST

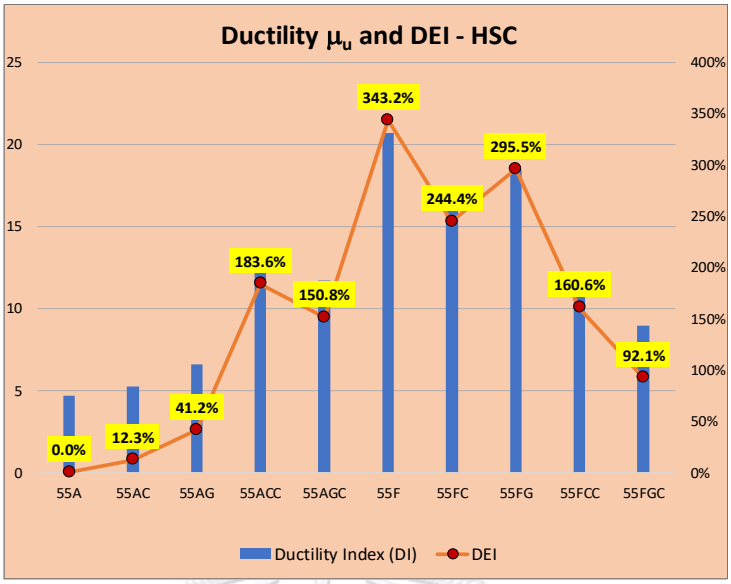

Figure 5.13 Ductility Index results and DEI (%)-HSC infilled CFST

Generally, the DEI for NSC at ambient, NSC fire-damaged, HSC fire-damaged are similar in trend. The more FRP layers, the easier to be rupture in the specimens. In contrast, for HSC at ambient has a different trend, when increasing the layer makes the specimens more ductile, this observation also agrees with the experiment from (Hu et al., 2011).

For one-layer wrapping, GFRP is better for ductility than CFRP (8% to 51% better). And one-layer GFRP is also the best for ductile improvement throughout the methods. For two-layer wrapping, the hybrid one (GC) shows the better in ductility than carbon two-layer (CC) for NSC infilled CFST (4% to 14% better). However, for HSC infilled, CC has the better improvement for ductility than GC (30% to 70%).

As can be seen, after fire-exposed, the specimens become more ductile (35.9% for NSC and 343.2% for HSC infilled). This can be explained by the more ductile property of steel after cooling down from fire-exposed period.

For NSC infilled, the DI for fire-damaged CFST decreased greater than undamaged CFST when using FRP wrap, around 59% and 42% respectively. For HSC infilled, DI for undamaged CFST increases 97% while decreases 145% for fire-damaged ones.

5.2.3 Composite modulus (Stiffness)

In this research, the stiffness is defined as the initial stiffness. It is slope of the line connected between the initial point (the 50th point of measurement) and the proportional limit point (the limit point for linear behavior, defined as R(x) > 0.99).

Figure 5.14 and Figure 5.15 show the composite modulus and EEI (5.3) results. The stiffness of specimens, generally, are seriously damaged after fire-exposed, especially for HSC infilled CFST columns (33% for NSC and 63% for HSC infilled).

For the undamaged specimens, the use of FRP wrapping causes the slight improvement in stiffness, HSC infilled is better enhanced in stiffness than NSC, 6.0% to 17.7% for NSC infilled and 13.6% to 38.0% for HSC infilled. The more layers, the stiffer in specimens. Although using G one-layer is not as good as C one-layer for stiffness (1.7% to 5.7% for NSC and 6% to 13.6% for HSC, respectively). But the appearance of GFRP in two-layer wrapping (hybrid) makes the specimen stiffer than using CFRP two-layer (17.7% to 38% for NSC and 13.4% to 28.9% for HSC, respectively).

For the fire-damaged specimens, the improvement is not in clear trend, even increasing number of FRP layer. It can be explained by the reason that, the fire exposure deteriorated seriously till the level that stiffness cannot be restored.

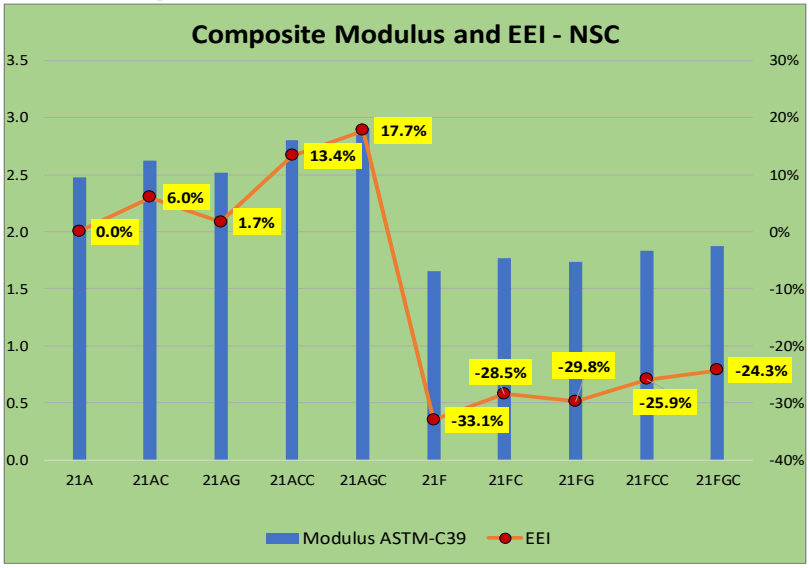

Figure 5.14 Composite modulus results and EEI (%)-NSC infilled CFST

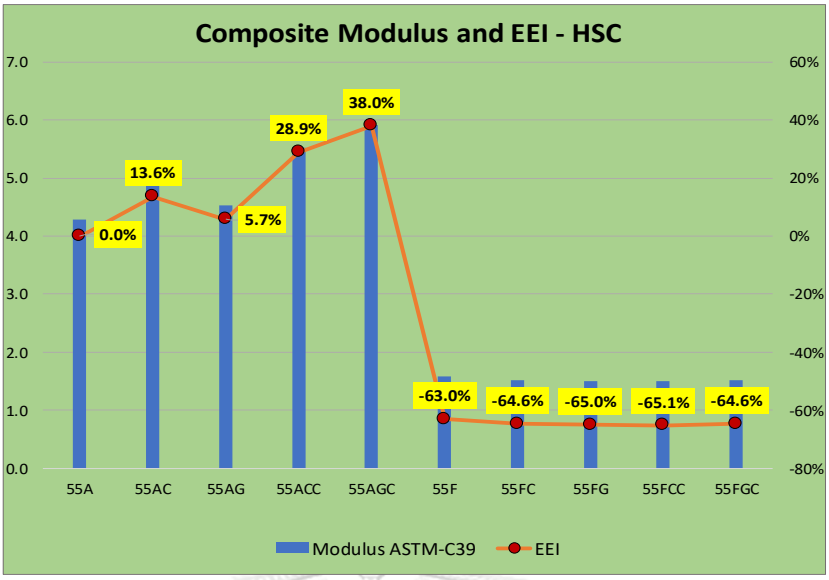

Figure 5.15 Composite modulus results and EEI (%)-HSC infilled CFST

5.3. Summary of test results

With slight differences on the results between specimens in the same group, both fire-test results and static-test results have shown the superior in experimental works and also reliable data.

Through the fire-test, by installing thermocouples on the specimens, the temperatures of furnace, steel tube, and concrete core were collected. Therefore, the level of damages by fire exposure can be estimated. The peak temperatures of furnace, steel tube and concrete core are about 1054°C, 1014°C, and 710°C respectively. The peak temperature of concrete has a "delay" (in cooling down phase) because of the low conductivity of concrete.

Through the static test, the load capacity, axial ductility and composite modulus (stiffness) were investigated to understand the compression behavior and effectiveness of FRP confinement for both fire-damaged and undamaged CFST columns.

The main conclusions are

1. The FRP wrap methods can enhance the load capacity. However, this method imposes to be more effective for increasing the load capacity for undamaged CFST columns than for the damaged CFST ones
2. Generally, although improving the load capacity, but the more FRP layers, the easier to be rupture. This phenomenon agreed with all situations except the HSC infilled CFST columns. The decrease level in ductility when applying FRP wrapping for fire-damaged specimens is greater than the undamaged ones.
3. Stiffness is seriously damaged after fire exposure. Although showing the good effectiveness for the undamaged CFST columns, FRP wrapping is a not good method for improving the stiffness for fire-damaged CFST columns.
4. The use of FRP, even with two layers, schemes of wrapping, cannot fully restore the load capacity, ductility and stiffnees of the fire-damaged CFST columns as the undamaged ones.
5. The use of Hybrid wrapping is the most effective to enhance the compression behavior of the CFST columns. It can prevent the effect of galvanic corrosion and prove as a good application for strengthening the fire-damaged behavior. Although having the competitive load capacity enhancement than CFRP, the superior in ductility enhancement by using GFRP is well-performed.

CHAPTER 6
ANALYTICAL MODELLING OF FRP-CONFINED FIRE-DAMAGED CFST COLUMNS

Many modelling approaches have been used in an attempt to predict the post-fire compression behavior of CFST columns. However, the available models to analyze and predict the FRP-confined fire-damaged CFST columns are still limited. Some of simplified formulas have been proposed based on experimental results (Shahidan et al., 2016; Wang et al., 2018).

In this chapter, the general analysis is proposed to understand and predict the compression behavior of FRP-confined fire-damaged CFST columns. The model is verified with experimental results described in Chapter 5.

6.1.1 Heat transfer analysis

6.1.2 2D finite Element Model

A commercial finite element analysis package ANSYS (ANSYS, 2004) is used to perform the heat transfer analysis to predict the temperature distributions in CFST columns cross-section fire exposure (heating and cooling down phases). The 2-D solid thermal element PLANE55 is used to mesh the CFST cross-section (Ding & Wang, 2008). The transition analysis type is applied on model to study the better heat transfer. Although the air gap between steel tube and concrete may affect to the results (Gillie, 2014), in this study, due to the simpler for throughout the model (with many steps), the perfect interface (no air gap) is assumed. The thermal properties (Table 6.1) are defined according to recommendations in (EN, 2005; Gillie, 2014):

Table 6.1 Thermal properties of material

Properties	Steel	Concrete
Density	7900 kg/m^3	2300 kg/m^3
Specific heat	460 J/(kg.K)	970 J/(kg.K)

Conductivity	45 w/mK	1.14 w/mK
Convection	25 w/mK	20 w/mK
Radiation rate	0.23	0.92

The applied thermal boundary conditions are followed the practical condition of the fire. In this study, the fire curve ISO-834 standard fire (CEN, 2002) is applied for heating stage:

$$T = T_0 + 345 \log_{10}(8t + 1)$$

For the cooling down stage, the thermal condition is modelled as closure as the condition of cooling down temperature inside the furnace. The applied thermal boundary condition for all stages are as shown in Figure 6.1.

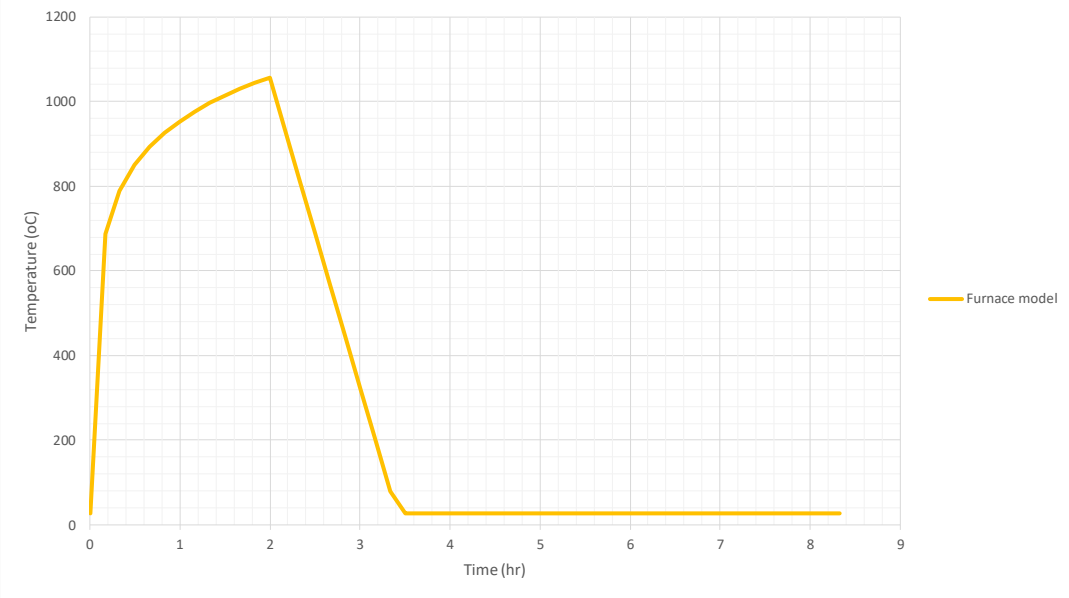

Figure 6.1 Modelling of furnace temperature for all stages

6.1.3 Verifications of FEM results

To examine the validity of the 2D heat transfer analysis, the fire-test experimental results are taken to verify. Figure 6.2 to Figure 6.4 show the results of temperature distribution by time. As shown in Figure 6.5 to Figure 6.8, good agreements between proposed model and experimental results data are observed, the maximum

differences are 2.5% and 4.5% for steel tube and concrete peak temperature, respectively.

Generally, the proposed model can predict accurately the peak temperature of the specimens (steel tube and concrete core). The proposed model not only shows the good predictions for peak temperature, but also the time-temperature distribution, especially in the heating phase.

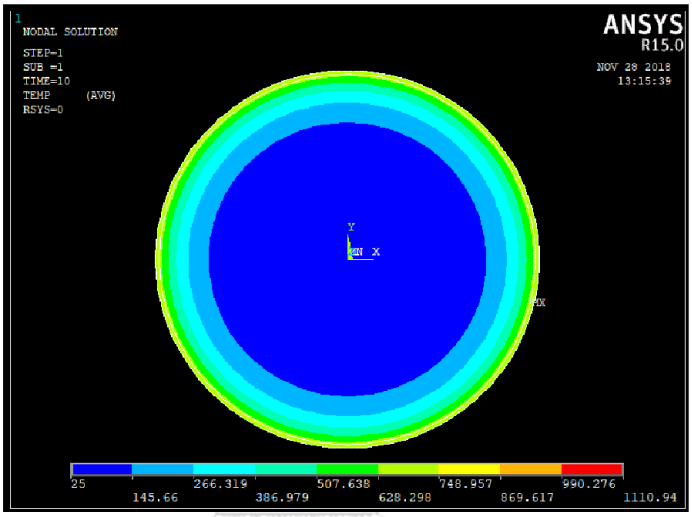

Figure 6.2 Temperature distribution at time=10 mins (heating stage)

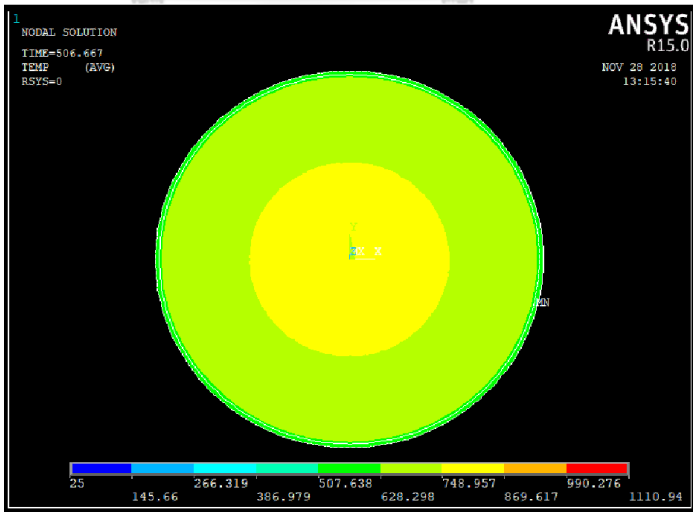

Figure 6.3 Temperature distribution at time=506 mins (cooling down stage)

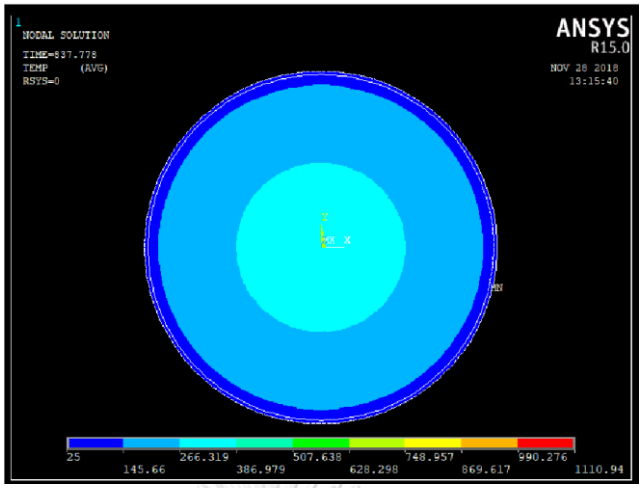

Figure 6.4 Temperature distribution at time=837 mins

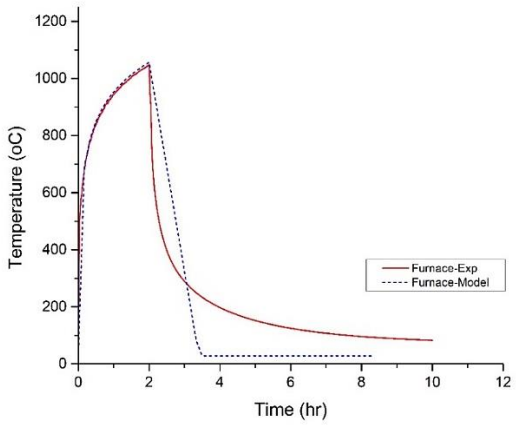

Figure 6.5 Furnace temperature (Model & Experiment 55FG1)

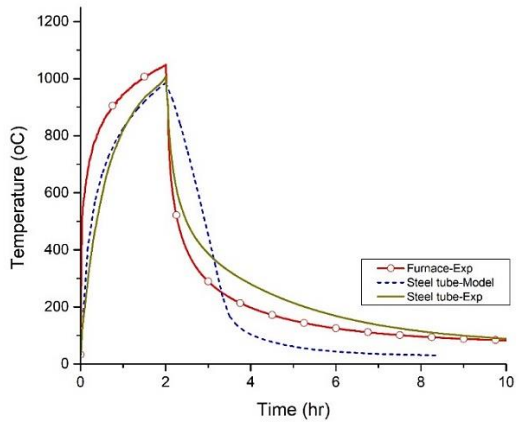

Figure 6.6 Steel tube temperature (Model & specimen 55FG1)

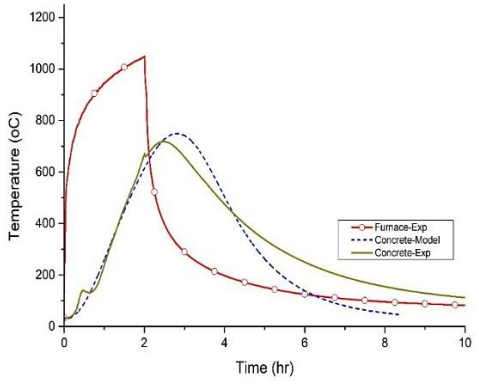

Figure 6.7 Centered concrete temperature (Model & specimen 55FG1)

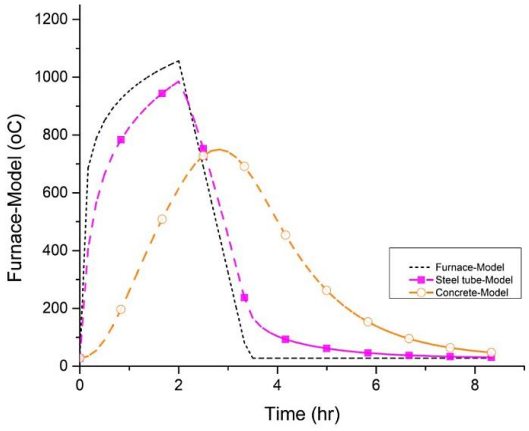

Figure 6.8 Specimen temperature (Model & specimen 55FG1)

6.2. Post-fire material properties

The cross-section temperature data from the heat transfer analysis model are then used along with the available post-fire material properties to predict the residual material properties of CFST columns. Such residual material properties for both steel and concrete are assumed to depend on the peak exposed temperature.

6.2.1 Post-fire material properties of steel (Han & Huo, 2003)

Residual yield strength (f_{yp}) and elastic modulus (E_{sp}) of steel:

$$f_{yp} = f_y \times \begin{cases} 1 & T \le 400^oC \\ 1 + 2.33 \times 10^{-4}(T-20) - 5.88 \times 10^{-7}(T-20)^2 & T > 400^oC \end{cases} \quad (6.1)$$

$$E_{sp} = E_s \times \begin{cases} 1 & T \le 600^oC \\ 1.431 - T/1400 & T > 600^oC \end{cases} \quad (6.2)$$

where f_y, E_s are yield strength and elastic modulus of steel tube at ambient condition.

6.2.1 Post-fire material properties of concrete (Chang et al., 2006)

Residual compressive strength (f_{cp}) and

$$f_{cp} = f_c \times \begin{cases} 1.01 - 0.00055 \times T & T \le 200^oC \\ 1.15 - 0.00125 \times T & 200^oC < T \le 800^oC \end{cases} \quad (6.3)$$

Corresponding strain (ε_{cp})

$$\varepsilon_{cp} = \varepsilon_c \begin{cases} 1 & T \le 200^oC \\ (-0.1f_c + 7.7)\left[\frac{\exp(-5.8+0.01T)}{1+\exp(-5.8+0.01T)} - 0.0219\right] + 1. & 200^oC < T \le 800^oC \end{cases} \quad (6.4)$$

Residual elastic modulus of unconfined concrete (E_{cp})

$$E_{cp} = E_c \times \begin{cases} -0.00165 \times T + 1.033 & T \le 125^oC \\ \frac{1}{1.2 + 18(0.0015 \times T)^{4.5}} & 125^oC < T \le 800^oC \end{cases} \quad (6.5)$$

where f_c, ε_c, E_c are compressive strength, corresponding strain and elastic modulus of concrete at ambient condition.

6.3. Confinement effect by FRP

The behavior of CFST is the behavior of fire-damaged CFST column, with the properties of the concrete and steel from above residual post-fire material properties.

The bonding between the concrete and steel is assumed to be intact

$$\begin{aligned} \varepsilon_{cz} &= \varepsilon_{sz} = \varepsilon_z \\ \varepsilon_{c\theta} &= \varepsilon_{s\theta} = \varepsilon_\theta \end{aligned} \tag{6.6}$$

where

ε_{cz} and ε_{sz} are the axial strains of the concrete and steel tube

$\varepsilon_{c\theta}$ and $\varepsilon_{s\theta}$ are the hoop strains of the concrete and steel tube

ε_z and ε_θ are the axial and hoop strains of the CFST column

6.3.1 The relationship between axial strain and hoop strain

The relationship between axial strain and hoop strain is

$$\begin{aligned} \varepsilon_z = \mathrm{LS}\left(\frac{f_{cp}}{30}\right)^m \Bigg\{ & \varepsilon_{cp}\left[1 + 0.75\left(\frac{-\varepsilon_\theta}{\varepsilon_{cp}}\right)\right]^{0.7} - \varepsilon_{cp}\exp\left[7\left(\frac{\varepsilon_\theta}{\varepsilon_{cp}}\right)\right] \\ & + 0.07(-\varepsilon_\theta)^{0.7}\left[1 + 26.8\left(\frac{f_r}{f_{cp}}\right)\right]\Bigg\} \end{aligned} \tag{6.7}$$

where

$\mathrm{LS} = \frac{\mathrm{LS}_2 - \mathrm{LS}_1}{\mathrm{H} - \mathrm{d}}(\mathrm{S} - \mathrm{d}) + \mathrm{LS}_1$ is the parameter reflecting the effect of external confinement, from $\mathrm{LS}_2 = 0.6466$ for unconfined CFST columns to $\mathrm{LS}_1 = 0.6650$ for FRP-confined CFST columns,

m is the parameter considering effect of concrete strength

$$\mathrm{m} = \begin{cases} 0 & f_{cp} \le 30 \\ -0.05 & f_{cp} > 30 \end{cases} \tag{6.8}$$

S is the center to center spacing of external confinement; d is diameter of external confinement; H is the total height of specimen. In this case, $S = d$.

f_r is the confining pressure from steel tube to the confined concrete.

6.3.2 Confining pressure

In the confined CFST column, the core concrete is confined by steel tube and also external confinement (FRP wrap). Thus, f_r is equal to the sum of the confining stress from the steel tube (f_{rs}) and external confinement (f_{rE})

$$f_r = f_{rs} + f_{rE} \tag{6.9}$$

where

f_{rs} is the confining stress from steel tube

$$f_{rs} = -\frac{2t}{D_0 - 2t}\sigma_{s\theta} \tag{6.10}$$

f_{rE} is the confining stress from external confinement. In this case, is confined by FRP

$$f_{rE} = -\frac{2t_{FRP}}{D_0 - 2t}\sigma_E \tag{6.11}$$

$\sigma_{s\theta}$ is the hoop stress provided by the steel tube; t_{FRP} is the thickness of FRP wrap; σ_E is the stress provided by external confinement (FRP); ε_{ssE}, E_{ssE}, σ_{ssE} are respectively the average hoop strain, elastic modulus and yield stress of FRP. Assume that $\varepsilon_{ssE} = \varepsilon_{s\theta}$.

σ_E is the stress provided by FRP

$$\sigma_E = \begin{cases} \varepsilon_{ssE}E_{ssE} & E_{ssE} \le \sigma_{ssE} \\ \varepsilon_{ssE}\sigma_{ssE} & E_{ssE} > \sigma_{ssE} \end{cases} \tag{6.12}$$

The three-dimensional stress-strain relationship of the steel tube can be evaluated by the hoop-axial strain relationships from Prandtl-Reuss theory. However, in this case, for CFST with thin-walled steel tube, it is able to ignore the small radial

stress (σ_{sR}) of the steel tube. Therefore, the steel tube stress can be assumed to be in plane stress.

Two-dimensional hoop-axial strain relationships (incremental form)

Elastic stage

$$\begin{Bmatrix} d\sigma_{sz}^{i} \\ d\sigma_{s\theta}^{i} \end{Bmatrix} = \frac{E_s}{1-v_s}\begin{bmatrix} 1 & v_s \\ v_s & 1 \end{bmatrix}\begin{Bmatrix} d\varepsilon_{sz}^{i} \\ d\varepsilon_{s\theta}^{i} \end{Bmatrix} \tag{6.13}$$

Plastic stage

$$\begin{Bmatrix} d\sigma_{sz}^{i} \\ d\sigma_{s\theta}^{i} \end{Bmatrix} = \frac{E_s}{S_z^2 + S_\theta^2 + 2v_s S_z S_\theta}\begin{bmatrix} S_\theta^2 & -S_z S_\theta \\ -S_z S_\theta & S_z^2 \end{bmatrix}\begin{Bmatrix} d\varepsilon_{sz}^{i} \\ d\varepsilon_{s\theta}^{i} \end{Bmatrix} \tag{6.14}$$

In particular,

$$S_z = \frac{1}{3}(2\sigma_{sz}^{i-1} - \sigma_{s\theta}^{i-1}) \tag{6.15}$$

$$S_\theta = \frac{1}{3}(2\sigma_{s\theta}^{i-1} - \sigma_{sz}^{i-1}) \tag{6.16}$$

The von Mises yield criterion is used to determine yield surface of the steel tube

$$\sigma_{sz}^2 - \sigma_{sz}\sigma_{s\theta} + \sigma_{s\theta}^2 = \sigma_{sy}^2 \tag{6.17}$$

For the confined core concrete, equations of the stress-strain curve (Attard & Setunge, 1996) is given as follow

$$\frac{f_{cc}}{f_{ccp}} = \frac{A\left(\frac{\varepsilon_z}{\varepsilon_{cc}}\right) + B\left(\frac{\varepsilon_z}{\varepsilon_{cc}}\right)^2}{1 + (A-2)\left(\frac{\varepsilon_z}{\varepsilon_{cc}}\right) + (B-1)\left(\frac{\varepsilon_z}{\varepsilon_{cc}}\right)^2} \tag{6.18}$$

$$\varepsilon_{cc} = \varepsilon_{co}\left[1 + \frac{(17 - 0.06f_c)f_r}{f_c}\right] \tag{6.19}$$

$$\frac{f_{ccp}}{f_c} = 1 + 4.1\left(\frac{f_r}{f_c}\right) \tag{6.20}$$

where $\mathbf{A}$ and $\mathbf{B}$ are parameters that govern the shape of stress-strain curve (Kwan et al., 2015) (Appendix A); $\mathbf{f_{cc}}$ is the confined concrete stress; $\mathbf{f_{ccp}}$ and $\boldsymbol{\varepsilon_{cc}}$ are the confined peak concrete stress and corresponding axial strain.

6.3.3 Compression behavior of FRP-confined fire-damaged CFST columns

The composite cross-section is divided into m layers. Each layer has its own peak exposed temperature and mechanical behavior. The steel tube is considered as one layer. The axial load capacity (F_t) is calculated as follows:

$$\mathbf{F_t = F_c + F_s} \tag{6.21}$$

$$\mathbf{F_t = \sum_{k=1}^{m} F_{ck} + F_s} \tag{6.22}$$

$$\mathbf{F_t = \sum_{k=1}^{m} f_{cck} A_{ck} + \sigma_{sz} A_s} \tag{6.23}$$

where $\mathbf{A_s}$ and $\mathbf{A_{ck}}$ are areas of steel tube and confined concrete of layer i, respectively; $\boldsymbol{\sigma_{sz}}$ is the axial stress of steel tube (defined as above); and $\mathbf{k}$ is the stress of confined concrete of layer $\mathbf{k}$.

6.4. Generation of axial load-strain curves

Based on layer discretization approach and equations, the iterative processes are introduced to obtain the axial load-strain curve of FRP-confined fire-damaged CFST column. The generation has two iterative processes (Figure 6.9 and Figure 6.10), one process used for determining the behavior of individual layer, the other one is the process that accumulate the behavior from all layers in order to get the total behavior of specimens. Details of processes are as below

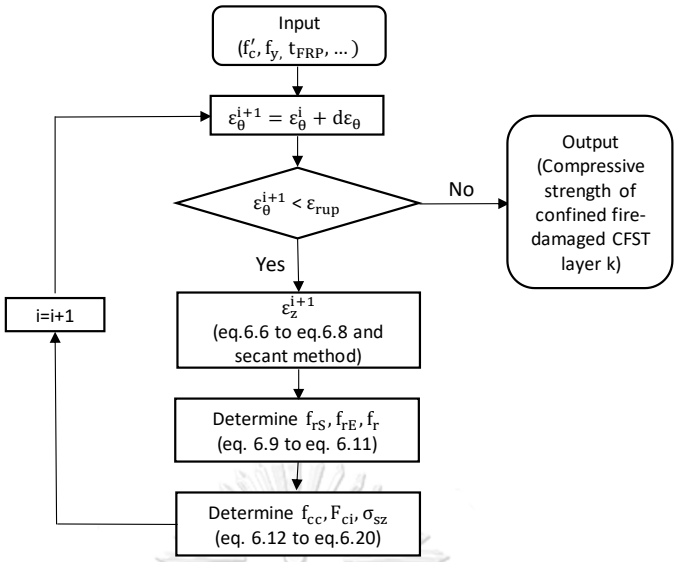

Figure 6.9 Iterative process 1 – Individual layer compressive behavior

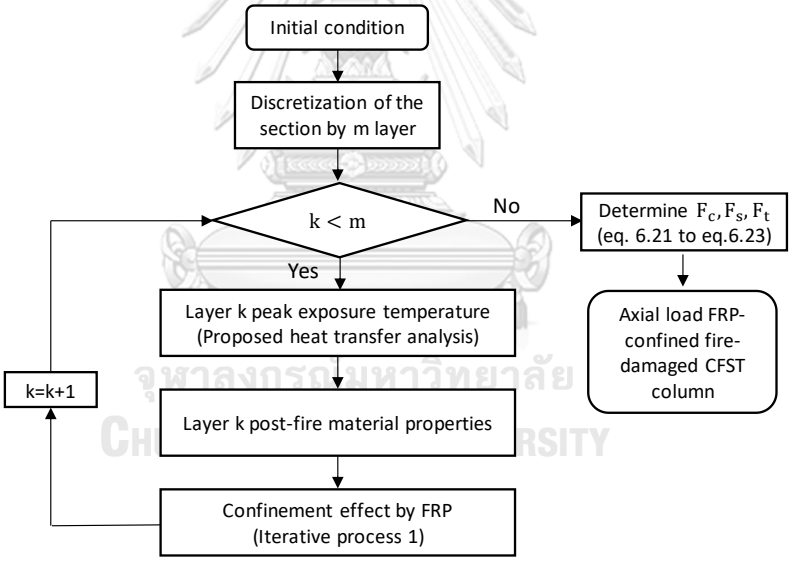

Figure 6.10 Iterative process 2– Compression behavior of specimens

6.5. Validation of proposed model

The proposed model to predict the compressive behavior of FRP-confined fire-damaged CFST columns are then verified with the conducted experimental results of this research.

Table 6.2 and Table 6.3 summarize and compare the predicted and experimental load capacity of specimens. The compressive behavior between proposed model and experiment are also shown in Figure 6.11 to Figure 6.30 by axial load-strain curves.

Table 6.2 Summary of predicted and experimental compressive strength values

No	Specimen Label	f_y (Mpa)	f_c' (Mpa)	Heating	CFRP wrap (layer)	GFRP wrap (layer)	$N_{predict}$ (kN)	N_{exp} (kN)	N_{pre}/N_{exp}
1	21A	400	NSC	-	-	-	1208	1207	**1.00**
2	21AC	400	NSC	-	1	-	1903	1838	**1.04**
3	21AG	400	NSC	-	-	1	1319	1326	**0.99**
4	21ACC	400	NSC	-	2	-	2139	2161	**0.99**
5	21AGC	400	NSC	-	1	1	1568	1574	**1.00**
6	21F	400	NSC	ISO	-	-	2381	2423	**0.98**
7	21FC	400	NSC	ISO	1	-	1298	1338	**0.97**
8	21FG	400	NSC	ISO		1	1902	1863	**1.02**
9	21FCC	400	NSC	ISO	2		1550	1496	**1.04**
10	21FGC	400	NSC	ISO	1	1	2344	2300	**1.02**
11	55A	400	HSC	-	-	-	607	692	**0.88**
12	55AC	400	HSC	-	1	-	805	849	**0.95**
13	55AG	400	HSC	-	-	1	786	794	**0.99**
14	55ACC	400	HSC	-	2	-	981	1001	**0.98**
15	55AGC	400	HSC	-	1	1	1008	1012	**1.00**
16	55F	400	HSC	ISO	-	-	1366	1306	**1.05**
17	55FC	400	HSC	ISO	1	-	803	800	**1.00**
18	55FG	400	HSC	ISO	-	1	1041	1048	**0.99**
19	55FCC	400	HSC	ISO	2	-	933	961	**0.97**
20	55FGC	400	HSC	ISO	1	1	1211	1222	**0.99**

Table 6.3 Comparison of the predicted and experimental results

Total of 20 specimens	Comparison of N_{pre}/N_{exp}
Max	1.05
Min	0.88
Mean	0.99
D(x)	0.036

The relationship axial load-axial curves strain between proposed models and experimental results for every tested specimen, are as follow

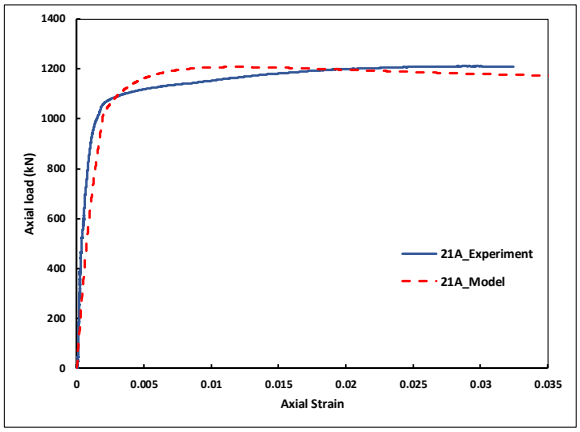

Figure 6.11 Specimen 21A (Axial load-strain curve; model and experiment results)

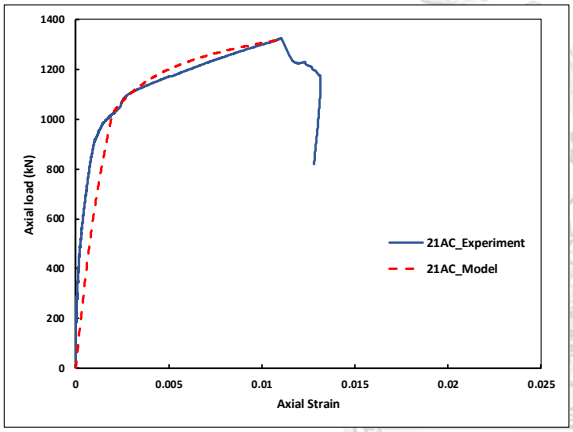

Figure 6.12 Specimen 21AC (Axial load-strain curve; model and experiment results)

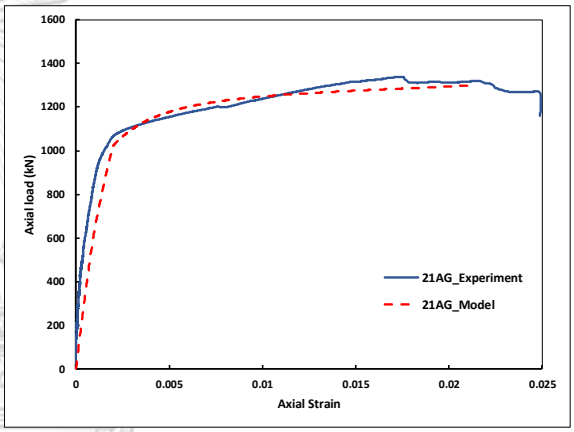

Figure 6.13 Specimen 21AG (Axial load-strain curve; model and experiment results)

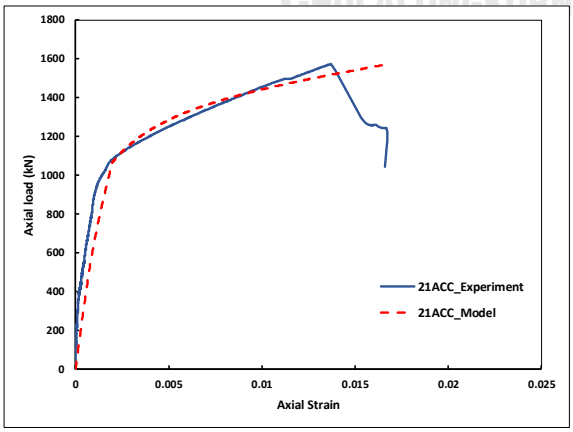

Figure 6.14 Specimen 21ACC (Axial load-strain curve; model and experiment results)

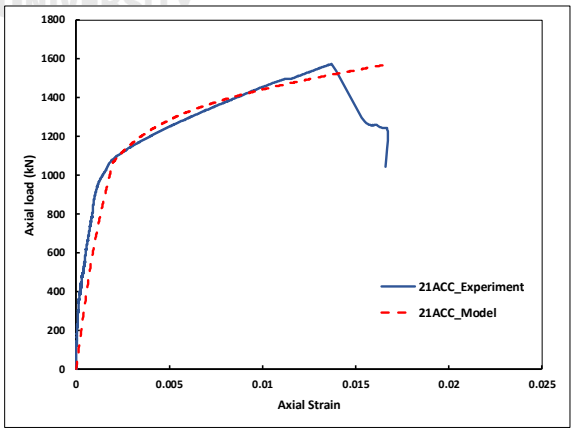

Figure 6.15 Specimen 21AGC (Axial load-strain curve; model and experiment results)

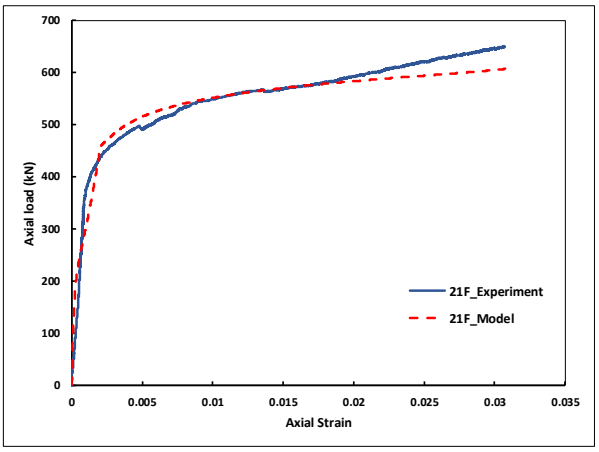

Figure 6.16 Specimen 21F (Axial load-strain curve; model and experiment results)

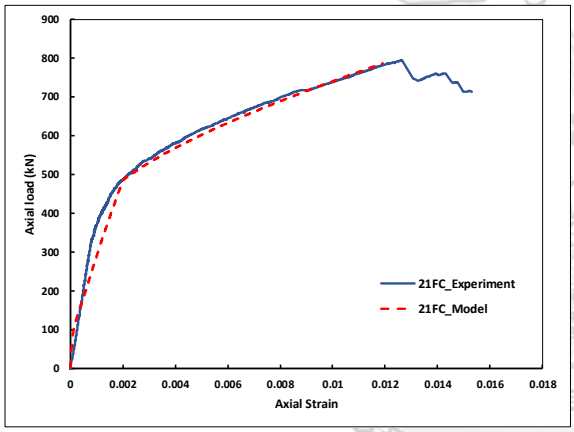

Figure 6.17 Specimen 21FC (Axial load-strain curve; model and experiment results)

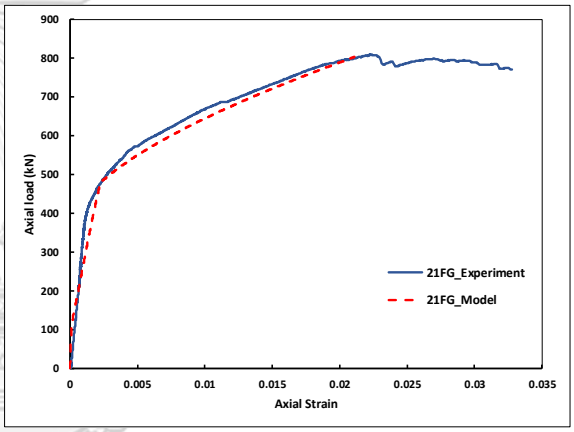

Figure 6.18 Specimen 21FG (Axial load-strain curve; model and experiment results)

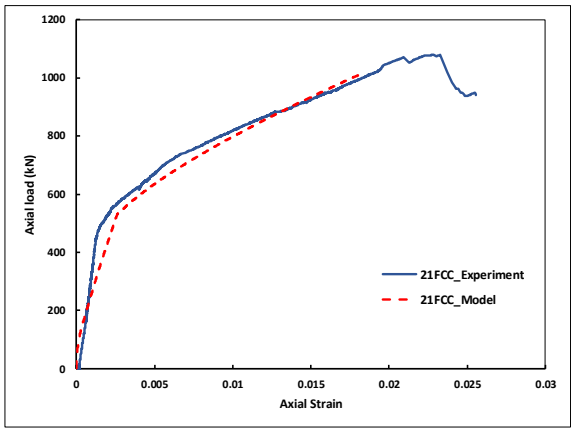

Figure 6.19 Specimen 21FCC (Axial load-strain curve; model and experiment results)

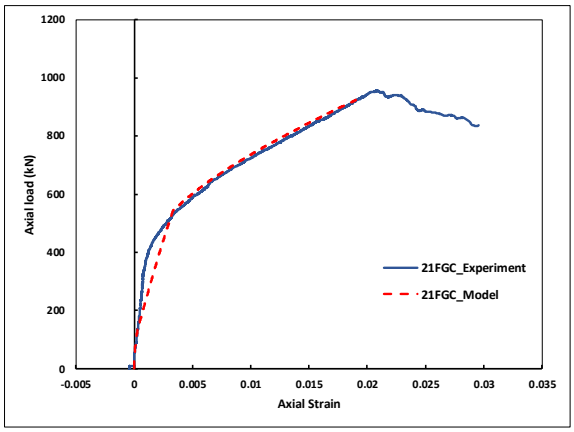

Figure 6.20 Specimen 21FGC (Axial load-strain curve; model and experiment results)

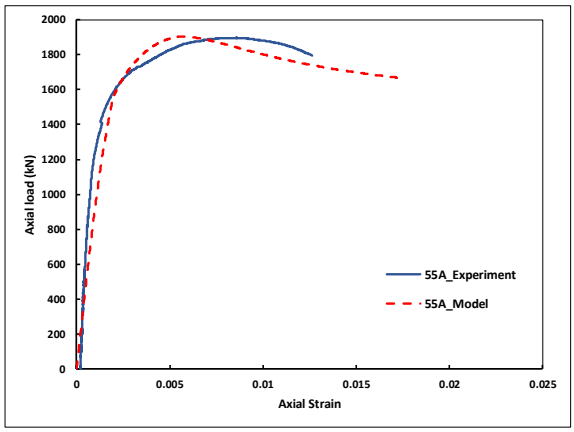

Figure 6.21 Specimen 55A (Axial load-strain curve; model and experiment results)

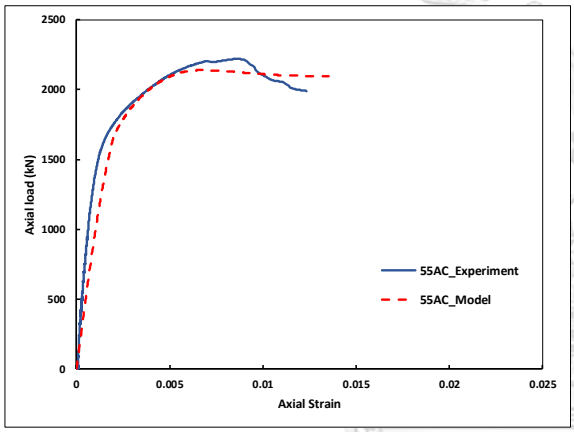

Figure 6.22 Specimen 55AC (Axial load-strain curve; model and experiment results)

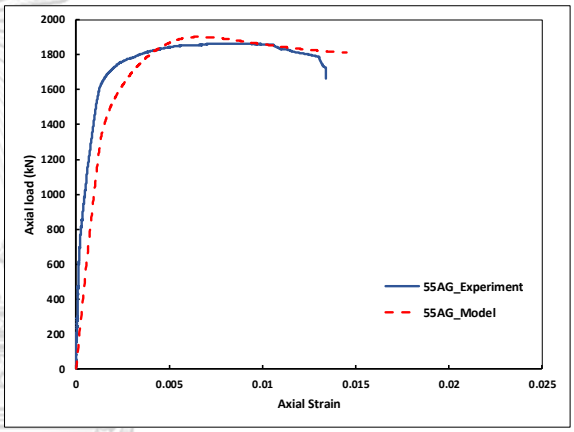

Figure 6.23 Specimen 55AG (Axial load-strain curve; model and experiment results)

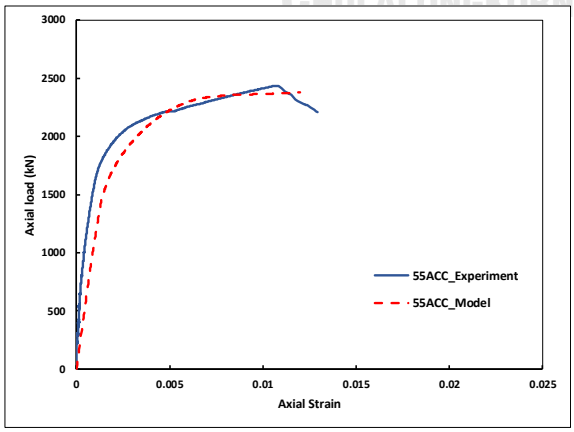

Figure 6.24 Specimen 55ACC (Axial load-strain curve; model and experiment results)

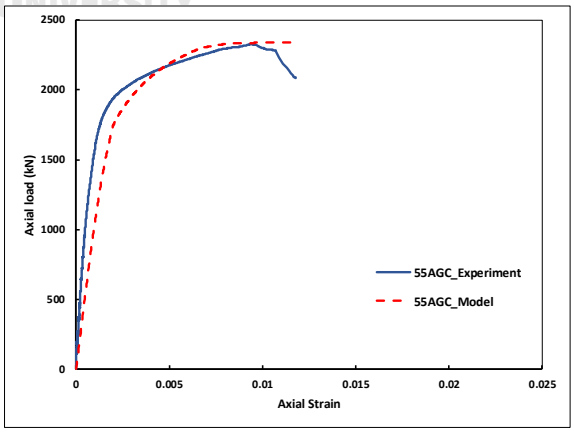

Figure 6.25 Specimen 55AGC (Axial load-strain curve; model and experiment results)

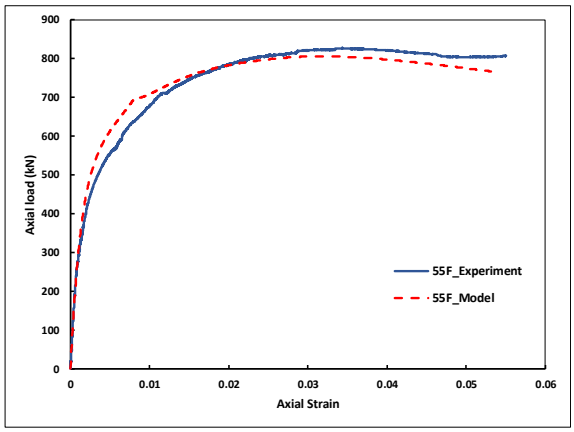

Figure 6.26 Specimen 55F (Axial load-strain curve; model and experiment results)

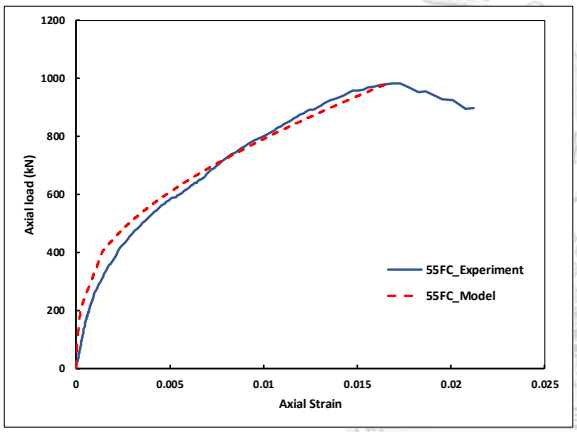

Figure 6.27 Specimen 55FC (Axial load-strain curve; model and experiment results)

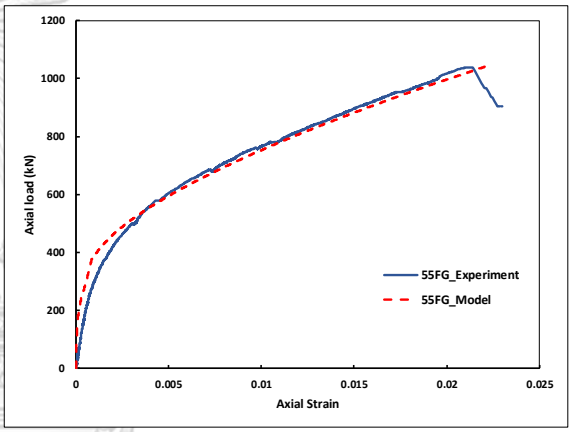

Figure 6.28 Specimen 55FG (Axial load-strain curve; model and experiment results)

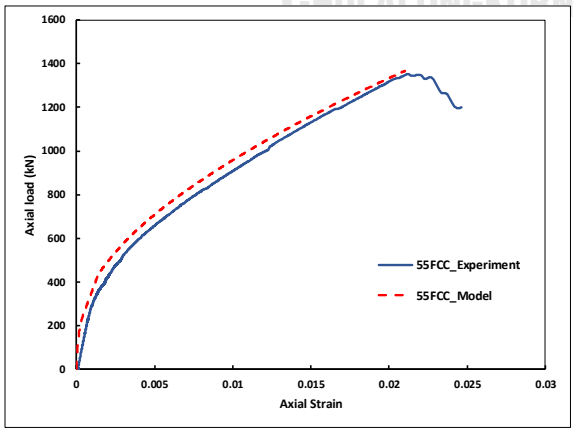

Figure 6.29 Specimen 55FCC (Axial load-strain curve; model and experiment results)

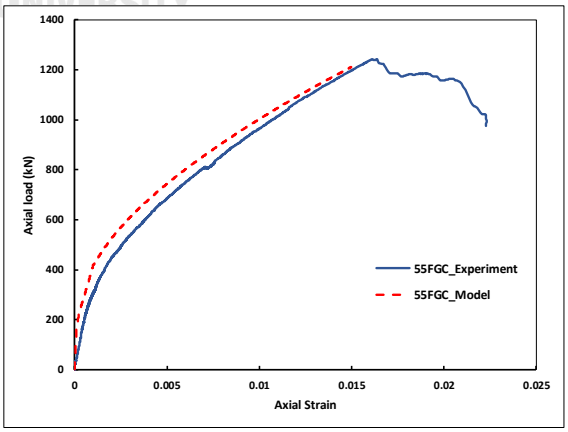

Figure 6.30 Specimen 55FGC (Axial load-strain curve; model and experiment results)

6.6. Summary of analytical results

Based on the theoretical background, the analysis for compressive behavior of FRP-confined fire-damaged CFST columns are proposed. The analytical results are in good agreement in axial load-strain data from experiment. Also, the validation of load capacity prediction is sufficiently accurate. The averaged mean value of 20 specimens is **0.99** with standard deviation of **0.036**.

CHAPTER 7
CONCLUSIONS AND RECOMMENDATIONS

In this research, both experimental and analytical studies are conducted to examine the compression behavior of FRP-confined for both fire-damaged and no fire-damaged (ambient) CFST columns at ambient conditions. The specific goals are to provide deeper understanding on post-fire residual strength of CFST columns and to estimate the effectiveness of using FRP wraps to strengthen on these damaged structures.

On the basis of the experimental and analytical studies, the compression behavior of FRP-confined fire-damaged CFST columns for both HSC and NSC infilled, the effectiveness of FRP wrap by types (GFRP, CFRP) and number of layers are clearly presented.

7.1. Conclusions

1) Although HSC infilled CFST columns are more seriously damaged by fire than NSC infilled CFST columns, the strengthening effectiveness for load-capacity from FRP wraps for HSC infilled CFST columns and NSC infilled CFST columns are similar.
2) FRP wrapping method showed as the better effective method for improving the load capacity of undamaged CFST columns than strengthening the CFST columns damaged by fire, for both NSC and HSC infill.
3) The more FRP layers applied, the specimens are more ductile. This phenomenon agrees with the NSC, HSC infilled fire-damaged CFST columns, NSC infilled at ambient. However, the opposite results were obtained from NSC infilled CFST columns at ambient.

4) Although the use of FRP can improve the stiffness of undamaged CFST columns. FRP wrapping is not effective to enhance the stiffness of fire-damaged CFST columns.
5) The use of glass fiber (GFRP) in hybrid wrapping is potential. It can prevent the effect of galvanic corrosion and prove as a good application for strengthening the fire-damaged behavior. Although having the competitive load capacity enhancement with CFRP wrapping, but the superior in ductility enhancement by using GFRP is well-performed.
6) Based on the FEM heat transfer analysis and herein research theoretical background, analytical models are proposed and showed the good agreement with the experimental results. With the axial load-strain curve obtained from the analysis, the compression behavior of FRP-confined fire-damaged CFST columns prediction can be fully predicted.

7.2. Recommendations

Further works are recommended to provide more knowledge and understanding for the behavior of fire-damaged CFST columns and the applications of FRP on these structures. Further works are required on the assessment of the other fire conditions and factors affecting the post-fire residual behavior such as geometry of specimens, the air gap between steel tube and concrete, or the sustained load as in real CFST columns.

Besides, the model should be verified with more experimental database in the future to obtain the better validation and wider range of uses. The models herein also need to improve for full-scale CFST columns (not tubular) and should be shorten in calculation approach in order to apply in practice.

REFERENCES

Abbas, H., Al-Salloum, Y., Alsayed, S., Alhaddad, M., & Iqbal, R. (2017). Post-heating response of concrete-filled circular steel columns. *KSCE Journal of Civil Engineering, 21*(4), 1367-1378.

ACI, A. J. A. C. I., Farmington Hills, USA. (2008). 440.2 R-08: Guide for the design and construction of externally bonded FRP systems for strengthening concrete structures.

ANSYS, I. (2004). ANSYS Release 9.0 Documentation. SAS IP. In: Inc.

Attard, M., & Setunge, S. (1996). Stress-strain relationship of confined and unconfined concrete. *ACI Master, 93*(5), 432-442.

Bank, L. C. (2006). *Composites for construction: Structural design with FRP materials*: John Wiley & Sons.

Barrington, J., Dickson, D., Bisby, L., & Stratford, T. (2011). Strain development and hoop strain efficiency in FRP confined square columns. *Special Publication, 275*, 1-20.

CEN, E. J. E. S. (2002). 1-2: Eurocode 1: Actions on structures–Part 1-2: General actions–Actions on structures exposed to fire.

Chang, Y.-F., Chen, Y.-H., Sheu, M.-S., Yao, G. C. J. C., & Research, C. (2006). Residual stress–strain relationship for concrete after exposure to high temperatures. *Cement and Concrete Research*, *36*(10), 1999-2005.

Ding, J., & Wang, Y. J. J. o. C. S. R. (2008). Realistic modelling of thermal and structural behaviour of unprotected concrete filled tubular columns in fire. *Journal of Construction Steel Research*, *64*(10), 1086-1102.

Dong, J., Wang, Q., & Guan, Z. (2013). Structural behaviour of recycled aggregate concrete filled steel tube columns strengthened by CFRP. *Engineering structures, 48*, 532-542.

Du, X., Chen, Y. L., Li, Y. C., Nie, D. X., & Huang, J. (2014). *Mechanical Properties of*

Polypropylene Fiber Concrete after High Temperature. Paper presented at the Applied Mechanics and Materials.

Ekmekyapar, T., & Al-Eliwi, B. J. (2016). Experimental behaviour of circular concrete filled steel tube columns and design specifications. *Thin-Walled Structures, 105*, 220-230.

EN, C. J. B., Belgium: Comité Européen de Normalisation. (2005). 1-2, Eurocode 4: Design of composite steel and concrete structures, Part 1.2: General rules-Structural fire design.

Eringen, A. C. J. I. J. o. E. S. (1983). Theories of nonlocal plasticity. *21*(7), 741-751.

Gillie, M. (2014). *Temperature Modeling for Concrete-Filled Steel Tube's Cross Section in Fire.* Paper presented at the 2014 International Conference on Mechanics and Civil Engineering (icmce-14).

Han, L.-H., Huo, J.-S., & Wang, Y.-C. J. J. o. C. S. R. (2005). Compressive and flexural behaviour of concrete filled steel tubes after exposure to standard fire. *Journal of Constructional Steel Research*, *61*(7), 882-901.

Han, L.-H., Huo, J.-s., & Yang, Y.-F. (2002). -Concrete-filled HSS columns after exposure to the Iso-834 standard fire. In *Advances in Steel Structures (ICASS'02)* (pp. 1127-1134): Elsevier.

Han, L.-H., & Huo, J.-s. J. J. o. S. E. (2003). Concrete-filled hollow structural steel columns after exposure to ISO-834 fire standard. *Journal of Structural Engineering*, *129*(1), 68-78.

Han, L.-H., Li, W., & Bjorhovde, R. (2014). Developments and advanced applications of concrete-filled steel tubular (CFST) structures: Members. *Journal of Constructional Steel Research, 100*, 211-228.

Hu, Y., Yu, T., & Teng, J. (2011). FRP-confined circular concrete-filled thin steel tubes under axial compression. *Journal of Composites for Construction, 15*(5), 850-860.

Kitada, T. J. E. s. (1998). Ultimate strength and ductility of state-of-the-art concrete-

filled steel bridge piers in Japan, *Engineering Structures*, *20*(4-6), 347-354.

Kwan, A., Dong, C., & Ho, J. (2015). Axial and lateral stress–strain model for FRP confined concrete. *Engineering Structures, 99*, 285-295.

Lai, M., & Ho, J. (2016). A theoretical axial stress-strain model for circular concrete-filled-steel-tube columns. *Engineering Structures, 125*, 124-143.

Lenwari, A., Rungamornrat, J., & Woonprasert, S. (2016). Axial compression behavior of fire-damaged concrete cylinders confined with CFRP sheets. *Journal of Composites for Construction, 20*(5), 04016027.

Lin, M.-L., & Tsai, K.-C. (2003). *Mechanical behavior of double-skinned composite steel tubular columns.* Paper presented at the Proceedings of the Joint NCREE-JRC Conference, Taipei, Taiwan.

Liu, D., Gho, W.-M., & Yuan, J. (2003). Ultimate capacity of high-strength rectangular concrete-filled steel hollow section stub columns. *Journal of Constructional Steel Research, 59*(12), 1499-1515.

Liu, L., & Lu, Y. (2010). Axial bearing capacity of short FRP confined concrete-filled steel tubular columns. *Journal of Wuhan University of Technology-Mater. Sci. Ed., 25*(3), 454-458.

Lu, Y., Li, N., & Li, S. (2014). Behavior of FRP-confined concrete-filled steel tube columns. *Polymers, 6*(5), 1333-1349.

Milanović, M., Cvetkovska, M., & Knežević, P. (2016). Load-bearing capacity of fire exposed composite columns. *Građevinar, 67*(12.), 1187-1197.

Mirmiran, A., & Shahawy, M. (1997). Behavior of concrete columns confined by fiber composites. *Journal of structural engineering, 123*(5), 583-590.

Nethercot, D. (2003). *Composite construction*: CRC Press.

O'Shea, M., & Bridge, R. (1994). *High strength concrete in thin-walled circular steel sections.* Paper presented at the Proceedings of the 6th International Symposium on Tubular Structures.

Prabhu, G. G., & Sundarraja, M. (2013). Behaviour of concrete filled steel tubular (CFST) short columns externally reinforced using CFRP strips composite. *Construction and Building Materials, 47*, 1362-1371.

Ravindran, E. S., & Hameed, E. A. S. (2016). An Experimental Study on Hybrid Fibre Reinforced Concrete Filled Steel Tube Columns.

Rush, D. I. (2013). Fire performance of unprotected and protected concrete filled steel hollow structural sections. *Thesis Book*.

Rush, D. I., Bisby, L. A., & Jowsey, A. (2015). Residual capacity of fire-exposed concrete-filled steel hollow section columns. *Engineering Structures, 100*, 550-563.

Scheuerman A, B. C. F. (2002 Mar 12.). An analysis of the cause of the collapse of the WTC towers &possible lessons learned to improve high-rise building life safety. *(Report No. 10 of the Nassau County Fire Training Academy and high-rise Fire Safety Director NYC)*.

Shahidan, S., Salwa, S., Zuki, M., Keong, C., & Jayaprakash, J. (2016). Repaired of fire-damaged concrete-filled double skin steel tubular (CFDST) columns with fiber reinforced polymer (FRP). *ARPN J. Eng. Appl. Sci., 11*, 3718-3372.

Tao, Z., Han, L. H., & Wang, L.-L. (2007a). Compressive and flexural behaviour of CFRP-repaired concrete-filled steel tubes after exposure to fire. *Journal of Constructional Steel Research, 63*(8), 1116-1126.

Tao, Z., Han, L. H., & Zhuang, J.-P. (2007b). Axial loading behavior of CFRP strengthened concrete-filled steel tubular stub columns. *Advances in Structural Engineering, 10*(1), 37-46.

Teng, J., Fernando, D., Yu, T., & Zhao, X. (2011). Treatment of steel surfaces for effective adhesive bonding. In *Advances in FRP composites in civil engineering* (pp. 865-868): Springer.

Teng, J., Yu, T., & Fernando, D. (2012). Strengthening of steel structures with fiber-reinforced polymer composites. *Journal of Constructional Steel Research, 78*, 131-143.

Uy, B. (1998). Concrete-filled fabricated steel box columns for multistorey buildings: behaviour and design. *Progress in Structural Engineering and Materials, 1*(2), 150-158.

Uy, B. (2001). Strength of short concrete filled high strength steel box columns. *Journal of Constructional Steel Research, 57*(2), 113-134.

Wakabayashi, M. (1987). *A historical study of research on composite construction in Japan.* Paper presented at the Composite construction in steel and concrete.

Wang, Tao, Z., Han, L.-H., Uy, B., Lam, D., & Kang, W.-H. J. E. S. (2017). Strength, stiffness and ductility of concrete-filled steel columns under axial compression. *Engineering Structures*, *135*, 209-221.

Wang, K., Chen, Y., Wan, J., Han, S., & Liao, L. (2018). Compressive behavior of post-heated circular CFST short columns externally strengthened with CFRP sheets. *Journal of Adhesion Science and Technology, 32*(8), 833-853.

Yao, Y., & Hu, X. X. (2015). Cooling behavior and residual strength of post-fire concrete filled steel tubular columns. *Journal of Constructional Steel Research, 112*, 282-292.

VITA

NAME	Dat Thanh Vu
DATE OF BIRTH	18 Sep 1994
PLACE OF BIRTH	Nha Trang, Viet Nam
INSTITUTIONS ATTENDED	- Ho Chi Minh University of Technology, Viet Nam - Chulalongkorn University, Thailand
HOME ADDRESS	Room 1226, CU i-house, Soi Chula 9, Wang Mai, Pathum Wan, Bangkok, 10330

APPENDIX A: CONSTANTS DEFINING SHAPE OF STRESS-STRAIN CURVE

The constants defining shape of the stress-strain curve A & B are given by:

For the ascending portion of the stress-strain curve

$$A = \frac{E_c \varepsilon_{cc}}{f_{cc}} \tag{A-1}$$

$$B = \frac{(A-1)^2}{0.55} - 1 \tag{A-2}$$

For the descending portion of the stress-strain curve

$$A = \left[\frac{\varepsilon_{2i} - \varepsilon_i}{\varepsilon_{cc}}\right]\left[\frac{\varepsilon_{2i}(f_i/\varepsilon i)}{(f_{cc} - f_i)} - \frac{4\varepsilon_i(f_{2i}/\varepsilon_{2i})}{(f_{cc} - f_{2i})}\right] \tag{A-3}$$

$$B = [\varepsilon_i - \varepsilon_{2i}]\left[\frac{(f_i/\varepsilon i)}{(f_{cc} - f_i)} - \frac{4(f_{2i}/\varepsilon_{2i})}{(f_{cc} - f_{2i})}\right] \tag{A-4}$$

where f_i and εi are the axial stress and axial strain at the inflexion point; f_{2i} is the axial stress at axial strain ε_{2i}; and ε_{2i} is equal to ($2\varepsilon i$-ε_{cc}). Their values vary with the concrete strength and confining stress, and given by:

$$\frac{f_i}{f_{cc}} = \frac{(1.41 - 0.17\ln(f_c')) - 1}{5.06\left(\frac{\sigma_r}{f_c'}\right)^{0.57} + 1} + 1 \tag{A-5}$$

$$\frac{\varepsilon_i}{\varepsilon_{cc}} = \frac{(2.50 - 0.30\ln(f_c')) - 2}{1.12\left(\frac{\sigma_r}{f_c'}\right)^{0.26} + 1} + 2 \tag{A-6}$$

$$\frac{\varepsilon_{2i}}{\varepsilon_{cc}} = \frac{(1.45 - 0.25\ln(f_c')) - 1}{6.35\left(\frac{\sigma_r}{f_c'}\right)^{0.62} + 1} + 1 \tag{A-7}$$

where f_{cc} and ε_{cc} are the peak axial stress and corresponding strain which can be used by the equations in Chapter 6.

APPENDIX B: COMPRESSIVE STRENGTH TEST OF CONCRETE

The infill concrete compressive strength was tested by plain standard concrete for both HSC and NSC concrete. Total of 10 plain cylinder specimens were casted, 5 for HSC and 5 for NSC. In each type of compressive strength, 2 cylinders were put into the fire furnace to obtain the compressive strength of plain concrete after fire test, however, it collapsed all. The others 6 specimens at ambient were tested for compressive strength, 3 specimens for HSC and 3 specimens for NSC. The results (calculated following ASTM C39) and procedures are shown as below:

Figure B-1 Concrete compressive strength before testing

Figure B-2 Concrete compressive strength on testing

Table B-1 Concrete compressive strength test results

Specimen	P max (kN)	Area (m2)	fc (Mpa)	fc - mean	Difference (%)	Status (<15%)	fc'- design (Mpa)	fc' (Mpa)
S21-1	484.4	0.0176	27.42		-1.23	ok		
S21-3	450.2	0.0176	25.49	27.77	-8.20	ok	24	**27.8**
S21-4	536.8	0.0176	30.39		9.44	ok		
S55-1	1019.9	0.0176	57.75		8.21	ok		
S55-2	872.1	0.0176	49.38	53.36	-7.46	ok	55	**53.4**
S55-4	935.3	0.0176	52.96		-0.75	ok		

APPENDIX C: TENSILE STRENGTH TEST OF FIBER REINFORCED POLYMER SHEETS COUPON

The coupon test of FRP sheets was conducted to obtain and examine the real properties of FRP. The procedures are followed strictly to ACI 440.2R-17.

A total of 10 coupons are conducted, 5 coupons for CFRP sheets and 5 coupons for GFRP sheets. The chosen sheets have the length around 45cm, together with both ends inside the tab of 35cm, so the established coupon FRP has the length of 80cm. The reason of having the long length is to fit with the tested machine.

There are 3 Strain Gage set up in each coupon specimens, all are located in the middle length, but in different positions. The values of dimensions and distances Figure B-1 as are: t=5mm; w=50mm; n=25mm; m=2mm.

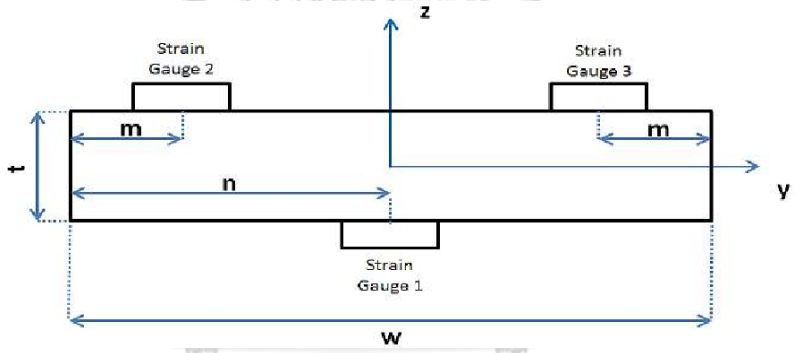

Figure C-1 Coupon's cross section

Figure C-2 Coupon specimens with set up SG

The tested results failure and modes of coupon specimens are shown as below:

Table C-1 CFRP coupon test results

CFRP					
CFRP-No		**2**	**3**	**4**	**5**
GFRP-Thick	mm	0.13	0.13	0.13	0.13
Thickness	mm	1.25	1.5	1.85	1.9
Width	mm	50	50	50	50
Length	mm	435	440	430	445
Elongation	mm	4.65	4.09	3.85	4.56
E-Modulus	Mpa	289100	274000	249500	291700
% Elongation at Test	%	1.07	0.93	0.90	1.02
% Elongation at Ultimate (Specification)	%	1.55	1.55	1.55	1.55
Tensile Strength	Mpa	4481	4247	3867	4521

Table C-2 GFRP coupon test results

GFRP					
GFRP-No		2	3	4	5
GFRP-Thick	mm	0.17	0.17	0.17	0.17
Thickness	mm	1.95	2.7	2.2	1.9
Width	mm	50	50	50	50
Length	mm	435	430	435	440
Elongation	mm	3.85	5.64	6.53	8.06
E-Modulus	Mpa	103100	109500	99520	95300
% Elongation at Test	%	0.89	1.31	1.50	1.83
% Elongation at Ultimate (Specification)	%	3.1	3.1	3.1	3.1
Tensile Strength	Mpa	3196	3395	3085	2954

Table C-3 FRP coupon test results

FRP-coupon results	CFRP	CFRP (spe)	GFRP	GFRP (spe)
E-Modulus	276075	225000	101855	70000
% Elongation at Ultimate (Spe)	1.55	1.55	3.1	3.1
Tensile Strength	4279	3500	3158	2250

Figure C-3 FRP Coupon's test failure modes

Total 10 specimens were tested, 1 specimen (GFRP-1) has the expected failure mode of FRP rupture. Other 9 specimens are failure by rupture near the tab, it is not as expected. The reasons explained by the insufficient thickness of tabs, so the concentration load occurred at that positions. Due to the test could not last long until expected failure, the Elongation at Ultimate is followed as the supplier's specifications for all of coupon specimens.

Figure C-4 shows the behavior of coupon test for both CFRP and GFRP. Noted that the data of the first specimens for both CFRP and GFRP were not collected well because of the high values of set up range in data logger.

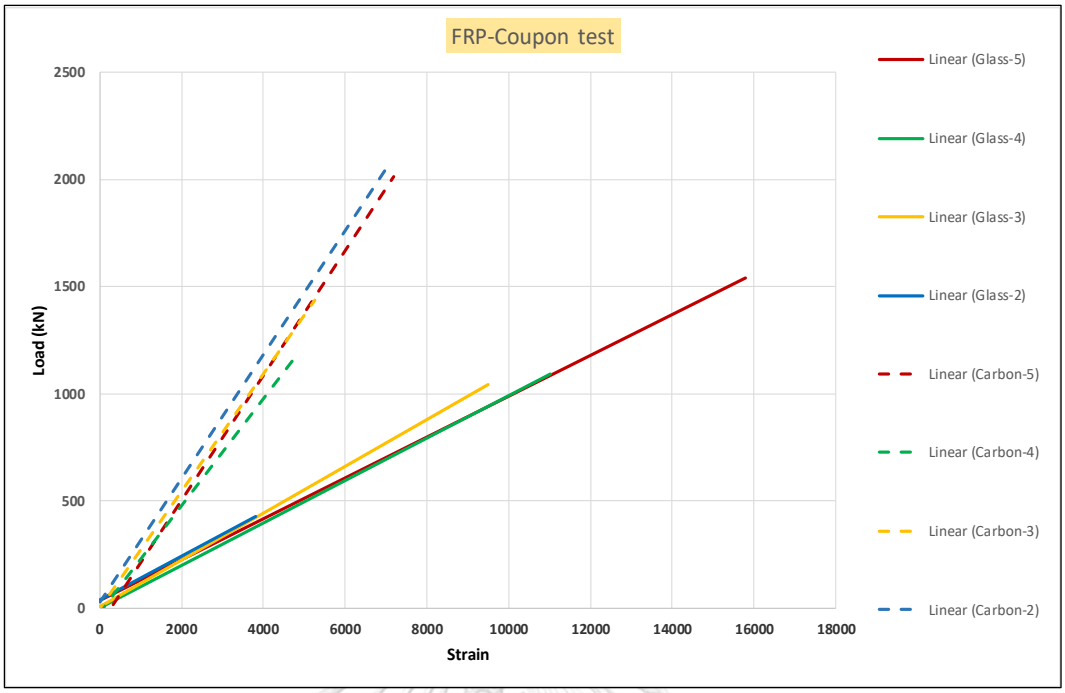

Figure C-4 Stress-strain curve of FRP coupons.

APPENDIX D: ANALYTICAL MODEL IN MATLAB CODE

1. Main model code

```
Analytical work
% Analytical work-verified by experiment

% 21-03-19
% Dat Thanh Vu
%-------------------------------------------------------------------
clear all

% Specimens properties
DAT_21AGC;

%-------------------------------------------------------------------
% Initial condition

et=0;sst=0;vmst=0;
ez=0;ssz=0;
ssr=0;

Ez=[];Et=[];vm=[];
Ssz=[];Sst=[];Ssr=[];Fcc=[];Fr=[];Ecc=[];

i=0;k=0;p=0;n=0;
%-------------------------------------------------------------------

% ----------------------SOLUTION-----------------------------------

% Stress-strain relationship for steel (Hooke's Law Generalization)
while ez<1.7/100
%     vmst=sqrt(2)/2*sqrt((ssz-sst)^2+(ssz-ssr)^2+(sst-ssr)^2);
        vmst=sqrt(ssz^2+sst^2-ssz*sst);
    if vmst < fy                % Elastic Range
        D=Es/(1-vs^2)*[1 vs;vs 1];
%         D=[K+4/3*G K-2/3*G K-2/3*G;
%             K-2/3*G K+4/3*G K-2/3*G;
%             K-2/3*G K-2/3*G K+4/3*G];
        det=-5e-6;
        p=p+1;
    else                        % Perfecly Plastic Range
        sz=1/3*(2*ssz-sst);
        st=1/3*(2*sst-ssz);
        D=Es/(sz^2+st^2+2*vs*sz*st)*[st^2 -sz*st;-sz*st sz^2];
        det=-5e-6;
        n=n+1;
    end

% Secant method to find converged axial strain

    % Initial bracket
    a=-0.001;b=0.03;
    fa=f(a,det,D,sst,et,ssz,ez);
```

```
    % Condition
        dx=inf;
        while abs(dx)>1e-5
            fb=f(b,det,D,sst,et,ssz,ez);
            dx=(b-a)*fb/(fb-fa);

            a=b;
            fa=fb;

            b=b-dx;
        end

% Hoop strain, stress; Axial strain, stress; confined concrete stress

    [fezb,ssz,sst,fr,frs,fre,de,ds]=f(b,det,D,sst,et,ssz,ez);
    ez=b;
    k=k+1;
    et=et+det;
    vm(k,1)=vmst;
    Ez(k,1)=ez;
    Et(k,1)=et;
    Ssz(k,1)=ssz;
    Sst(k,1)=sst;
    ssr=fr;
    Ssr(k,1)=ssr;
    Fr(k,1)=fr;
    Frs(k,1)=frs;
    Fre(k,1)=fre;
 %--------Attard model (complex but wide range of fc)----------------
-
 %%Kwan 2016 paper
        % Peak stress and correcponding strain
    ecc=eco*(1+(17-0.06*fc)*fr/fc);
    fccp=fc*(1+4.1*(fr/fc));
%     fccp=fccpe;
%     ecc=eccpe;
%     fc=4.1*fr-fccp;
%     eco=ecc/(1+(17-0.06*fc)*fr/fc);
    coe=ez/ecc;
    Ecc(k,1)=ecc;
    if ez<ecc
        % Assending branch
        fpl=0.45*fccp;
        A=Ecit*ecc/fccp;
        B=((A-1)^2/anphat*(1-fpl/fccp)+A^2*(1-
anphat)/anphat^2*fpl/fccp*(1-fpl/fccp)-1);

    else
        % Descending branch
        fi=fccp*((0.41-0.17 *log(fc))/(5.06*(fr/fc)^0.57+1)+1);
        f2i=fccp*((0.45-0.25*log(fc))/(6.35*(fr/fc)^0.62+1)+1);
        ei=ecc*((0.5-0.3*log(fc))/(1.12*(fr/fc)^0.26+1)+2);
        e2i=2*ei-ecc;
        Ei=fi/ei; E2i=f2i/e2i;

        A=((e2i-ei)/ecc)*(e2i*Ei/(fccp-fi)-4*ei*E2i/(fccp-f2i));
```

```
        B=(ei-e2i)*(Ei/(fccp-fi)-4*E2i/(fccp-f2i));
    end
    fcc=fccp*((A*coe+B*coe^2)/(1+(A-2)*coe+(B+1)*coe^2));
    Fcc(k,1)=fcc;
end
% Find the load and capacity of concrete, steel and CFST
Fs=Ssz*As*10^3; %kN
Fc=Fcc*Ac*10^3; %kN
Ft=Fs+Fc;       %kN
```

2. Confining pressure code (for secant method)

```
function [f,ssz,sst,fr,frs,fre,de,ds]=f(x,det,D,sst,et,ssz,ez)

%-------------------------------------------------------------------------
% Input properties
% Specimen name:
DAT_21AGC;
%-------------------------------------------------------------------------
% Strain increment
desz=x-ez;
dest=det;

de=[desz;dest];
ds=D*de;

% Axial and hoop stress of steel tube
    ssz=ssz+ds(1,1);
    sst=sst+ds(2,1);

% Confining stress from steel tube
    frs=-2*t/(D0-2*t)*sst;

% Confining stress from FRP
    if et*Efrp>syfrp
        se=syfrp;    % Assume efrp=esteel in hoop direction
    else
        se=Efrp*et;
    end

    fre=-2*tfrp/(D0-2*t)*se;

% Confining pressure for confined concrete
    fr=frs+fre;
% Function
    Ls=0.6466;
    if fc>30
        m=-0.05;
    else
        m=0;
    end

f=Ls*(fc/30)^m*(eco*(1+0.75*(-et/eco))^0.7-
eco*exp(7*(et/eco))+0.07*(-et)^0.7*(1+26.8*(fr/fc)))-x;
```

APPENDIX E: EXPERIMENTAL RESULTS OF SPECIMENS

Name: **21FC_1**

Test order: 1

No: 7-1

Concrete Strength	Fire damaged	CFRP	GFRP	Batch
21	ISO 2-hour	1	-	1

Ultimate strength	$\varepsilon_{L,p}$	ε_u	ε_y	Ductility	Composite modulus	Failure mode
$N_{max}(kN)$	-	-	-	$DI = \frac{\varepsilon_u}{\varepsilon_y}$	$E_{sc} = \frac{f_{sc,p} - f_{50}}{\varepsilon_{L,p} - \varepsilon_{50}}$	FRP rupture
589.6	317	11341	2527	4.49	1.61	

Load-Axial Strain	Axial stress- Axial strain	Hoop strain-Axial Strain
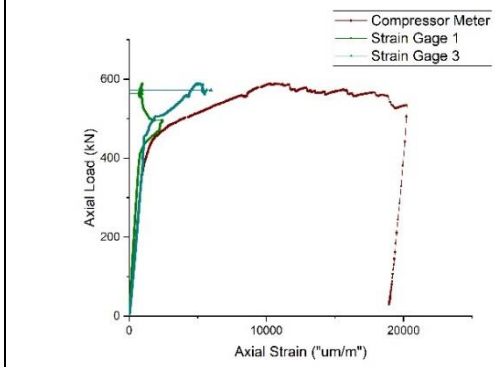	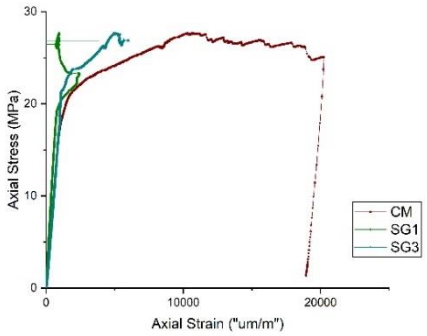	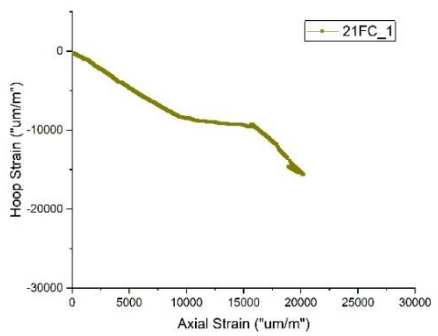

Notes:

- SG1 is changed direction because of FRP enlarged by hoop strain
- First tested specimen. Different result compared with 21FC batch 2

Name: **21FC_2**

Test order: 21

No: 7-2

Concrete Strength	Fire damaged	CFRP	GFRP	Batch
21	ISO 2-hour	1	-	2

Ultimate strength	$\varepsilon_{L,p}$	ε_u	ε_y	Ductility	Composite modulus	Failure Mode
$N_{max}(kN)$	-	-	-	$\mu_u = \frac{\varepsilon_u}{\varepsilon_y}$	$E_{sc} = \frac{f_{sc,p} - f_{50}}{\varepsilon_{L,p} - \varepsilon_{50}}$	FRP rupture
793.9	344	12637	1231	10.27	1.89	

Load-Axial Strain	Axial stress- Axial strain	Hoop strain-Axial Strain
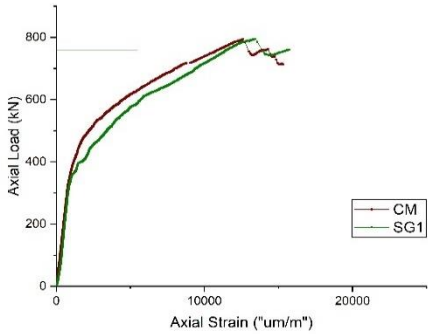	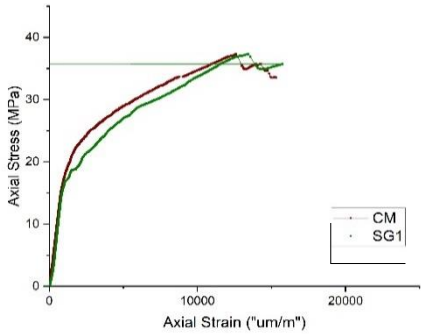	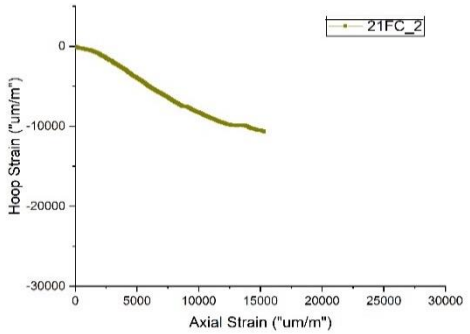

Name: **55FC_1**

Test order: 2

No: 17-1

Concrete Strength	Fire damaged	CFRP	GFRP	Batch
55	ISO 2-hour	1	-	1

Ultimate strength	$\varepsilon_{L,p}$	ε_u	ε_y	Ductility	Composite modulus	Failure mode
$N_{max}(kN)$	-	-	-	$\mu_u = \frac{\varepsilon_u}{\varepsilon_y}$	$E_{sc} = \frac{f_{sc,p} - f_{50}}{\varepsilon_{L,p} - \varepsilon_{50}}$	FRP rupture
918.9	345	12589	1269	**9.92**	**1.70**	

Load-Axial Strain	Axial stress- Axial strain	Hoop strain-Axial Strain
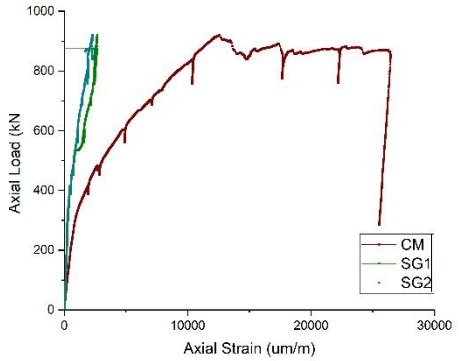	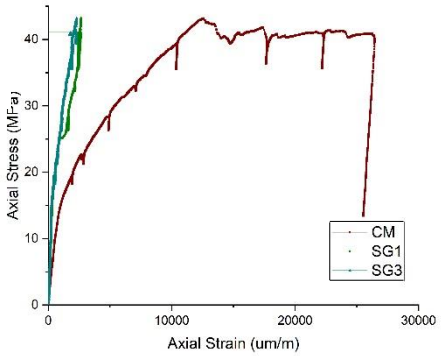	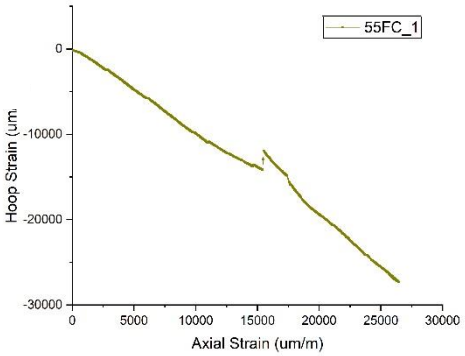

Notes: - The more not continuous in load control, the more difference in the SG and CM.

Name: **55FC_2**

Test order: 22

No: 17-2

Concrete Strength	Fire damaged	CFRP	GFRP	Batch
55	ISO 2-hour	1	-	2

Ultimate strength	$\varepsilon_{L,p}$	ε_u	ε_y	Ductility	Composite modulus	Failure mode
$N_{max}(kN)$	-	-	-	$\mu_u = \frac{\varepsilon_u}{\varepsilon_y}$	$E_{sc} = \frac{f_{sc,p} - f_{50}}{\varepsilon_{L,p} - \varepsilon_{50}}$	FRP rupture
985.2	371	17503	1461	**11.98**	**1.33**	

Load-Axial Strain	Axial stress- Axial strain	Hoop strain-Axial Strain
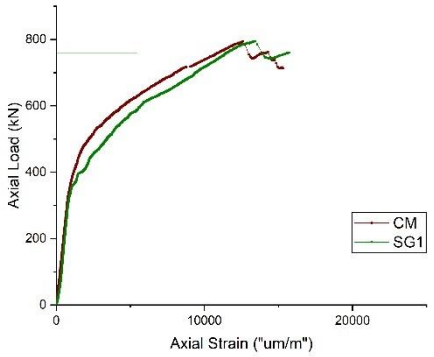	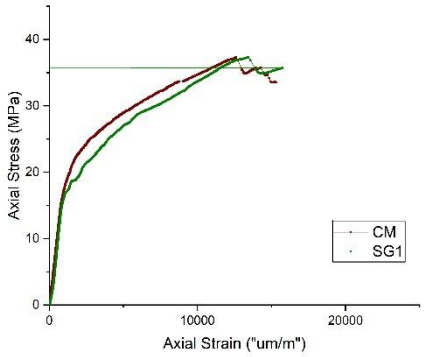	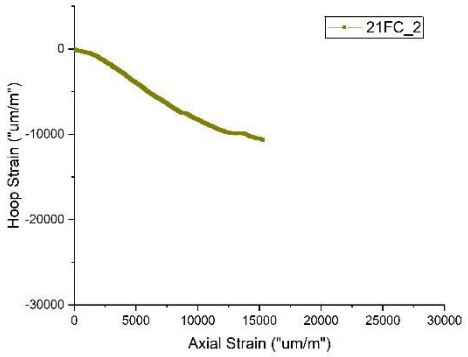

Notes:

Name: **21AC_1**

Test order: 3

No: 2-1

Concrete Strength	Fire damaged	CFRP	GFRP	Batch
21	-	1	-	1

Ultimate strength	$\varepsilon_{L,p}$	ε_u	ε_y	Ductility	Composite modulus	Failure mode
$N_{max}(kN)$	-	-	-	$\mu_u = \frac{\varepsilon_u}{\varepsilon_y}$	$E_{sc} = \frac{f_{sc,p} - f_{50}}{\varepsilon_{L,p} - \varepsilon_{50}}$	FRP rupture
1324.7	88.4	11074	1003	11.04	2.62	

Load-Axial Strain	Axial stress- Axial strain	Hoop strain-Axial Strain
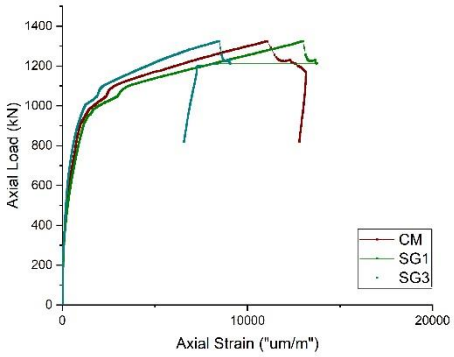	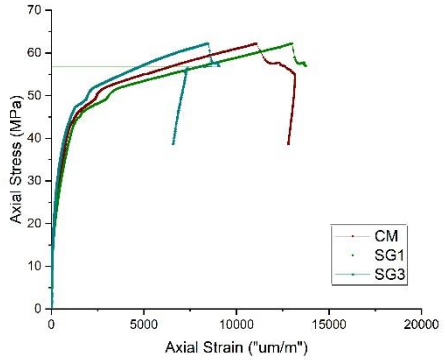	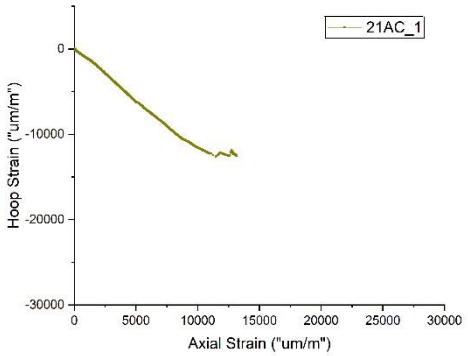

Notes:

Name: **21AC_2**

Test order: 23

No: 2-2

Concrete Strength	Fire damaged	CFRP	GFRP	Batch
21	-	1	-	2

Ultimate strength	$\varepsilon_{L,p}$	ε_u	ε_y	Ductility	Composite modulus	Failure mode
$N_{max}(kN)$	-	-	-	$\mu_u = \frac{\varepsilon_u}{\varepsilon_y}$	$E_{sc} = \frac{f_{sc,p} - f_{50}}{\varepsilon_{L,p} - \varepsilon_{50}}$	FRP rupture
1327.6	98	-	-	-	-	

Load-Axial Strain	Axial stress- Axial strain	Hoop strain-Axial Strain
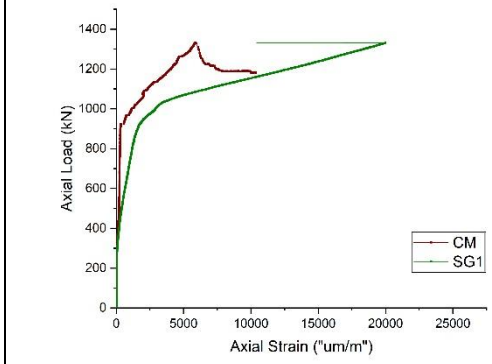	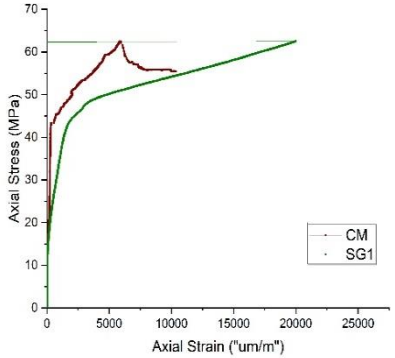	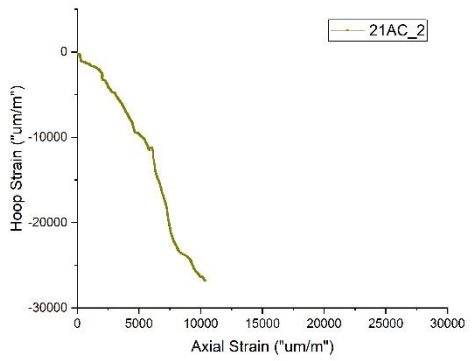

Notes: - Compressor meter got problem

Name: **55AC_1**

Test order: 4

No: 12-1

Concrete Strength	Fire damaged	CFRP	GFRP	Batch
55	-	1	-	1

Ultimate strength	$\varepsilon_{L,p}$	ε_u	ε_y	Ductility	Composite modulus	Failure mode
$N_{max}(kN)$	-	-	-	$\mu_u = \frac{\varepsilon_u}{\varepsilon_y}$	$E_{sc} = \frac{f_{sc,p} - f_{50}}{\varepsilon_{L,p} - \varepsilon_{50}}$	FRP rupture
2104.2	93	7205	1477	4.88	4.83	

Load-Axial Strain	Axial stress- Axial strain	Hoop strain-Axial Strain
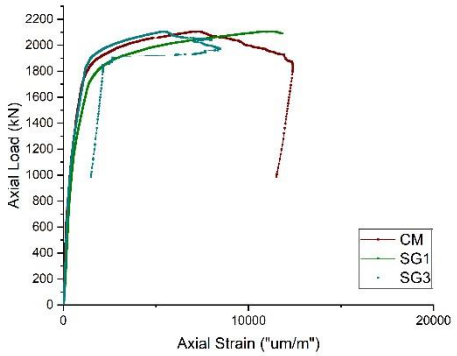	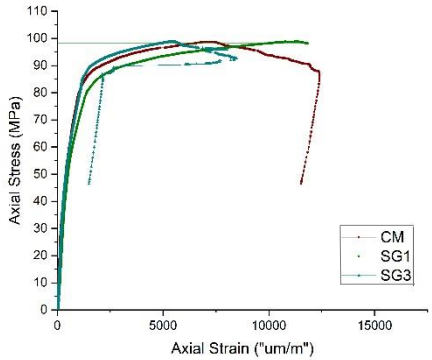	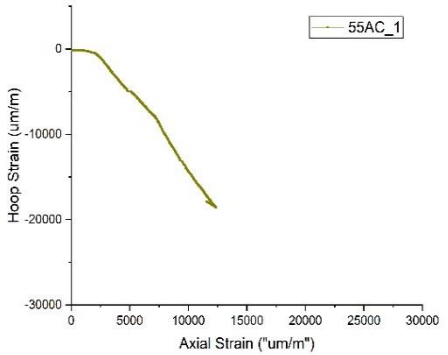

Notes:

Name: **55AC_2**

Test order: 24

No: 12-2

Concrete Strength	Fire damaged	CFRP	GFRP	Batch
55	-	1	-	2

Ultimate strength	$\varepsilon_{L,p}$	ε_u	ε_y	Ductility	Composite modulus	Failure mode
$N_{max}(kN)$	-	-	-	$\mu_u = \frac{\varepsilon_u}{\varepsilon_y}$	$E_{sc} = \frac{f_{sc,p} - f_{50}}{\varepsilon_{L,p} - \varepsilon_{50}}$	FRP rupture
2218.5	158	8896	1287	5.61	4.91	

Load-Axial Strain	Axial stress- Axial strain	Hoop strain-Axial Strain
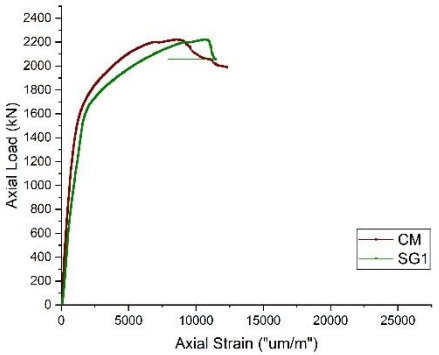	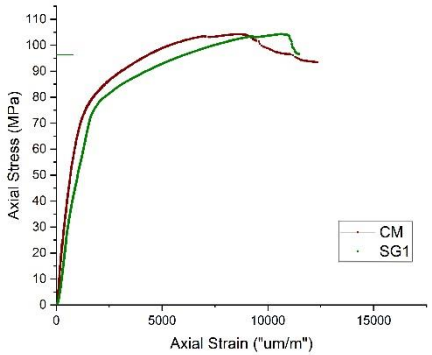	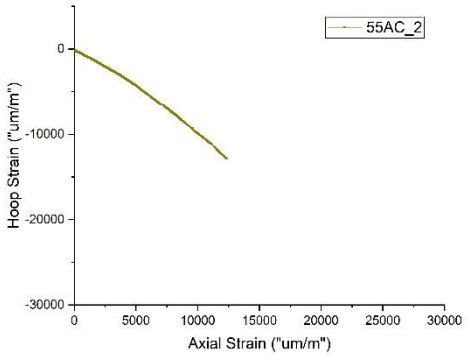

Notes:

Name: **21FCC_1**

Test order: 5

No: 9-1

Concrete Strength	Fire damaged	CFRP	GFRP	Batch
21	ISO 2-hours	2	-	1

Ultimate strength	$\varepsilon_{L,p}$	ε_u	ε_y	Ductility	Composite modulus	Failure mode
$N_{max}(kN)$	-	-	-	$\mu_u = \frac{\varepsilon_u}{\varepsilon_y}$	$E_{sc} = \frac{f_{sc,p} - f_{50}}{\varepsilon_{L,p} - \varepsilon_{50}}$	FRP rupture
945.4	261	-	-	-	-	

Load-Axial Strain	Axial stress- Axial strain	Hoop strain-Axial Strain
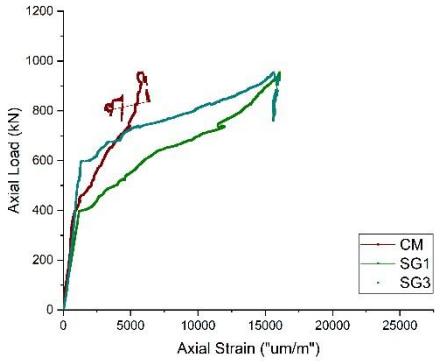	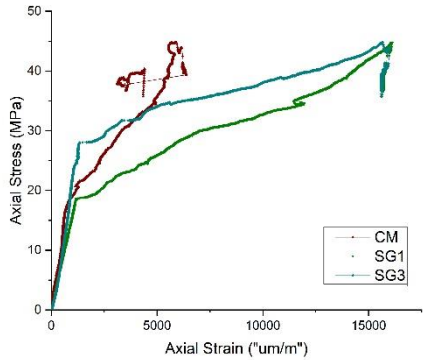	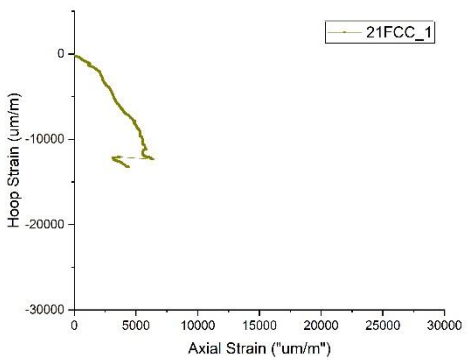

Notes: - Compressor meter works unwell.

Name: **21FCC_2**

Test order: 25

No: 9-2

Concrete Strength	Fire damaged	CFRP	GFRP	Batch
21	ISO 2-hours	2	-	2

Ultimate strength	$\varepsilon_{L,p}$	ε_u	ε_y	Ductility	Composite modulus	Failure mode
$N_{max}(kN)$	-	-	-	$\mu_u = \frac{\varepsilon_u}{\varepsilon_y}$	$E_{sc} = \frac{f_{sc,p} - f_{50}}{\varepsilon_{L,p} - \varepsilon_{50}}$	FRP rupture
1078.8	242	23248	1374	16.92	1.83	

Load-Axial Strain	Axial stress- Axial strain	Hoop strain-Axial Strain
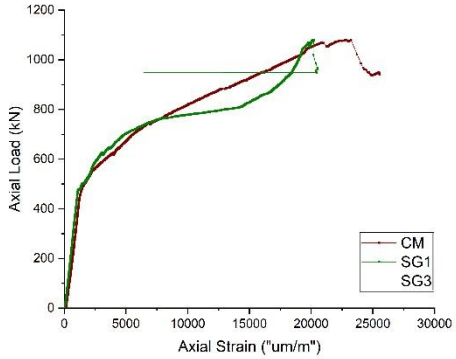	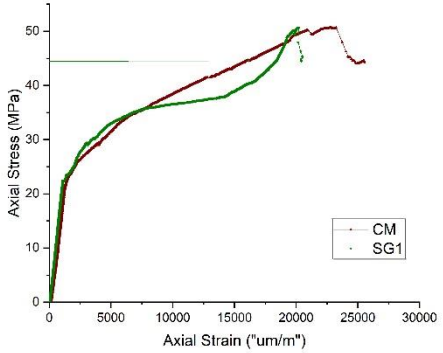	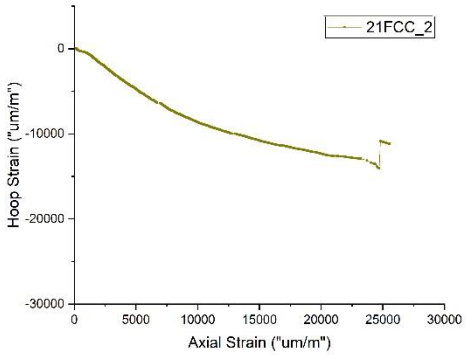

Notes:

Name: **55FCC_1**

Test order: 6

No: 19-1

Concrete Strength	Fire damaged	CFRP	GFRP	Batch
55	ISO 2-hours	2	-	1

Ultimate strength	$\varepsilon_{L,p}$	ε_u	ε_y	Ductility	Composite modulus	Failure mode
$N_{max}(kN)$	-	-	-	$\mu_u = \frac{\varepsilon_u}{\varepsilon_y}$	$E_{sc} = \frac{f_{sc,p} - f_{50}}{\varepsilon_{L,p} - \varepsilon_{50}}$	FRP rupture
1367.4	601	21100	1674	**12.60**	**1.48**	

Load-Axial Strain	Axial stress- Axial strain	Hoop strain-Axial Strain
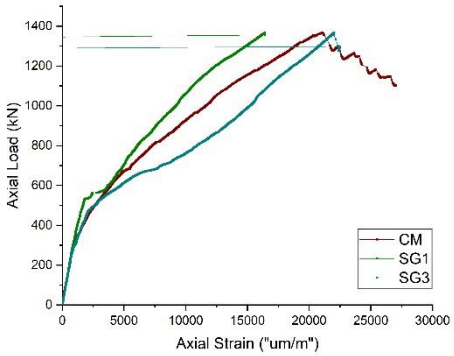	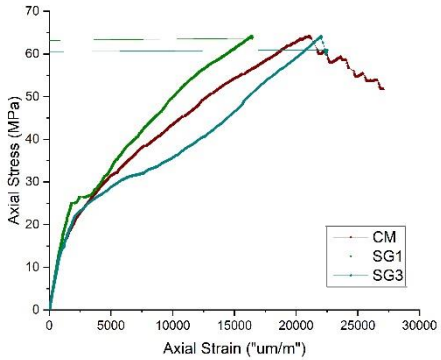	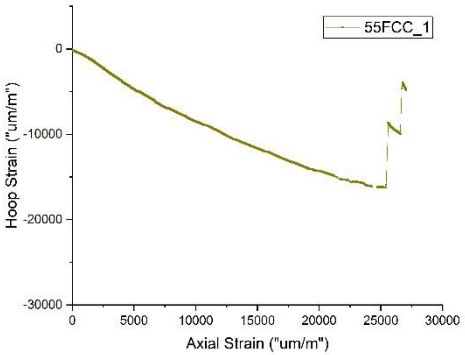

Notes:

Name: **55FCC_2**

Test order: 26

No: 19-2

Concrete Strength	Fire damaged	CFRP	GFRP	Batch
55	ISO 2-hours	2	-	2

Ultimate strength	$\varepsilon_{L,p}$	ε_u	ε_y	Ductility	Composite modulus	Failure mode
$N_{max}(kN)$	-	-	-	$\mu_u = \frac{\varepsilon_u}{\varepsilon_y}$	$E_{sc} = \frac{f_{sc,p} - f_{50}}{\varepsilon_{L,p} - \varepsilon_{50}}$	FRP rupture
1350.8	541	21053	1797	11.72	1.51	

Load-Axial Strain	Axial stress- Axial strain	Hoop strain-Axial Strain
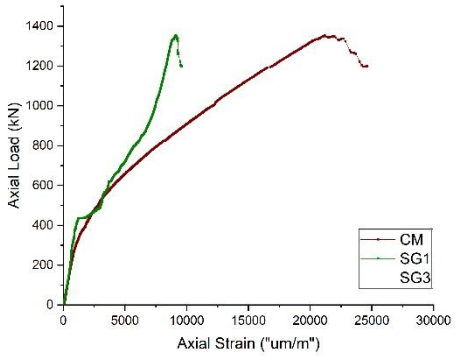	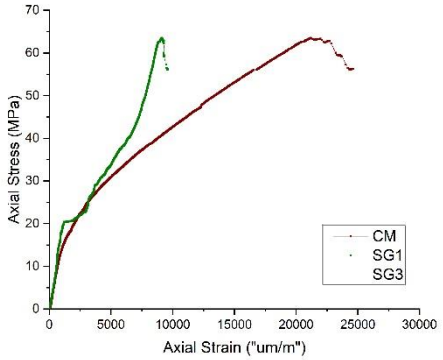	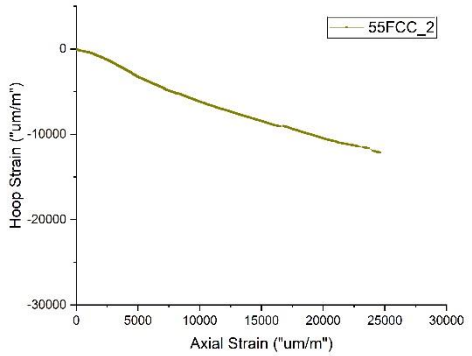

Notes: - Similar between 2 batch 55FCC

Name: **21ACC_1**

Test order: 7

No: 4-1

Concrete Strength	Fire damaged	CFRP	GFRP	Batch
21	-	2	-	1

Ultimate strength	$\varepsilon_{L,p}$	ε_u	ε_y	Ductility	Composite modulus	Failure mode
$N_{max}(kN)$	-	-	-	$\mu_u = \frac{\varepsilon_u}{\varepsilon_y}$	$E_{sc} = \frac{f_{sc,p} - f_{50}}{\varepsilon_{L,p} - \varepsilon_{50}}$	FRP rupture
1574.5	40	12232	990	12.36	2.61	

Load-Axial Strain	Axial stress- Axial strain	Hoop strain-Axial Strain
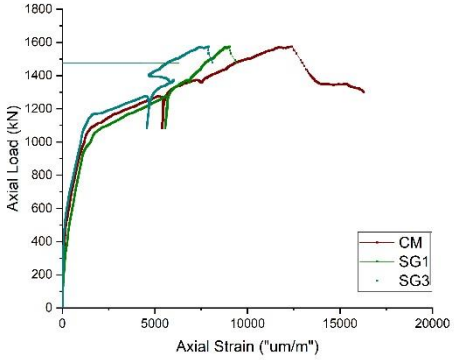	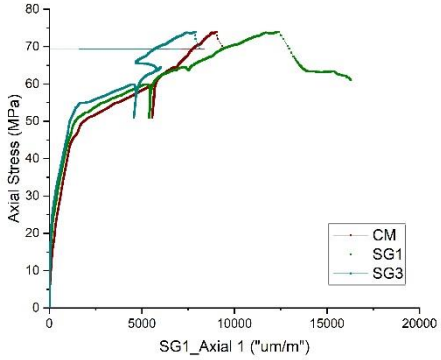	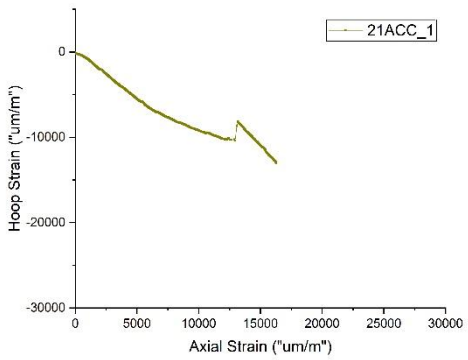

Notes:

Name: **21ACC_2**

Test order: 27

No: 4-2

Concrete Strength	Fire damaged	CFRP	GFRP	Batch
21	-	2	-	2

Ultimate strength	$\varepsilon_{L,p}$	ε_u	ε_y	Ductility	Composite modulus	Failure mode
$N_{max}(kN)$	-	-	-	$\mu_u = \frac{\varepsilon_u}{\varepsilon_y}$	$E_{sc} = \frac{f_{sc,p} - f_{50}}{\varepsilon_{L,p} - \varepsilon_{50}}$	FRP rupture
1573.3	195	13191	1027	12.84	2.99	

Load-Axial Strain	Axial stress- Axial strain	Hoop strain-Axial Strain
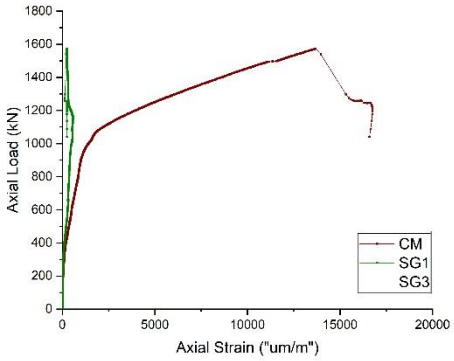	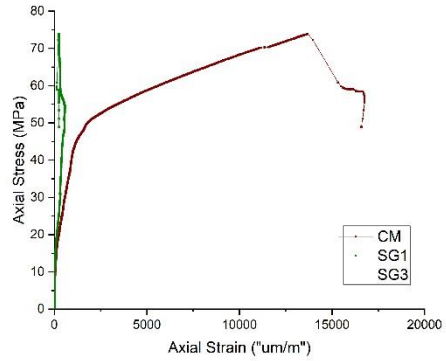	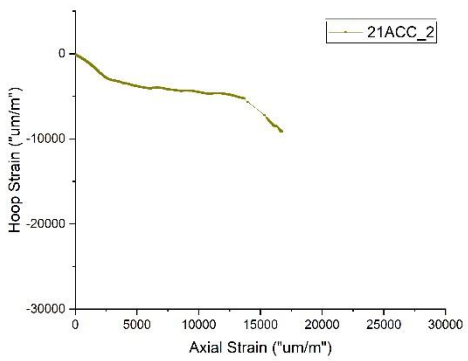

Notes: - SG works unwell. Similar between 2 batch 21ACC

Name: **55ACC_1**

Test order: 8

No: 14-1

Concrete Strength	Fire damaged	CFRP	GFRP	Batch
55	-	2	-	1

Ultimate strength	$\varepsilon_{L,p}$	ε_u	ε_y	Ductility	Composite modulus	Failure mode
$N_{max}(kN)$	-	-	-	$\mu_u = \frac{\varepsilon_u}{\varepsilon_y}$	$E_{sc} = \frac{f_{sc,p} - f_{50}}{\varepsilon_{L,p} - \varepsilon_{50}}$	FRP rupture
2412.3	186	11431	864	**13.23**	**4.95**	

Load-Axial Strain	Axial stress- Axial strain	Hoop strain-Axial Strain
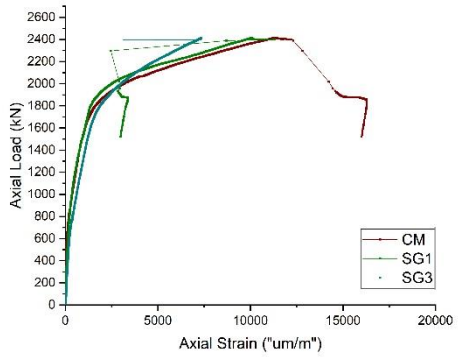	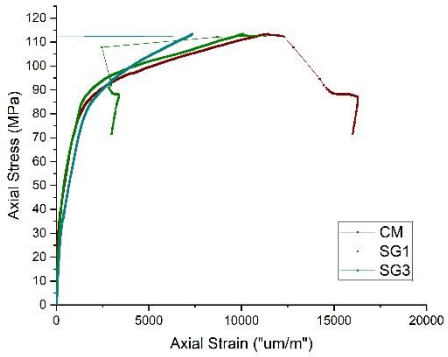	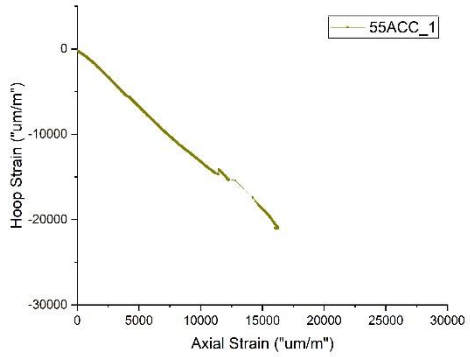

Notes:

Name: **55ACC_2**

Test order: 28

No: 14-2

Concrete Strength	Fire damaged	CFRP	GFRP	Batch
55	-	2	-	2

Ultimate strength	$\varepsilon_{L,p}$	ε_u	ε_y	Ductility	Composite modulus	Failure mode
$N_{max}(kN)$	-	-	-	$\mu_u = \frac{\varepsilon_u}{\varepsilon_y}$	$E_{sc} = \frac{f_{sc,p} - f_{50}}{\varepsilon_{L,p} - \varepsilon_{50}}$	FRP rupture
2434.5	258	10855	820	**13.24**	**6.11**	

Load-Axial Strain	Axial stress- Axial strain	Hoop strain-Axial Strain
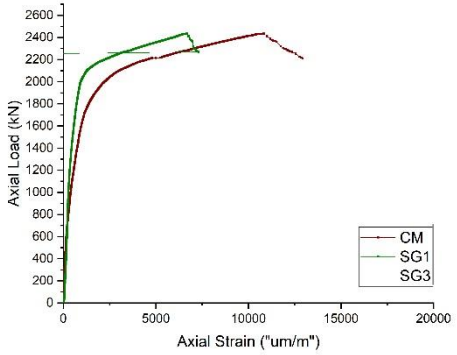	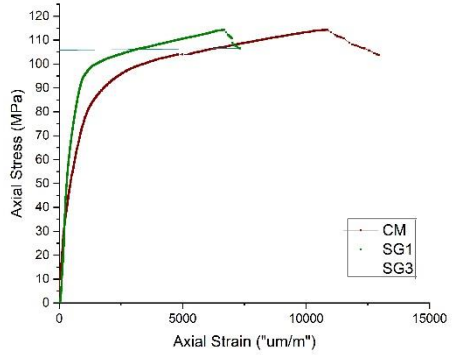	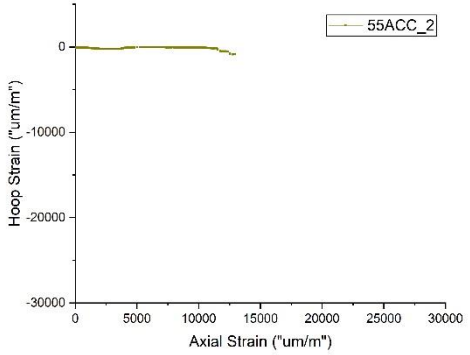

Notes: - Transverse Compressor meter works unwell.

Name: **21FGC_1**

Test order: 9

No: 10-1

Concrete Strength	Fire damaged	CFRP	GFRP	Batch
21	ISO 2-hours	1	1	1

Ultimate strength	$\varepsilon_{L,p}$	ε_u	ε_y	Ductility	Composite modulus	Failure mode
$N_{max}(kN)$	-	-	-	$\mu_u = \frac{\varepsilon_u}{\varepsilon_y}$	$E_{sc} = \frac{f_{sc,p} - f_{50}}{\varepsilon_{L,p} - \varepsilon_{50}}$	FRP rupture
965.6	496	14917	707	**21.10**	**1.99**	

Load-Axial Strain	Axial stress- Axial strain	Hoop strain-Axial Strain
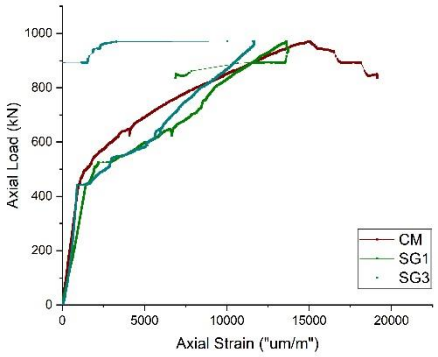	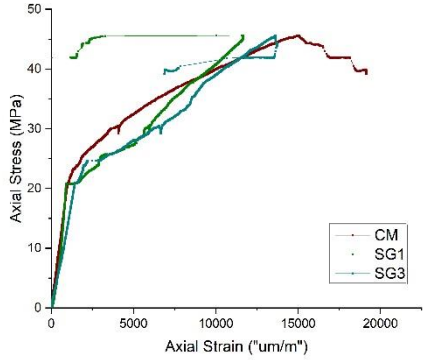	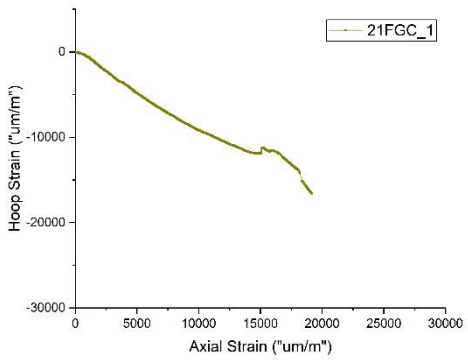

Notes:

Name: **21FGC_2**

Test order: 29

No: 10-2

Concrete Strength	Fire damaged	CFRP	GFRP	Batch
21	ISO 2-hours	1	1	2

Ultimate strength	$\varepsilon_{L,p}$	ε_u	ε_y	Ductility	Composite modulus	Failure mode
$N_{max}(kN)$	-	-	-	$\mu_u = \frac{\varepsilon_u}{\varepsilon_y}$	$E_{sc} = \frac{f_{sc,p} - f_{50}}{\varepsilon_{L,p} - \varepsilon_{50}}$	FRP rupture
955.9	521	19226	1033	**18.61**	**1.76**	

Load-Axial Strain	Axial stress- Axial strain	Hoop strain-Axial Strain
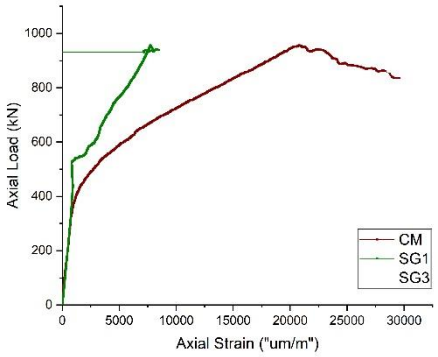	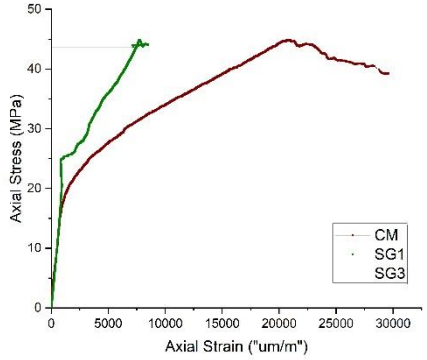	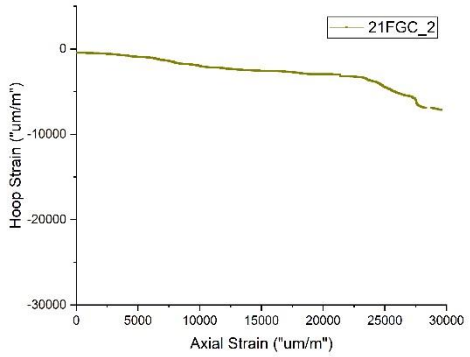

Notes:

Name: **55FGC_1**

Test order: 10

No: 20-1

Concrete Strength	Fire damaged	CFRP	GFRP	Batch
55	ISO 2-hours	1	1	1

Ultimate strength	$\varepsilon_{L,p}$	ε_u	ε_y	Ductility	Composite modulus	Failure mode
$N_{max}(kN)$	-	-	-	$\mu_u = \frac{\varepsilon_u}{\varepsilon_y}$	$E_{sc} = \frac{f_{sc,p} - f_{50}}{\varepsilon_{L,p} - \varepsilon_{50}}$	FRP rupture
1241.6	134	16310	1809	**9.02**	**1.55**	

Load-Axial Strain	Axial stress- Axial strain	Hoop strain-Axial Strain
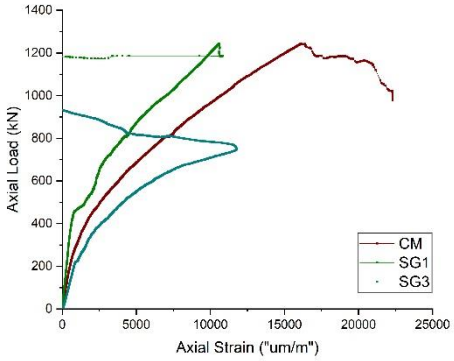	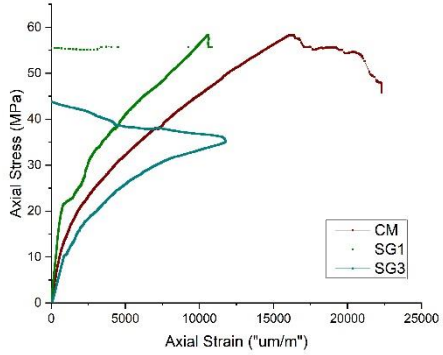	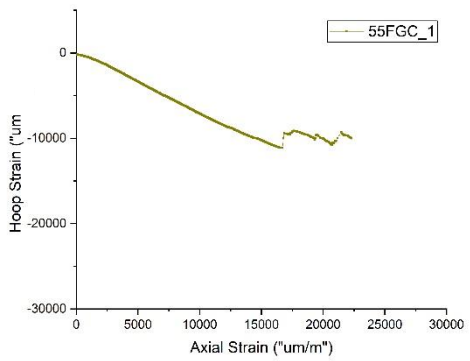

Notes: - SG3 is changed direction because of the FRP enlarge by hoop strain.

Name: **55FGC_2**

Test order: 30

No: 20-2

Concrete Strength	Fire damaged	CFRP	GFRP	Batch
55	ISO 2-hours	1	1	2

Ultimate strength	$\varepsilon_{L,p}$	ε_u	ε_y	Ductility	Composite modulus	Failure mode
$N_{max}(kN)$	-	-	-	$\mu_u = \frac{\varepsilon_u}{\varepsilon_y}$	$E_{sc} = \frac{f_{sc,p} - f_{50}}{\varepsilon_{L,p} - \varepsilon_{50}}$	FRP rupture
1202.8	117	16373	1838	**8.91**	**1.49**	

Load-Axial Strain

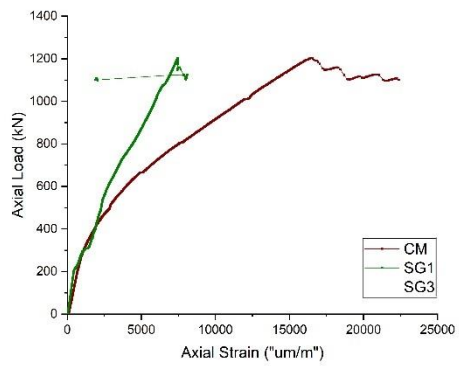

Axial stress- Axial strain

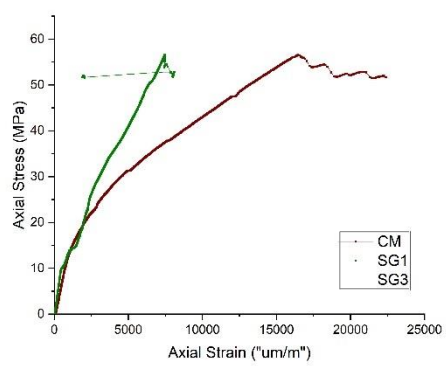

Hoop strain-Axial Strain

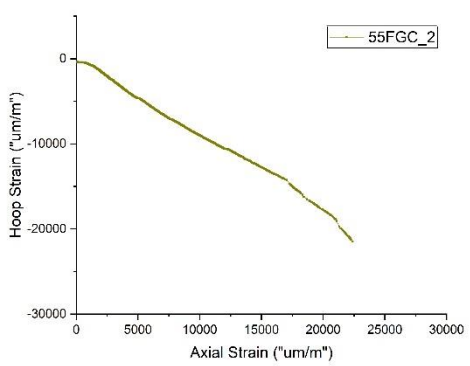

Notes:

Name: **21AGC_1**

Test order: 11

No: 5-1

Concrete Strength	Fire damaged	CFRP	GFRP	Batch
21	-	1	1	1

Ultimate strength	$\varepsilon_{L,p}$	ε_u	ε_y	Ductility	Composite modulus	Failure mode
$N_{max}(kN)$	-	-	-	$\mu_u = \frac{\varepsilon_u}{\varepsilon_y}$	$E_{sc} = \frac{f_{sc,p} - f_{50}}{\varepsilon_{L,p} - \varepsilon_{50}}$	FRP rupture
1447.2	63	-	-	-	-	

Load-Axial Strain	Axial stress- Axial strain	Hoop strain-Axial Strain
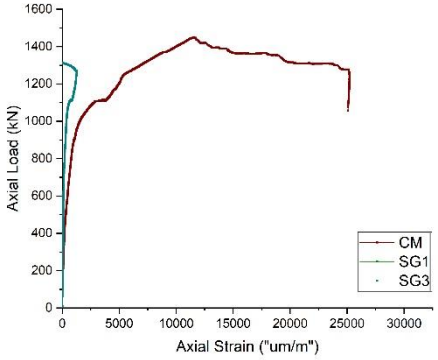	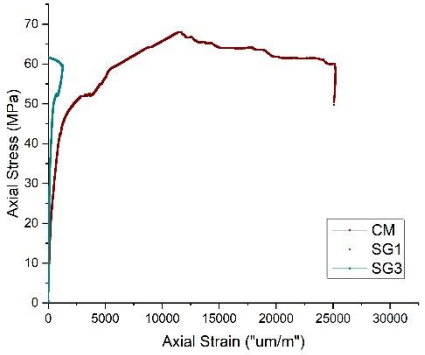	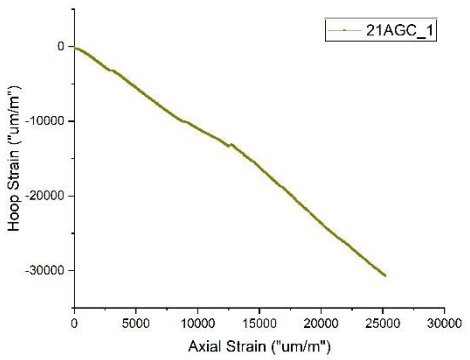

Notes: - SG1 is broken before test. SG3 works unwell.

Name: **21AGC_2**

Test order: 31

No: 5-2

Concrete Strength	Fire damaged	CFRP	GFRP	Batch
21	-	1	1	2

Ultimate strength	$\varepsilon_{L,p}$	ε_u	ε_y	Ductility	Composite modulus	Failure mode
$N_{max}(kN)$	-	-	-	$\mu_u = \frac{\varepsilon_u}{\varepsilon_y}$	$E_{sc} = \frac{f_{sc,p} - f_{50}}{\varepsilon_{L,p} - \varepsilon_{50}}$	FRP rupture
1545.5	80.4	16572	1220	13.58	2.87	

Load-Axial Strain

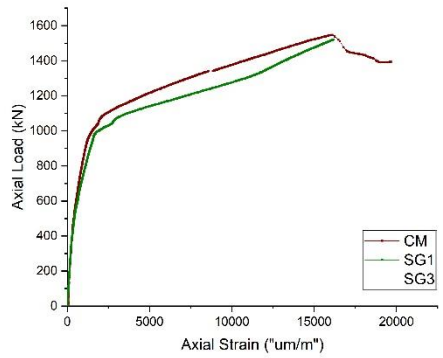

Axial stress- Axial strain

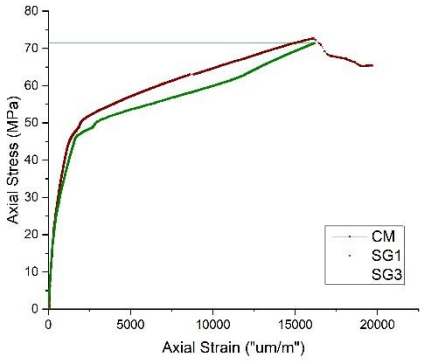

Hoop strain-Axial Strain

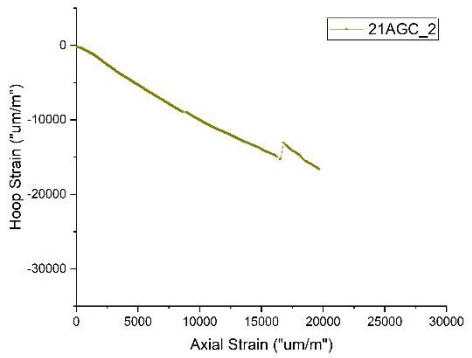

Notes:

Name: **55AGC_1**

Test order: 12

No: 15-1

Concrete Strength	Fire damaged	CFRP	GFRP	Batch
55	-	1	1	1

Ultimate strength	$\varepsilon_{L,p}$	ε_u	ε_y	Ductility	Composite modulus	Failure mode
$N_{max}(kN)$	-	-	-	$\mu_u = \frac{\varepsilon_u}{\varepsilon_y}$	$E_{sc} = \frac{f_{sc,p} - f_{50}}{\varepsilon_{L,p} - \varepsilon_{50}}$	FRP rupture
2270.8	59	9753	806	**12.10**	**5.44**	

Load-Axial Strain	Axial stress- Axial strain	Hoop strain-Axial Strain
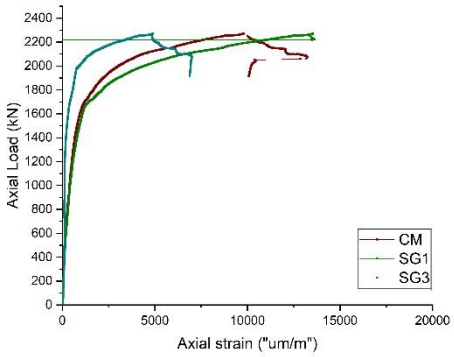	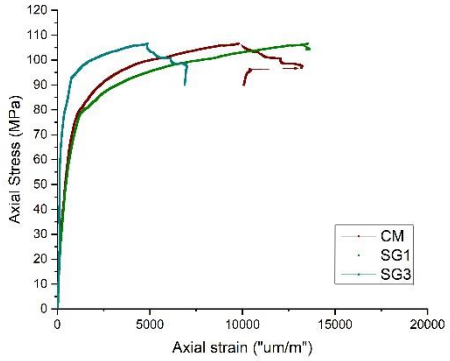	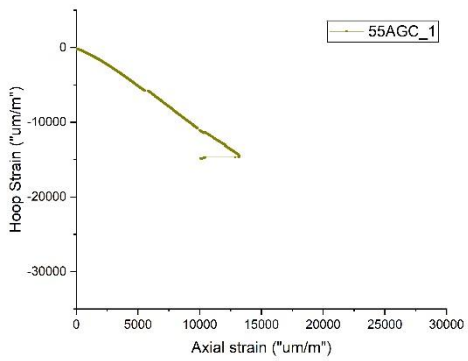

Notes:

Name: **55AGC_2**

Test order: 32

No: 15-2

Concrete Strength	Fire damaged	CFRP	GFRP	Batch
55	-	1	1	2

Ultimate strength	$\varepsilon_{L,p}$	ε_u	ε_y	Ductility	Composite modulus	Failure mode
$N_{max}(kN)$	-	-	-	$\mu_u = \frac{\varepsilon_u}{\varepsilon_y}$	$E_{sc} = \frac{f_{sc,p} - f_{50}}{\varepsilon_{L,p} - \varepsilon_{50}}$	FRP rupture
2328.3	56	9430	834	**11.31**	**6.39**	

Load-Axial Strain	Axial stress- Axial strain	Hoop strain-Axial Strain
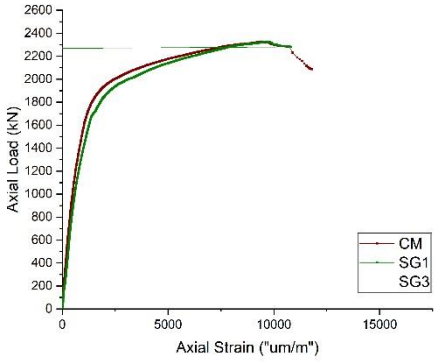	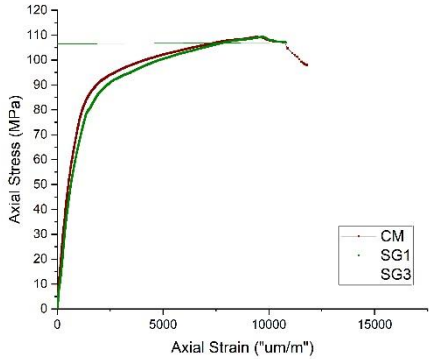	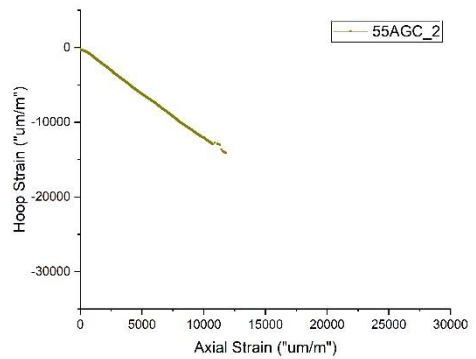

Notes: - Good control. Good curves.

Name: **21F_1**

Test order: 13

No: 6-1

Concrete Strength	Fire damaged	CFRP	GFRP	Batch
21	ISO 2-hour	-	-	1

Ultimate strength	$\varepsilon_{L,p}$	ε_u	ε_y	Ductility	Composite modulus	Failure mode
$N_{max}(kN)$	-	-	-	$\mu_u = \frac{\varepsilon_u}{\varepsilon_y}$	$E_{sc} = \frac{f_{sc,p} - f_{50}}{\varepsilon_{L,p} - \varepsilon_{50}}$	Top buckling (Stop because on high hoop strain, exceed LVDT gage length)
650.2	509	30711	876	35.06	1.66	

Load-Axial Strain	Axial stress- Axial strain	Hoop strain-Axial Strain
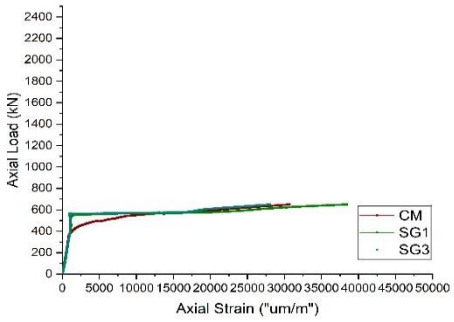	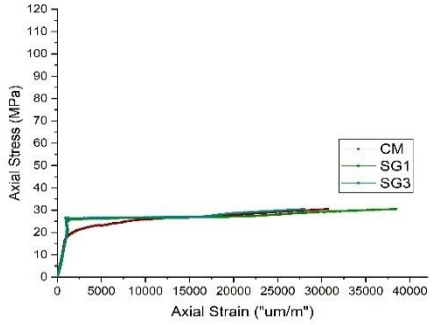	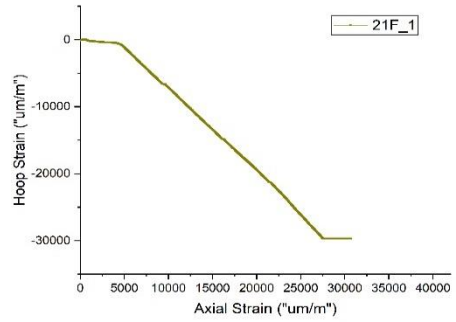

Notes: - No drop on curve. Not able to calculate ductility

Name: **21F_2**

Test order: 33

No: 6-2

Concrete Strength	Fire damaged	CFRP	GFRP	Batch
21	ISO 2-hour	-	-	2

Ultimate strength	$\varepsilon_{L,p}$	ε_u	ε_y	Ductility	Composite modulus	Failure mode
$N_{max}(kN)$	-	-	-	$\mu_u = \frac{\varepsilon_u}{\varepsilon_y}$	$E_{sc} = \frac{f_{sc,p} - f_{50}}{\varepsilon_{L,p} - \varepsilon_{50}}$	Mid buckling (Stop because on high hoop strain, exceed LVDT gage length)
734.5	597	-	-	-	-	

Load-Axial Strain	Axial stress- Axial strain	Hoop strain-Axial Strain
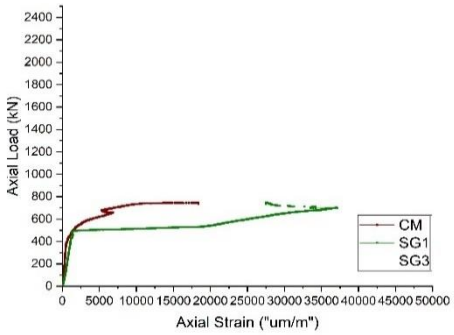	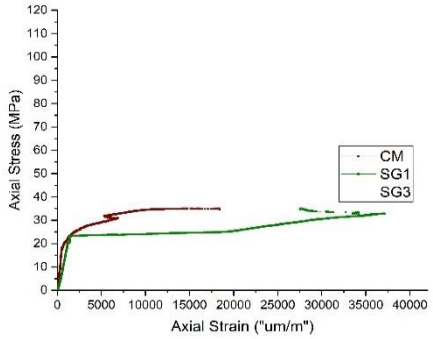	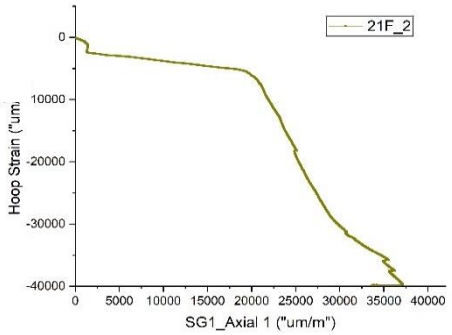

Notes: - No drop on curve. Not able to calculate ductility. Axial LVDT worked unwell.

Name: **55F_1**

Test order: 14

No: 16-1

Concrete Strength	Fire damaged	CFRP	GFRP	Batch
55	ISO 2-hour	-	-	1

Ultimate strength	$\varepsilon_{L,p}$	ε_u	ε_y	Ductility	Composite modulus	Failure mode
$N_{max}(kN)$	-	-	-	$\mu_u = \frac{\varepsilon_u}{\varepsilon_y}$	$E_{sc} = \frac{f_{sc,p} - f_{50}}{\varepsilon_{L,p} - \varepsilon_{50}}$	Mid buckling (Stop because on high hoop strain, exceed LVDT gage length)
825.4	500	35130	1768	19.87	1.54	

Load-Axial Strain

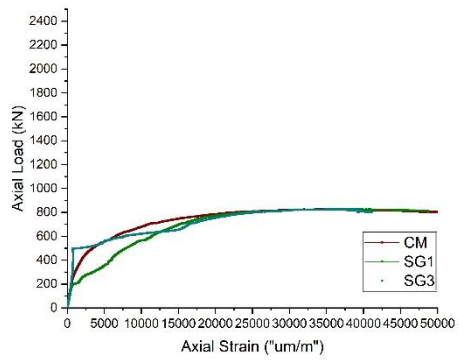

Axial stress- Axial strain

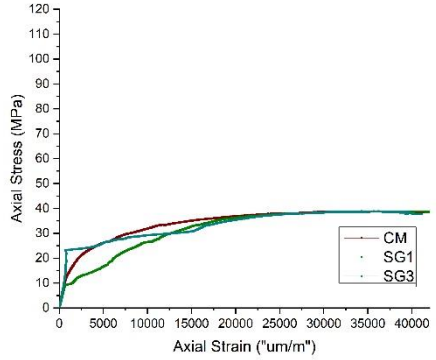

Hoop strain-Axial Strain

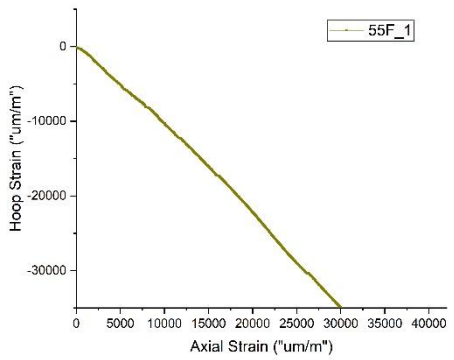

Notes: - No drop on curve. Not able to calculate ductility. Good control. Good curve

Name: **55F_2**

Test order: 34

No: 16-2

Concrete Strength	Fire damaged	CFRP	GFRP	Batch
55	ISO 2-hour	-	-	2

Ultimate strength	$\varepsilon_{L,p}$	ε_u	ε_y	Ductility	Composite modulus	Failure mode
$N_{max}(kN)$	-	-	-	$\mu_u = \frac{\varepsilon_u}{\varepsilon_y}$	$E_{sc} = \frac{f_{sc,p} - f_{50}}{\varepsilon_{L,p} - \varepsilon_{50}}$	Top buckling (Stop because on high hoop strain, exceed LVDT gage length)
872.6	490	36118	1681	**21.49**	**1.63**	

Load-Axial Strain

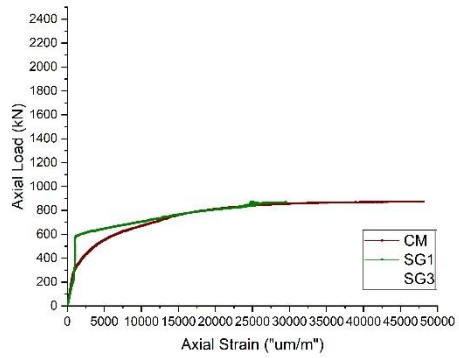

Axial stress- Axial strain

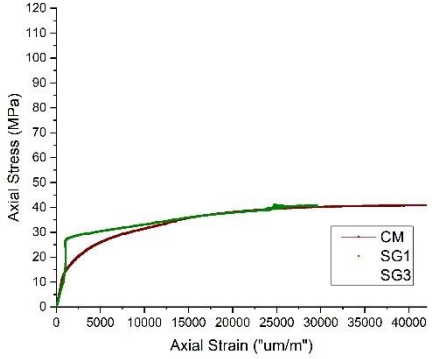

Hoop strain-Axial Strain

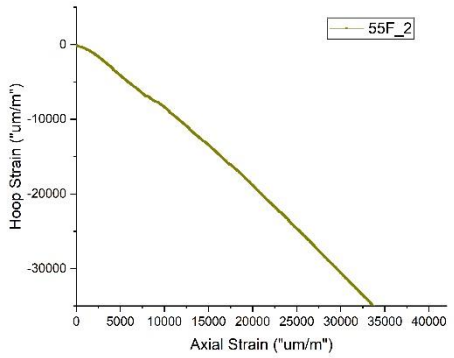

Notes: - No drop on curve. Not able to calculate ductility. Good control. Good curve

Name: **21A_1**

Test order: 15

No: 1-1

Concrete Strength	Fire damaged	CFRP	GFRP	Batch
21	-	-	-	1

Ultimate strength	$\varepsilon_{L,p}$	ε_u	ε_y	Ductility	Composite modulus	Failure mode
$N_{max}(kN)$	-	-	-	$\mu_u = \frac{\varepsilon_u}{\varepsilon_y}$	$E_{sc} = \frac{f_{sc,p} - f_{50}}{\varepsilon_{L,p} - \varepsilon_{50}}$	Mid buckling (Stop because on high hoop strain, exceed LVDT gage length)
1203.9	97	29147	1150	25.35	2.29	

Load-Axial Strain

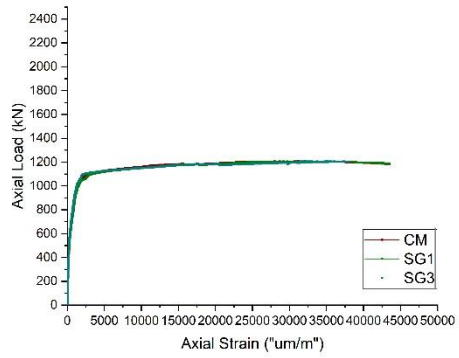

Axial stress- Axial strain

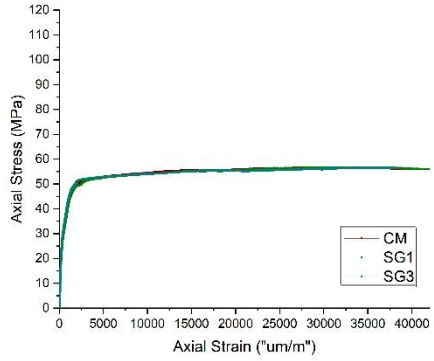

Hoop strain-Axial Strain

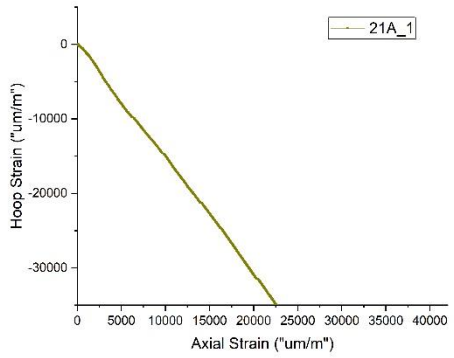

Notes: - No drop on curve. Not able to calculate ductility. Good control. Good curve

Name: **21A_2**

Test order: 35

No: 1-2

Concrete Strength	Fire damaged	CFRP	GFRP	Batch
21	-	-	-	2

Ultimate strength	$\varepsilon_{L,p}$	ε_u	ε_y	Ductility	Composite modulus	Failure mode
$N_{max}(kN)$	-	-	-	$\mu_u = \frac{\varepsilon_u}{\varepsilon_y}$	$E_{sc} = \frac{f_{sc,p} - f_{50}}{\varepsilon_{L,p} - \varepsilon_{50}}$	Mid buckling (Stop because on high hoop strain, exceed LVDT gage length)
1209.8	90	27443	1046	26.24	2.66	

Load-Axial Strain	Axial stress- Axial strain	Hoop strain-Axial Strain
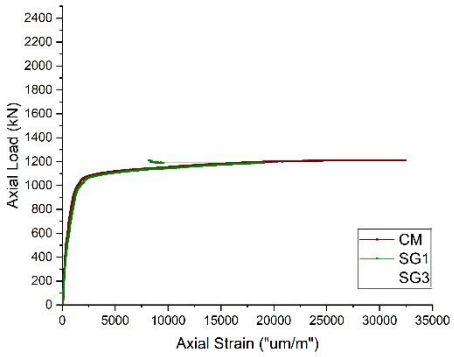	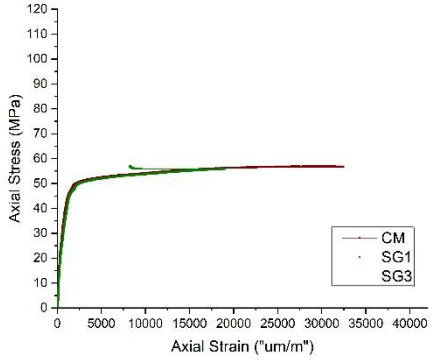	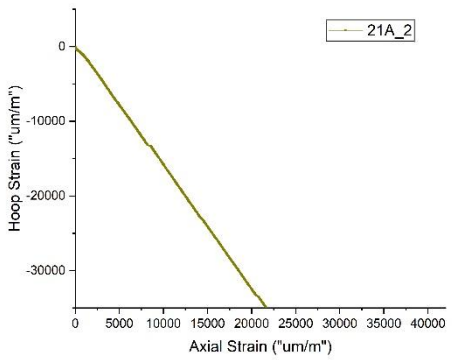

Notes: - No drop on curve. Not able to calculate ductility. Good control. Good curve

Name: **55A_1**

Test order: 16

No: 11-1

Concrete Strength	Fire damaged	CFRP	GFRP	Batch
55	-	-	-	1

Ultimate strength	$\varepsilon_{L,p}$	ε_u	ε_y	Ductility	Composite modulus	Failure mode
$N_{max}(kN)$	-	-	-	$\mu_u = \frac{\varepsilon_u}{\varepsilon_y}$	$E_{sc} = \frac{f_{sc,p} - f_{50}}{\varepsilon_{L,p} - \varepsilon_{50}}$	Mid buckling
1780.7	774	4950	1067	**4.64**	**4.08**	

Load-Axial Strain	Axial stress- Axial strain	Hoop strain-Axial Strain
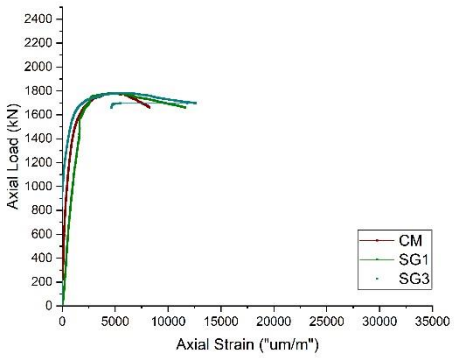	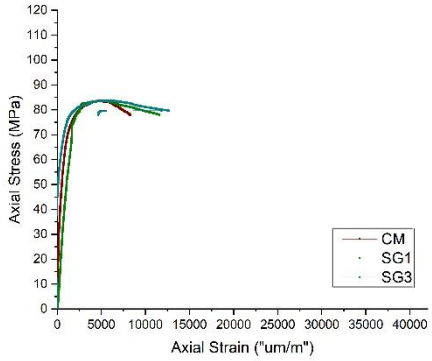	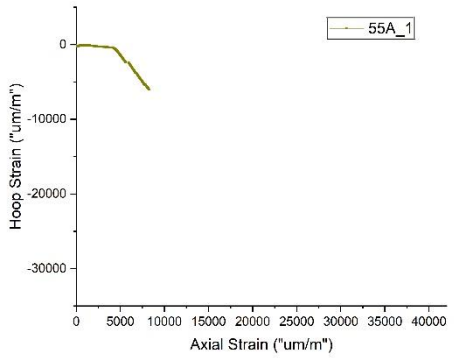

Notes:

No: 11-2

Name: **55A_2**

Test order: 36

Concrete Strength	Fire damaged	CFRP	GFRP	Batch
55	-	-	-	2

Ultimate strength	$\varepsilon_{L,p}$	ε_u	ε_y	Ductility	Composite modulus	Failure mode
$N_{max}(kN)$	-	-	-	$\mu_u = \frac{\varepsilon_u}{\varepsilon_y}$	$E_{sc} = \frac{f_{sc,p} - f_{50}}{\varepsilon_{L,p} - \varepsilon_{50}}$	Mid buckling
1895.4	727	8207	1749	**4.69**	**4.50**	

Load-Axial Strain

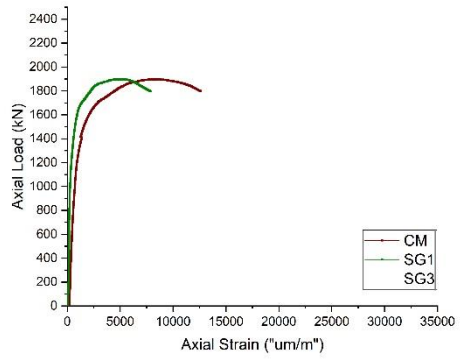

Axial stress- Axial strain

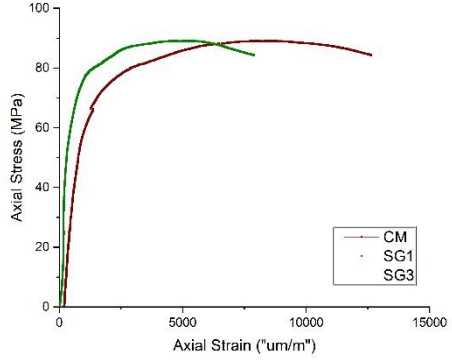

Hoop strain-Axial Strain

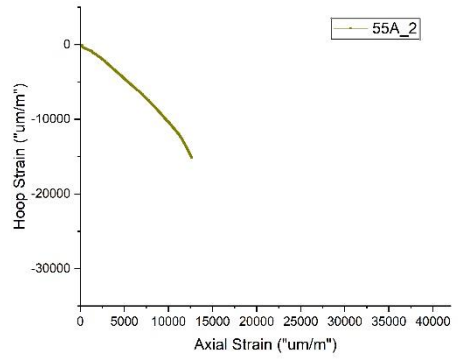

Notes:

Name: **21FG_1**

Test order: 17

No: 8-1

Concrete Strength	Fire damaged	CFRP	GFRP	Batch
21	ISO 2-hour	-	1	1

Ultimate strength	$\varepsilon_{L,p}$	ε_u	ε_y	Ductility	Composite modulus	Failure mode
$N_{max}(kN)$	-	-	-	$\mu_u = \frac{\varepsilon_u}{\varepsilon_y}$	$E_{sc} = \frac{f_{sc,p} - f_{50}}{\varepsilon_{L,p} - \varepsilon_{50}}$	FRP rupture
789.6	904	20682	914	**22.63**	**1.73**	

Load-Axial Strain	Axial stress- Axial strain	Hoop strain-Axial Strain
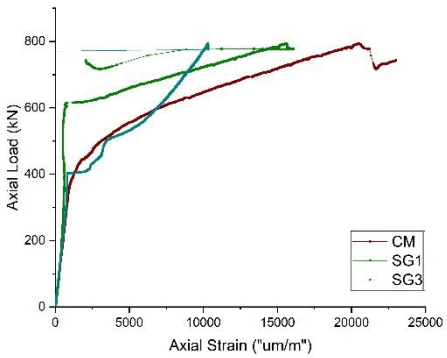	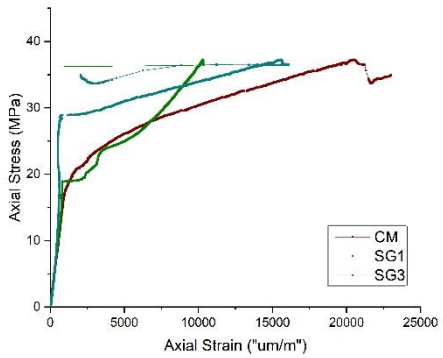	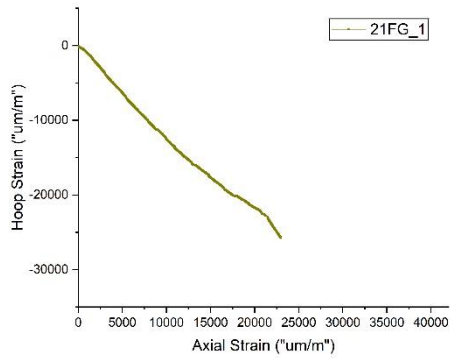

Notes: - Nominal yield point does not make sense.

Name: **21FG_2**

Test order: 37

No: 8-2

Concrete Strength	Fire damaged	CFRP	GFRP	Batch
21	ISO 2-hour	-	1	2

Ultimate strength	$\varepsilon_{L,p}$	ε_u	ε_y	Ductility	Composite modulus	Failure mode
$N_{max}(kN)$	-	-	-	$\mu_u = \frac{\varepsilon_u}{\varepsilon_y}$	$E_{sc} = \frac{f_{sc,p} - f_{50}}{\varepsilon_{L,p} - \varepsilon_{50}}$	FRP rupture
810.4	1006	22477	1006	**22.34**	**1.74**	

Load-Axial Strain	Axial stress- Axial strain	Hoop strain-Axial Strain
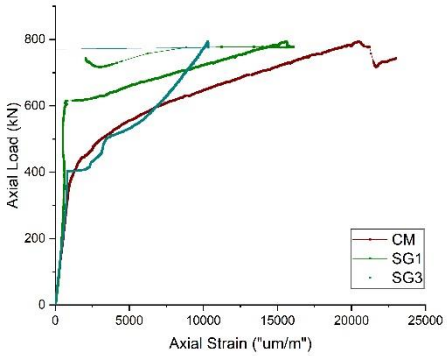	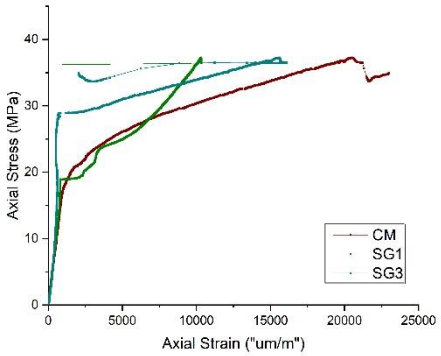	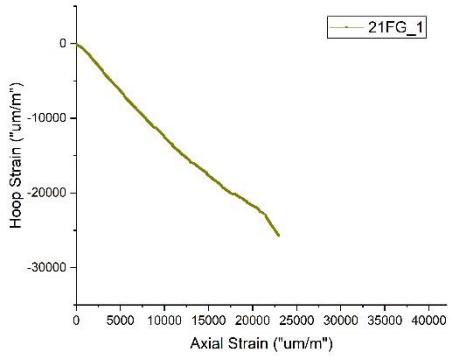

Notes: - Nominal yield point does not make sense.

Name: **55FG_1**

Test order: 18

No: 18-1

Concrete Strength	Fire damaged	CFRP	GFRP	Batch
55	ISO 2-hour	-	1	1

Ultimate strength	$\varepsilon_{L,p}$	ε_u	ε_y	Ductility	Composite modulus	Failure mode
$N_{max}(kN)$	-	-	-	$\mu_u = \frac{\varepsilon_u}{\varepsilon_y}$	$E_{sc} = \frac{f_{sc,p} - f_{50}}{\varepsilon_{L,p} - \varepsilon_{50}}$	FRP rupture
1038.2	291	20325	1137	**17.88**	**1.62**	

Load-Axial Strain	Axial stress- Axial strain	Hoop strain-Axial Strain
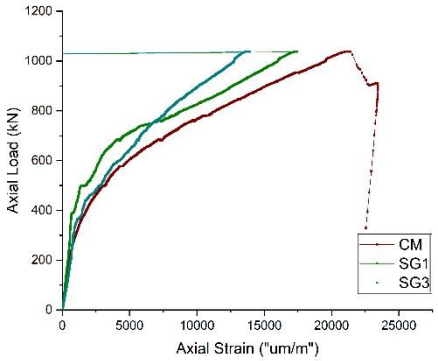	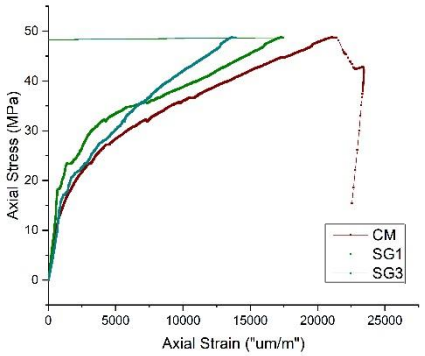	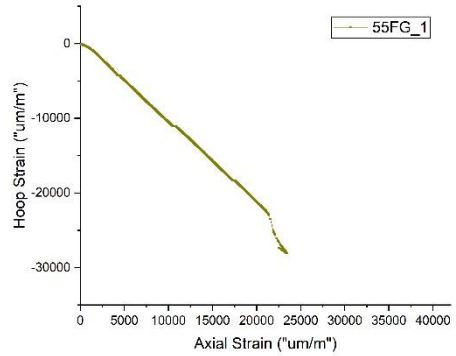

Notes: - Nominal yield point does not make sense.

Name: **55FG_2**

Test order: 38

No: 18-2

Concrete Strength	Fire damaged	CFRP	GFRP	Batch
55	ISO 2-hour	-	1	2

Ultimate strength	$\varepsilon_{L,p}$	ε_u	ε_y	Ductility	Composite modulus	Failure mode
$N_{max}(kN)$	-	-	-	$\mu_u = \frac{\varepsilon_u}{\varepsilon_y}$	$E_{sc} = \frac{f_{sc,p} - f_{50}}{\varepsilon_{L,p} - \varepsilon_{50}}$	FRP rupture
1058.7	261	22415	1178	**19.03**	**1.38**	

Load-Axial Strain

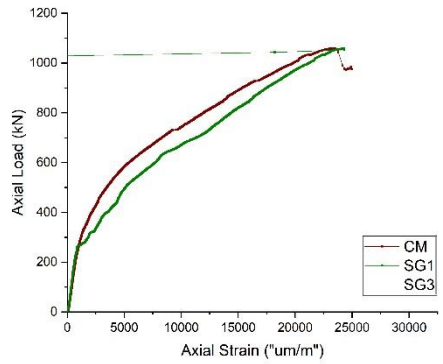

Axial stress- Axial strain

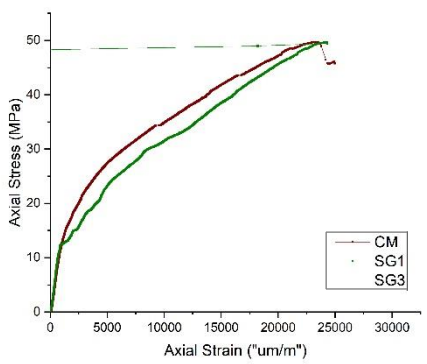

Hoop strain-Axial Strain

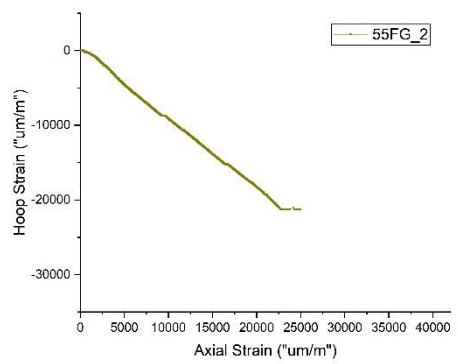

Notes: - Nominal yield point does not make sense.

Name: **21AG_1**

Test order: 19

No: 3-1

Concrete Strength	Fire damaged	CFRP	GFRP	Batch
21	-	-	1	1

Ultimate strength	$\varepsilon_{L,p}$	ε_u	ε_y	Ductility	Composite modulus	Failure mode
$N_{max}(kN)$	-	-	-	$\mu_u = \frac{\varepsilon_u}{\varepsilon_y}$	$E_{sc} = \frac{f_{sc,p} - f_{50}}{\varepsilon_{L,p} - \varepsilon_{50}}$	FRP rupture
1337.6	792	18358	989	**18.56**	**2.51**	

Load-Axial Strain	Axial stress- Axial strain	Hoop strain-Axial Strain
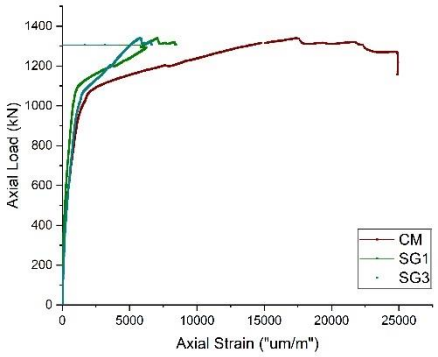	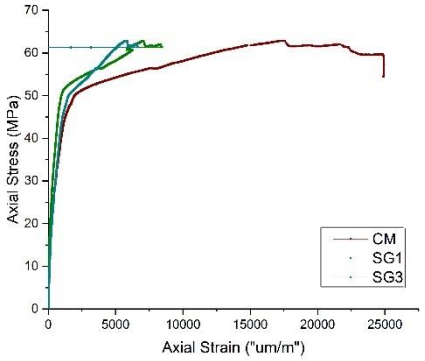	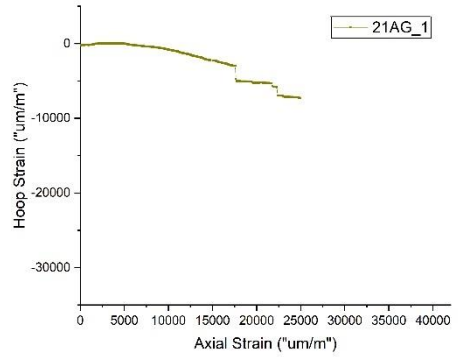

Notes:

Name: **55AG_1**

Test order: 20

No: 13-1

Concrete Strength	Fire damaged	CFRP	GFRP	Batch
21	-	-	1	2

Ultimate strength	$\varepsilon_{L,p}$	ε_u	ε_y	Ductility	Composite modulus	Failure mode
$N_{max}(kN)$	-	-	-	$\mu_u = \frac{\varepsilon_u}{\varepsilon_y}$	$E_{sc} = \frac{f_{sc,p} - f_{50}}{\varepsilon_{L,p} - \varepsilon_{50}}$	FRP rupture
1862.5	178	8657	1232	**6.59**	**4.53**	

Load-Axial Strain

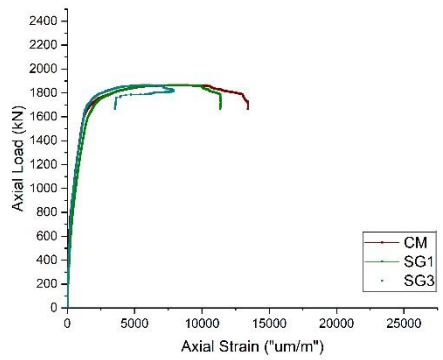

Axial stress- Axial strain

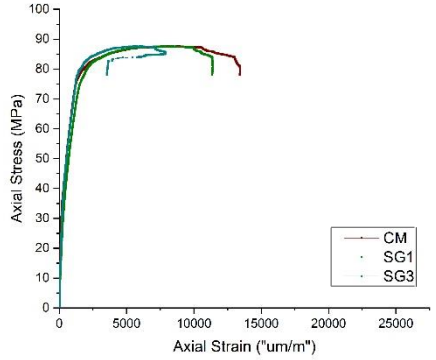

Hoop strain-Axial Strain